EFFECT OF LONG TERM ELEVATED TEMPERATURE EXPOSURE ON THE MECHANICAL PROPERTIES AND WELDABILITY OF CAST DUPLEX STAINLESS STEELS

SANJAY B. SHENDYE

B. Tech., Indian Institute of Technology, Bombay, 1983.

A thesis submitted to the faculty
of the Oregon Graduate Center
in partial fulfillment of the
requirements for the degree
Master of Science
in
Materials Science and Engineering

August, 1985

The thesis ' Effect of Long Term Elevated Temperature Exposure on the Mechanical Properties and Weldability of Cast Duplex Stainless Steels ', by Sanjay B. Shendye has been examined and approved by the following examination committee :

Jack H. Devletian
Associate Professor
Thesis Research Advisor

William E. Wood
Professor

Anthony E. Bell
Research Scientist

ACKNOWLEDGEMENT

I thank Prof. J. H. Devletian for his guidance and support throughout this work. I also thank Drs. W. E. Wood and A. E. Bell for agreeing to examine my thesis. Thanks are due to The Metal Properties Council and the Welding Research Council for funding this work, and to ESCO Corporation, Portland, Oregon, for providing the material required for this work. I am also thankful to L. Finch, ESCO Corporation, Portland, Oregon, for providing equipment required to carry out this work. I also appreciate deeply the help provided by R. Turpin, D. Roberts, and L. Fuller during the course of this work. Special thanks are due to Ms. B. Ryall for the excellent drawings.

TABLE OF CONTENTS

LIST OF TABLES

LIST OF FIGURES

Page

Page

Page

Page

ABSTRACT

Effect of Long Term Elevated Temperature Exposure on the Mechanical Properties and Weldability of Cast Duplex Stainless Steels

Sanjay B. Shendye
Oregon Graduate center, 1985

Supervising Professor : Jack H. Devletian

Stainless steel castings of the type CF-3M, CG-8M and CF-3C were studied to determine the effect of exposure at 316, 427 and 594 ^{0}C (600, 800 and 1100 ^{0}F) for the durations up to 14,000 hrs. Substantial reduction in the room temperature CVN impact toughness resulted after aging these castings. Also, hardness and microhardness values increased with aging time. The ferrite contents of castings decreased with increasing aging time at 594 and 427 ^{0}C (1100 and 800 ^{0}F), but the ferrite content increased after aging at 316 ^{0}C (600 ^{0}F).

The weldability of these castings (as measured by the varestraint test) was found to be excellent. No significant change in the weldability and hot cracking susceptibility was found as a result of aging the castings at 594 and 427 ^{0}C (1100 and 800 ^{0}F) up to 10,000 hours. Only after the ferrite content exceeded about 22 FN did a noticeable increase in the hot cracking tendency occur. Higher sulphur contents gave rise to greater hot cracking tendency of the weld metal.

INTRODUCTION

A duplex alloy possesses a two phase microstructure. The term is generally used for alloys in which the phases are present in substantial amounts. A duplex stainless steel is one in which the two phases are 'stainless' i.e the two phases have more than 12 % Cr. The most common phases in stainless steel are face centered cubic (FCC) austenite (γ), body centered cubic (BCC) ferrite (α) and martensite. The predominant phases in most stainless steels are austenite and ferrite, and all the discussion here will be confined to such alloys.

Cast duplex stainless steels are used extensively to fabricate piping for the chemical, petrochemical and nuclear industries. In the nuclear industry they are used to fabricate pump casings and valve bodies for light water reactors and primary coolant piping in pressurized water reactors [1]. The ferrite phase of duplex stainless steel generally improves the tensile strength, resistance to stress corrosion cracking, the soundness of castings, weldability, and formability. However, the presence of ferrite in these steels leads to the precipitation of several detrimental phases such as carbides, brittle Cr rich phases such as sigma (σ) and the chi (χ) phase, and a Cr rich BCC phase α', in the ferrite or along the ferrite/austenite grain boundaries during elevated temperature exposure. The precipitation of these embrittling phases leads to deterioration of the properties.

Solidification cracking in stainless steels is reduced by appropriately adjusting their ferrite content which is controlled with the help of a Schaeffler/DeLong diagram [2] for welds and a Schoeffer diagram [3] for castings.

The ferrite content [4] of the duplex stainless steels is generally maintained between 5 - 40%. Recent studies have shown that it is the nature of solidification which is important, rather than just the final amount of ferrite produced.

The objective of this investigation was to study the long term aging characteristics of cast stainless steels aged at 316, 427 and 594 ^{0}C (600, 800 and 1100 ^{0}F respectively), by determining the mechanical properties such as Charpy V-notch (CVN) impact energy and hardness, and ferrite content. The second objective was to determine the weldability of the stainless steels by the varestraint test after embrittlement due to aging.

LITERATURE REVIEW

SOLIDIFICATION :

Isothermal sections of the Fe-Cr-Ni system have been published by Bain and Griffiths [5], Pugh and Nisbet [6] and recently by Rivlin [7]. Figure 1 shows the isothermal sections of the Fe-Cr-Ni system at 650°C and 400°C. A convenient way of considering the Fe-Cr-Ni system is the vertical section [8] as shown in Figure 2 for 70% Fe. The vertical section provides good information of the Fe-Cr-Ni system, although tie lines can not be drawn on them. The high temperature ferrite in Figure 2 has been denoted as δ ; it is however, the same BCC phase as the α phase. The ferrite can form via a diffusionless shear process and when it does, it is referred to as martensite. Alloys containing less than 18 Cr_{eq} and more than 12 Ni_{eq} begin to solidify as primary austenite while alloys with a higher Cr_{eq} begin to solidify as primary ferrite. The schematic vertical section in Figure 2 was developed for welds, however it can also be applied to castings.

The Cr_{eq} and Ni_{eq} for castings [3] is given by :

$$Cr_{eq} = Cr(\%) + 1.5\ Si(\%) + 1.4\ Mo(\%) + Cb(\%) - 4.99 \quad (1a)$$

$$Ni_{eq} = (\%Ni) + 30\ (\%C) + 0.5\ (\%Mn) + 26\ (\%N - 0.02) + 2.77 \quad (1b)$$

The Cr_{eq} and the Ni_{eq} for welds [2] is given by the following relation :

$$Cr_{eq} = (\%Cr) + (\%Mo) + 1.5\ (\%Si) + 0.5\ (\%Cb) \quad (1c)$$

$$Ni_{eq} = Ni(\%) + 30\ (\%C + \%N) + 0.5\ (\%Mn) \quad (1d)$$

Stainless steel welds containing more than approximately 3 - 4% ferrite at

room temperature solidified as primary ferrite [9]. Various ferrite morphologies result due to increasing the amount of ferrite in the austenite matrix, such as lacy, vermicular, globular and acicular ferrite [10]. These terms are used to describe the ferrite morphology of both welds and castings. The ferrite morphology is important because it affects the mechanical properties of castings.

In general the ferrite content of castings is expressed in terms of volume percent ferrite and the ferrite content of welds in terms of arbitrary number called the ferrite number (FN). Even in case of castings the ferrite content is determined in terms of FN, but since the ferrite in castings is larger, a calibration curve can be obtained to convert the FN to % ferrite by metallographic point count method or any other accepted method [3]. The methods used to obtain the calibration curve to convert FN to % ferrite as in case of castings can not be used for weld metal due to the extreme fineness of the ferrite in case of weld metal, which could lead to errors in the ferrite measurement methods as described in the AWS A4.2 - 74.

In general, duplex stainless steel castings contain 5 - 40 % ferrite in the austenite matrix. When primary ferrite is the first phase to solidify, the dendrites become enriched in ferrite stabilizing elements such as Cr, Mo, Si etc. Various theories have been put forward to explain the beneficial effects of ferrite in stainless steels. Linnert and Bloom [11] believed that reduced cracking tendency with the presence of ferrite was due to increased grain boundary area, thus reducing the effective width of grain boundary. Parks [12] has reported that the favorable effect of ferrite was due to its capacity for dissolving larger quantities of elements, such as P, Si, and Nb than austenite, and this reduces the

segregation and thereby strengthens the grain boundary. Thomas [13] believed that the beneficial action of ferrite was due to its presence in a finely dispersed form, which prevents the formation of cracks or their propagation, once they are formed. It can be seen from the above theories, that the reason for the beneficial effect of ferrite in reducing the crackability of stainless steel is not precisely known. It is however, important to have primary ferrite as the first phase to solidify during solidification, to reduce the crackability of stainless steel [14–16]. The above theories have been put forward for welds, however, similar arguments hold for castings.

The complexity of commercial alloys presents difficulty in the study of their solidification mechanics. As a result, most information on the solidification mechanics of metals has been based upon room temperature metallographic examination of the solidification structure of castings and welds. In castings, the cooling rates are low for diffusion controlled processes to modify both the microstructure and the pattern of microsegregation during cooling. The cooling rates for most weldments on the other hand, are considerably faster so as to suppress most diffusion controlled reactions in the solid state such as precipitation of σ, α' and χ phases. Microsegregation and the solidification structure of the weld metal is therefore better preserved as compared to the castings.

EFFECT OF AGING ON MECHANICAL PROPERTIES :

Several investigators [17–45] have investigated the effect of aging on the properties of austenitic, ferritic and duplex stainless steels. Figure 3 shows the

time temperature diagram [43] for the precipitation of phases in a duplex stainless steel, U50. These precipitates may precipitate in the ferrite and/or along the ferrite/austenite boundary.

Aging in the temperature range of 540 - 926 ^{0}C (1000 - 1700 ^{0}F) produces σ phase in the ferrite of duplex stainless steels [16–19,45]. The σ phase is known to be a Fe - Cr rich, brittle, non-magnetic phase with a tetragonal lattice structure. The σ phase precipitates more easily in ferrite than in austenite, because during solidification, ferrite becomes enriched in Cr; moreover the rate of diffusion in ferrite is much faster than in austenite. Some elements such as Mo, Si, V and Nb promote the tendency to form σ phase [21]. These elements are ferrite stabilizers and thus are segregated into ferrite during solidification, which results in an increase in the Cr_{eq}/Ni_{eq} ratio. Such an increase in the Cr_{eq}/Ni_{eq} ratio promotes the precipitation of σ phase.

Apart from the influence of Cr_{eq}/Ni_{eq} ratio on the ferrite content, the solution annealing temperature has also been reported to influence the ferrite content of stainless steel [46]. An increase in the solution annealing temperature causes a change in the chemical composition of ferrite, and an increase in the ferrite content. A higher solution annealing temperature raises the Cr and the Mo contents of ferrite. Both the increase in ferrite content, and the change in chemical composition of ferrite can influence σ phase precipitation [46].

The σ phase often forms as a continuous grain boundary layer; it is also observed as a blocky intergranular precipitate [47] or as platelets in which case

the interface with the matrix often provides a path of relatively easy fracture. Because of the complexity of σ phase crystal structure and low mobility of Cr at temperatures where σ phase is stable, the nucleation and growth rates are slow, at least in the absence of cold work. Experimental data on aging behaviour of ferritic stainless steels show evidence of σ phase formation [48] in severely cold worked stainless steel at temperatures as low as 482^{0}C.

Shortsleeve and Nicholson [49] have reported ' C - curve ' shape characteristic, typical of a nucleation and growth process, for σ phase formation in ferritic alloys aged from 594 - 830 ^{0}C (1100 - 1525 ^{0}F). Although increasing the C content was shown to increase the Cr content required for σ phase formation, presence of certain carbides was shown to accelerate the formation of σ phase. Foley [50] has suggested that σ phase nucleation times are lowered by carbide formation due to straining of the lattice adjacent to carbide particle.

The amount and distribution of the σ phase depends on the distribution of the parent ferrite phase. The extent of the embrittling effect of σ phase similarly depends on the amount and distribution of the ferrite phase. Networks containing more than 6% ferrite have been observed to produce continuous σ networks during complete decomposition [21]. These continuous networks of the σ phase provide an easy path for the propagation of fracture. It has been established [45] that precipitation of the σ phase in stainless steels seriously reduces their impact toughness. Apart from the impact toughness, σ phase also affects tensile properties, hardness and the ferrite content. In general the tensile

strength and hardness are increased, and % elongation to fracture and the ferrite content is decreased [17,18,21,45].

The σ phase in stainless steels has been observed by optical microscopy [17,18,39,45], Mossbauer spectroscopy [51], transmission electron microscopy [37,43] and x-ray crystallography [17,24]. Ferrite measurements [18,45] have also been used as a method to detect the formation of σ phase, which is non-magnetic.

At lower temperatures ranging from 400 to 500 ^{0}C (752 - 932 ^{0}F) α' phase precipitates in ferrite [1,42,43,52]. The α' precipitates are Cr rich with a BCC structure. The phenomenon of 475 ^{0}C (885 ^{0}F) embrittlement has been extensively studied for Fe-Cr alloys and several theories have been put forward to explain the phenomenon. They are as follows :

1) Embrittlement is due to precipitation of a phase which is a precursor to the σ phase forming at higher temperatures,

2) Alloying and impurity elements lead to the embrittlement, and,

3) Precipitation of a Cr rich α' phase is responsible for the embrittlement.

It has been suggested [53] that 475 ^{0}C (885 ^{0}F) embrittlement is a precursor for the precipitation of the σ phase that forms at higher temperatures. This concept is inconsistent with the observation that at higher temperatures where σ phase is formed there is no evidence of this precursor. The precursor model is therefore no longer widely held.

The effects of impurities and alloy additions other than Cr on 475 ^{0}C (885 ^{0}F) embrittlement have been summarized by Lena and Hawkes [53]. Elements such as Mo, Si, Nb, Ti and P increase the degree of embrittlement. However, even in high purity Fe-Cr alloys containing very low levels of impurities and alloy additions, severe embrittlement occurs [34]. Hence, the theory that impurity and alloy additions promote the 475 ^{0}C (885 ^{0}F) embrittlement has received little attention.

The widely held view for the 475 ^{0}C (885 ^{0}F) embrittlement recognizes the precipitation of a Cr rich α' phase. This phase was observed in the electron microscope in 1953 by Fisher et al [54]. Their observations have been corroborated by others [34,35]. Lagneborg [35] has suggested that the formation of α' is due to a spinodal decomposition of ferrite of overall composition into $\alpha + \alpha'$ during cooling in the vicinity of 475 ^{0}C (885 ^{0}F). This type of transformation can be described with the aid of Figures 4 a and 4 b. Figure 4 a represents a schematic free energy *vs* composition diagram for a temperature T'. Figure 4b represents a phase diagram. For % X less than A the α phase is stable, for % X greater than B, α' phase is stable and between A and B the two phases coexist. Points C and D are the inflection points on the free energy curve, i.e., points where $d^2F(X)/dX^2 = 0$. In alloys with compositions between C and D, any local compositional fluctuations tending to cause a phase separation will result in lowering the free energy. Between A and C and B and D such fluctuations do not lower the free energy. The locus of these spinodal points is drawn as the dotted line on the phase diagram. Inside the spinodal region, phase

separation is extremely rapid with no incubation time required. Thus in some alloys the transformation can be avoided during air cooling, but in others water quenching is required to prevent this phenomenon.

The 475^{0}C embrittlement in Fe-Cr alloys could also result from an eutectoid transformation of $\sigma > \alpha + \alpha'$. The eutectoid transformation [43] is limited kinetically, and therefore in practice never observed. A nucleation and growth type of mechanism [34] is also reported for the formation of the α' phase in ferritic stainless steels, containing 14 - 18% Cr. The nuclei of the α' phase have been observed to form on the dislocations. The precipitation of the α' phase on the dislocations hinder their movement and this results in the reduced impact toughness. It is suggested by Grobner [34] that nucleation rate of α' phase is more important than its growth rate.

The ferrite content of cast structure has a pronounced effect on embrittlement behaviour at low aging temperatures, alike the behaviour at higher aging temperatures where σ phase precipitates in ferrite. Increasing ferrite content, increases the susceptibility to embrittlement [1,45] at lower aging temperatures, because higher amounts of ferrite in stainless steel can lead to a higher amount of embrittling phases.

The extensive information available on the embrittlement behaviour of single phase binary Fe-Cr ferritic alloys can be used to predict possible mechanisms of low temperature embrittlement in duplex stainless steels. Data on thermal aging of single phase ferritic alloys indicate that increasing the Cr, Mo or

Ti content in ferrite decreases the time required for low temperature embrittlement [1]. Variations in Mn or Si content have no effect on the aging behaviour. For single phase Fe-Cr-Ni alloys, an increase in Ni content promotes α' precipitation [29] in ferrite. Interstitial elements such as carbon and nitrogen also accelerate the embrittlement [33,35,55] of single phase ferritic steels.

The kinetics of embrittlement [1,34,37,42] due to the σ and α' phases are evaluated by considering the aging phenomenon to be a thermally activated process expressed by Arrhenius relationship. The Arrhenius relationship is given by the following expression :

$$J = A \exp -(U/RT) \tag{2}$$

where, J is the precipitation rate, A is a constant, U is the activation energy, R is gas constant and T is the temperature in ^{0}K. Since the reaction time is inversely proportional to the reaction rate the Arrhenius relation may be written as follows :

$$t = t_0 \exp(U/RT) \tag{3}$$

where, t is the reaction time in hours, t_0 is the reaction constant in hours, U and R have the same meaning as in Equation 2.

The activation energy of σ phase formation can be obtained by plotting the rate of precipitation as a function of $1/T$, where, T is the temperature in ^{0}K. The activation energy for AISI 316 steel was determined by Barcik [37] to be

178 KJ/mole. In case of duplex stainless steels the activation energy would be expected to be lower than that for 316 stainless steel because the diffusion rates are much faster in ferrite which already exists in the duplex steel.

The activation energy [42] of α' phase formation has been determined by examining the CVN impact energy of the castings produced by different aging times and temperatures. The impact energy has been shown as a function of an aging parameter P, which represents the degree of aging reached after 10^P hours at 400 ^{0}C (752 ^{0}F). Arrhenius extrapolation [42] has been used to determine the equivalent aging time at other temperatures. The aging parameter P is defined by the following relationship by Trautwein and Gysel [42] for cast type CF 8 and CF 8M stainless steel :

$$P(t,T) = \log_{10}(t) + 0.4343\ U/R\ [\ 1/673 - 1/T\ ] \qquad (4)$$

where, t, T, U and R have the same meaning as in equation (1) above. P is defined to be equal to 1 for aging 10 hours at 400 ^{0}C (752 ^{0}F). Trautwein and Gysel [42] have reported an activation energy of 24,000 $\pm$ 1000 cal/mole for formation of embrittling phases in the lower temperature range. Recent investigations have described the activation energy [1] as a function of chemical composition of the cast material, given by :

$$Q(KJ/mole) = -\ 182.6 + 19.9\ (\%Si) + 11.08\ (\%Cr) + 14.4\ (\%Mo) \qquad (5)$$

Apart from σ and α' phases, the other phases [43] which are likely to precipitate in a duplex stainless steel are :

1) $M_{23}C_6$ - This precipitation is rapid, requiring less than 1 minute to form at 800 ^{0}C (1498 ^{0}F). The precipitates are predominantly found at the ferrite/austenite phase boundaries, but are also found at the ferrite/ferrite boundary and to a lesser degree inside the ferrite grains.

2) Chi (χ), R phases - Aging between 600 - 700 ^{0}C (1112 - 1292 ^{0}F) for more than 6 to 10 hours results in the formation of the χ phase. The χ phase, like σ phase, is brittle and undesirable. It has an ordered cubic structure consisting mainly of Fe, Cr and Mo. The R phase, consisting mainly of Fe and Mo is also undesirable.

3) γ_2 precipitation in α - Aging in the temperature range of 600 - 800 ^{0}C (1112 - 1472 ^{0}F) results in the reduction in the ferrite content via ferrite $>$ austenite transformation. This austenite (γ_2) is morphologically different than the bulk austenite (γ), but possesses approximately the same composition as that of the bulk austenite (γ).

The amount of precipitates of $M_{23}C_6$, χ and the γ_2 phase is small in comparison to the σ or the α' phase and they precipitate in the ferrite simultaneously along with σ and the α' and therefore the effect of individual phases on the mechanical properties of the steel can't be determined.

At temperatures lower than 400 ^{0}C (752 ^{0}F) the embrittlement of cast duplex stainless steels is probably due to precipitation of phases other than α'. Recently, Chopra and Chung [52] have reported precipitation of several phases

other than α' in the ferrite of the ferritic and alloys of the type CF 8 and CF 8M aged between 300 - 475 ^{0}C (572 - 885 ^{0}F). The various phases are :

1) Type P - These are platelet shaped precipitates producing strong strain field contrast in the bright field images and giving rise to streaking of the ferrite diffraction spots.

2) Type M - $M_{23}C_6$ type precipitates rich in Ni and Si with a lattice constant slightly larger than the $M_{23}C_6$ phase. They are primarily found near dislocations, indicating some degree of immobilization of the dislocations by precipitates. They are relatively small in size , about 10 nm.

3) Type X - These precipitates have a fine size, small volume fraction and are observed near dislocations, indicating they also may lead to the immobilization of the dislocations leading to reduction in toughness.

4) Type ML - These precipitates are observed in association with type M precipitates, coating the type M precipitates and dislocations.

Table 1 gives the time - temperature history of the alloys and the various phases [52] which precipitate in the ferrite. Based on the work reported by Chopra and Chung [52], it may be concluded that phases other than α' may be responsible for the degradation of mechanical properties of cast duplex stainless steels aged at temperatures less than 400 ^{0}C (752 ^{0}F).

Thermal aging of cast duplex stainless steels at temperatures between 288

and 500 ^{0}C (551 - 932 ^{0}F) affects the mechanical properties [1,22,42,45] in several ways. In general, thermal aging causes an increase in hardness and tensile strength and a decrease in the ductility, CVN impact strength and J_{IC} fracture toughness of the material. However, the low cycle properties and fatigue crack propagation are not significantly modified by aging. Chopra and Ayrault [1] have reported a 80% decrease in the impact strength of CF 8M stainless steel after aging for 3000 hours at 427 ^{0}C (800 ^{0}F). Substantial reductions in the impact strength [42] have also been reported for several cast CF 8 and CF 8M stainless steels after aging for 10,000 to 70,000 hours at temperatures as low as 300 ^{0}C (572 ^{0}F).

WELDABILITY OF STAINLESS STEELS :

Stainless steels are used in the fabrication of several types of equipment used in the nuclear, aerospace, petroleum and marine industry. It is thus important to study the weldability of stainless steels. Stainless steel weldments are prone to hot cracking. It is believed that most cracks in the weldments originate when the weld is in a semi-solid condition, and some may occur during cooling. Cracking may also occur during thermal stress relieving treatment or during service. Base metal cracks are thought to form during or immediately after the welding operation. In general, weld and base metal thickness, restraint, composition and joint geometry are all important factors affecting the cracking tendency of stainless steels.

The development of hot cracks in welds may be explained on the basis of

hot tearing theory for castings [14]. Low melting point constituents which segregate at the grain boundaries of the grains are believed responsible for the cracking. The base metal cracking may thus be due to liquation of the fusible grain boundary segregates. The base metal surrounding the weld metal is stressed initially in compression during the welding operation, due to thermal expansion of the hot metal in the fusion zone. The peak temperatures experienced by regions surrounding the weld are sufficient to cause melting of the fusible segregate constituents. Tensile forces are produced in the heat affected zone (HAZ) as a result of cooling, and these result in separation of the liquid film region, thus producing a HAZ crack. The orientation of the HAZ crack with respect to the weld will depend on geometry of the weld.

The weld metal cracks do not appear at the time when HAZ cracks are formed since the high proportion of liquid and semi-solid mass of weld metal still has the capacity to absorb the strains in HAZ or base metal. When the weld metal is almost solidified (liquid film stage), a high strain concentration is developed at the tip of HAZ and the weld metal, resulting in separation of the weld metal as an extension of the HAZ crack. Weld metal becomes prone to cracking if it contains a high proportion of low melting constituents such as sulphides.

To study the problem of weldability several weldability tests such as Fissure Bend Test [56], Cast Pin Tear Test [13] and Varestraint Test [56,57] have been devised to rate the relative hot cracking tendencies of commercial stainless

steels. The varestraint test was used to evaluate the weldability of stainless steels investigated in this work.

The varestraint test (variable restraint test) was originally [57] developed to evaluate susceptibility of materials to hot cracking. It has proved to be unique in its adaptability to both evaluation of relative weldability and studies of the mechanisms of hot cracking. The test utilizes a small laboratory scale specimen supported as a cantilever beam as shown schematically in Figure 5.

From the geometry of the system, nominal value of suddenly applied augmented longitudinal strain in the outer fibers of the test specimen can be calculated as follows :

$$\epsilon = t / 2R \tag{6}$$

where, ϵ is the augmented strain, t is the specimen thickness and R is the radius of the die block. The desired augmented strain can be applied to the weld at any instant during the welding process, by substituting a die block with the appropriate radius of curvature. The magnitude of the longitudinal strain is essentially independent of the welding variables and hence the effect of weld composition, welding process and other parameters influencing the microstructural features of the weld can be isolated from the mechanical effect of externally imposed restraint.

Three criteria [57] are used to evaluate the results of varestraint test. They are :

a) Cracking threshold - the minimum strain required to cause cracking.

b) Total crack length - the sum of the lengths of all the cracks observed.

c) Maximum crack length - the length of the longest crack.

The cracking threshold and total crack length criteria provide quantitative indices for comparing hot cracking tendency. The maximum crack length provides both an indication of the relative hot cracking temperature range and a rapid quantitative means of assessing hot cracking sensitivity. It is possible to determine the mechanisms of hot cracking in welds, if the cracking temperature range, the specific location at which cracking initiates, the direction of propagation of cracks and the influence of microsegregation and solidification structure on the hot cracking sensitivity can be accurately defined.

With the varestraint test it is possible to apply a controlled augmented strain at a predetermined location and time with respect to the welding arc. The instant of formation and location of the cracks can thus be predetermined by controlling the point of application of augmented strain during welding. In addition, the temperature distribution along the weld can be controlled by proper choice of welding variables.

The test parameters used in the varestraint test such as the travel speed, amperage and specimen thickness are the principal parameters which control the cracking response [58] of the weld. Lundin [58] has proposed that once a crack is initiated it would propagate readily over a cracking temperature range. This

cracking temperature range would be characteristic of the material being tested. In this temperature range the weld metal grain boundary would possesses essentially no ductility and be unable to accommodate strain by plastic deformation. At temperatures below this cracking range, the grain boundary recovers some measure of ductility; additional crack extension requires much greater augmented strains since much of the strain is being absorbed by plastic deformation.

The thermal gradient in weld metal determines the distance over which the cracking temperature extends. It follows that any variable which significantly affects the thermal gradient in the weld should affect the maximum and the total crack length values in a predictable fashion. In general, any variable which increases the thermal gradient [58] in the weld metal decreases the cracking response of the weld.

EXPERIMENTAL PROCEDURE

The experimental procedure will be described in this section.

MATERIALS AND SPECIMEN PREPARATION :

The chemical analysis and solution annealing treatments of the castings investigated is given in Table 2. The material was received in the form of keel blocks in the solution annealed and water quenched (SAWQ) condition. The locations of the CVN impact and the varestraint specimens in the keel block is illustrated in Figure 6. The dimensions of the CVN impact and the varestraint specimens were in accordance with the standards ASTM E23 and AWS B4.0, respectively. A broaching machine was used to V-notch the CVN impact specimens.

AGING TREATMENT :

The various temperatures and times used for aging the alloys is given in Table 3. The oversize CVN impact and varestraint blanks removed from the keel blocks were aged at 316, 427 and 594 ^{0}C (600, 800 and 1100 ^{0}F) and 427 and 594 ^{0}C (800 and 1100 ^{0}F) respectively, in electrically heated air furnaces. The furnaces maintained the prescribed temperatures within $\pm 10^0$ C. The specimens were removed from the furnaces after appropriate aging time, and air cooled.

MECHANICAL PROPERTIES :

Standard CVN impact specimens were obtained from the aged blanks

after grinding and milling. Two CVN specimens were tested for each aging time and aging temperature at room temperature. A Tinius Olsen impact testing machine capable of measuring a maximum of 264 ft-lbs was used. The broken CVN impact specimens were saved for microstructure, hardness, ferrite content evaluation and fractography. The impact testing was performed in accordance with ASTM E23.

Hardness was measured by a Rockwell hardness tester. The hardness was measured at 5 locations on the broken CVN impact specimens. Knoop microhardness (50 gm load) of the ferrite phase of SAWQ castings and those aged at 427 ^{0}C (800 ^{0}F) and 316 ^{0}C (600 ^{0}F) was measured. The microhardness was measured at 10 different ferrite locations per specimen.

WELDABILITY :

The varestraint test was performed in accordance with AWS B4.0 to evaluate the weldability of the SAWQ and the aged castings. The time and temperatures used for aging the varestraint blanks are given in Table 3. Varestraint specimens (12" x 2" x 1/2") were obtained from the aged blanks after milling and grinding in accordance with AWS B4.0. The crack lengths in the weld metal were measured with an optical microscope at a magnification of 80x. Welding parameters (Table 4) used in the varestraint test were designed to provide an autogenous weld bead at least 13 mm (1/2") wide for an accurate assessment of the cracking susceptibility. Figure 7 shows the actual set up of the varestraint test jig and specimen. A small portion of the welded specimen

removed for the examination of cracks in the weld metal and HAZ is shown in Figure 8.

FERRITE MEASUREMENT :

A Fischer ferrite-scope was used to evaluate the ferrite content of both impact specimens and the welds. Ferrite number was measured at 6 locations on the broken CVN impact specimens. The ferrite scope was calibrated in accordance with ASTM A799. Figure 9 shows the calibration curve [59] used to convert the ferrite number (FN) obtained from the ferrite scope to ferrite content for castings.

OPTICAL MICROSCOPY AND FRACTOGRAPHY :

Small specimens were removed from the welded and the broken CVN impact bars for microstructural evaluation. The specimens were ground in 120, 240, 400 and 600 grits and then successively polished on selvyt cloth impregnated with 5μm, 0.3 μm and 0.05 μm size alumina particles suspended in water. The σ phase and the carbides were identified by electrolytic etching [17] with 5N KOH at 3 - 4 V for 4 - 5 seconds. Murakami's reagent (3 - 10 gm $K_3\,FeCN_6$ + 10 gm oxalic acid + 100 ml water) was used to reveal the carbides alone. Electrolytic etching (3 - 4 V, 4 - 5 sec.) with saturated NaOH solution [39] was used to reveal the χ phase in the specimens aged at 594 ^{0}C (1100 ^{0}F). Electrolytic etching with 10% oxalic acid was used [45] to reveal the ferrite and austenite in the microstructure of specimens aged at 427 and 316 ^{0}C (800 and 600 ^{0}F). Elec-

trolytic etching with both 5N KOH and 10% oxalic acid was used to etch the base metal, HAZ and the weld metal microstructure of the specimen aged at 594 ^{0}C (1100 ^{0}F).

The fracture surface of the broken CVN impact specimens was observed in a scanning electron microscope at an accelerating potential of 25 KV. The fracture surface examination verified the decrease in the CVN impact toughness that was observed after aging.

RESULTS

SOLIDIFICATION OF CASTINGS :

The solidification structure of all the castings is shown in Figure 10. The first phase to solidify was primary ferrite in all the castings. Alloys CF 3M and CF 3C with Cr_{eq}/Ni_{eq} ratio of 1.12 and 1.28 solidified with a vermicular ferrite morphology, and the rest of the alloys with acicular ferrite morphology. Continuous network of ferrite was seen in all the alloys with acicular ferrite morphology. Ferrite and austenite phases were present in all the alloys.

MECHANICAL PROPERTIES OF CASTINGS :

The effect of Cr_{eq}/Ni_{eq} ratio on the CVN impact energy of castings in the SAWQ is shown in Figure 11. Table 5 gives the CVN impact energy, ferrite content and Cr_{eq}/Ni_{eq} ratio of all castings. Higher Cr_{eq}/Ni_{eq} ratio of the casting resulted in lower CVN impact energy. The Cr_{eq}/Ni_{eq} ratio of the castings have been calculated based on Equations 1 a and 1 b.

The CVN impact energy of the castings aged at 594 ^{0}C (1100 ^{0}F) reduced substantially (Figure 12) with increasing aging time. Figure 13 shows the effect of aging at 427 ^{0}C (800 ^{0}F) on the CVN impact energy of the castings. A significant decrease in the CVN impact energy resulted at the said aging temperature. A small decrease in CVN impact energy resulted after aging at 316 ^{0}C (600 ^{0}F) as shown in Figure 14. Figures 15 - 19 depict the CVN impact energy of individual castings at the 3 aging temperatures. Table A in the appendix lists the CVN impact energy of the castings.

The effect of aging on hardness of the castings is shown in Figures 20 - 24. Figures 25 - 29 show the effect of aging at 427 and 316 ^{0}C (800 and 600 ^{0}F) on the knoop hardness of the ferrite phase of castings. The hardness and knoop hardness (ferrite) values increased with aging time at the said aging temperatures. Tables B and C in the appendix list the hardness and the microhardness of the castings.

FERRITE CONTENT OF CASTINGS :

The ferrite content of castings decreased with aging time after aging at 594 and 427 ^{0}C (1100 and 800 ^{0}F). However, after long aging time at 316 ^{0}C (600 ^{0}F) the ferrite content increased slightly. The ferrite content of castings after aging is illustrated in Figures 30 - 34. Table D in the appendix lists the ferrite content of aged castings.

WELDABILITY :

The weldability of castings was excellent (Figure 35) in both the unaged and aged castings. The total crack length (TCL) increased when the FN of the weld exceeded about 22 FN. The ferrite content of weld metal was higher than that of the casting, on which the weld was deposited (Figure 36). Although the TCL in all the castings was small, higher amounts of sulphur produced more cracking (Figure 37). No major difference was found in the cracking susceptibility of the castings which contained Mo (CF 3M and CG 8M) and those which contained Cb (CF 3C). Tables E and F in the appendix list the total crack

length and the FN of weld metal of each of the castings, respectively. No cracking was observed in heat affected zone (HAZ) and the base metal in of any of the castings.

The first phase to solidify was primary ferrite in all the welds. Vermicular ferrite morphology was observed in the weld metal of alloy CF 3M containing 7% ferrite in SAWQ condition, and acicular ferrite morphology was observed in the weld metal microstructures of the remaining alloys as shown in Figure 38.

The hardness of weld metal, HAZ and the base metal is listed in Table G in the appendix. The weld metal hardness was found to be higher than that of HAZ and base metal. The HAZ exhibited the least hardness of all three, the weld metal, HAZ and the base metal in case of aged castings. In case of SAWQ castings, the weld metal had a greater hardness than HAZ and the base metal.

OPTICAL MICROSCOPY :

Typical micrographs of castings (containing Mo) aged at 594 ^{0}C (1100 ^{0}F) reveal the precipitation of σ phase and carbides in ferrite as shown in Figure 39. Figure 40 shows the micrographs of castings containing Cb additions (CF 3C) aged at 594 ^{0}C (1100 ^{0}F). A micrograph of alloy CF 3M (20% ferrite in the SAWQ condition) in Figure 41 shows the precipitation of χ phase in the ferrite. χ phase was not observed in any of the other alloys. Carbide precipitation (revealed by Murakami's reagent) was observed in castings of the type

CF 3M and CF 3C (Figure 42) and it was negligibly small in castings containing Cb. Aging the castings at 316 and 427 ^{0}C (600 and 800 ^{0}F) did not produce any observable (optical) changes in the microstructure as shown in Figure 43. The micrographs of the weld metal, HAZ and base metal (weld deposited on aged castings) are shown in Figures 44 and 45. The micrograph of the HAZ (Figure 45) reveals the dissolution of the σ phase. No difference was found in the microstructure of the SAWQ varestraint specimens and those that were aged at 427 ^{0}C (800 ^{0}F). σ phase did not reform in the HAZ.

FRACTOGRAPHY :

Figures 46 - 48 are the scanning electron micrographs of the fracture surface of broken CVN impact specimens. A ductile mode of fracture was evident in both the SAWQ and those aged at 316 ^{0}C (600 ^{0}F), however, a brittle fracture was observed in specimens aged at 594 and 427 ^{0}C (1100 and 800 ^{0}F). Large number of inclusions (mainly sulphides and silicates, as determined by energy dispersive x-ray analysis) were found in castings aged at 316 ^{0}C (600 ^{0}F).

DISCUSSION

SOLIDIFICATION OF CASTINGS :

The first phase to solidify was primary ferrite in all the castings investigated. This can be explained on the basis of Figure 2. All the alloys have a sufficiently high Cr_{eq}/Ni_{eq} ratio which to put them into the region where primary ferrite is the first phase to solidify. The chemical composition of the alloys CF 3M and CF 3C with Cr_{eq}/Ni_{eq} ratio of 1.12 and 1.28 lies close to the 3 phase $L+\delta+\gamma$ region but still on the primary ferrite side and therefore, the primary ferrite solidifies with a vermicular morphology. The primary ferrite forming in the initial stages of solidification, subsequently transforms to austenite, γ, during cooling to room temperature, leaving behind a vermicular ferrite morphology. The Cr_{eq}/Ni_{eq} ratio of other steels is higher than that of alloy CF 3M (1.12) or CF 3C (1.28) and therefore the ferrite morphology is acicular. Figure 10 clearly indicates the vermicular and acicular ferrite morphology of various castings. Widmanstatten austenite was not found in any of the castings since higher amounts of ferrite would be required for Widmanstatten austenite formation.

The chemical composition of the castings given in Table 2 indicates that C + N contents of castings greatly influence the Cr_{eq}/Ni_{eq} ratio i.e. greater C + N with similar contents of other alloying elements promote larger Cr_{eq}/Ni_{eq} ratio and thus lower the amount of ferrite in the casting. This is due to strong austenitizing tendency of C and N. Alloys of the type CF 3C have Cb addi-

tions instead of Mo, however, Cb did not affect ferrite morphology. This is because the amount of Cb in the castings is low and it has a lower ferrite stabilizing potential as compared to Molybdenum.

MECHANICAL PROPERTIES OF BASE METAL :

Castings having larger Cr_{eq}/Ni_{eq} ratios had lower CVN impact energies in the SAWQ condition, as shown in Figure 11. A larger Cr_{eq}/Ni_{eq} ratio implies a higher amount of ferrite in the casting. This leads to a continuous network of ferrite, which provides a preferred path for propagation of crack. Crack propagation is easier in ferrite than austenite, since ferrite has a lower toughness and ductility as compared to austenite.

The decrease in CVN impact energy (Figure 12) after aging at 594 ^{0}C (1100 ^{0}F) was due to precipitation of σ phase in ferrite as has been observed by many workers [17,18,45]. The micrographs in Figures 39, 40 and 41 indicate the formation of σ phase in the ferrite of castings after aging at 594 ^{0}C (1100 ^{0}F). At lower aging times such as 10 hours, probably carbide precipitation occurs (Figure 42), along with the σ phase and the decrease in the CVN impact energy may probably be due to both the phases. In alloys of the type CF 3C (Cb addition) there was no evidence of precipitation of either the carbides or the σ phase after aging for 200 hours. This may be due to the strong carbide forming tendency of Cb, and therefore there may not be sufficient precipitation of $M_{23}C_6$ type carbides, which were revealed by etching with 5 N KOH or the Murakami's reagent.

The significant decrease in CVN impact energy after aging at 427 ^{0}C (800 ^{0}F) may be due to the α' phase and a small decrease in CVN energy after aging at 316 ^{0}C (600 ^{0}F) may probably be due to precipitation of phases other than α' such as X, M, ML etc. (Table 1) in the ferrite phase of castings, as shown in Figures 13 and 14 respectively. The phases listed in Table 1 can only be revealed by special techniques such as transmission electron microscopy, and thus no observable changes were detected in the microstructures (Figure 43). Based on the work done by Chopra and Ayrault [1] and Chopra and Chung [52], on CF 8 and CF 8M type alloys, the decrease in CVN impact energy at 316 ^{0}C (600 ^{0}F) may only be attributed to the precipitation of phases other than α' (Table 1) ,but the decrease in the CVN impact energy at the aging temperature of 427 ^{0}C (800 ^{0}F) is more likely to be due to α' phase.

Since 427 ^{0}C (800 ^{0}F) is close to 475 ^{0}C (885 ^{0}F) embrittlement temperature, where α' is observed in cast alloys of the type CF 8 and CF 8M the driving force at 427 ^{0}C (800 ^{0}F) may be sufficient enough to promote α' phase. Moreover, the ferrite content of the specimens aged at 427 ^{0}C decreased with aging time, which corroborates the possibility of α' phase (non-magnetic) precipitation in ferrite. The ferrite content increased slightly in alloys aged at 316 ^{0}C (600 ^{0}F) after long aging times, which indicates that α' did not precipitate at that aging temperature. The reason for the increase in ferrite content after aging at 316 ^{0}C (600 ^{0}F) is not known.

The decrease in CVN impact energy was the greatest after aging at

594 °C (1100 °F) as compared to the impact energy after aging at 427 and 316 °C (800 and 600 °F) as shown in Figures 15 - 19. This is probably due to the difference in the nature and distribution of the precipitates forming at the said temperatures. The σ phase was blocky in shape and was distributed along the boundaries between the ferrite and the austenite, providing an easy path for the propagation of fracture, leading to a lower value of impact energy. Conversely, the α' phase has been reported to precipitate in the form of fine particles [43] throughout the ferrite which may hinder the propagation of fracture and may lead to higher impact energy.

Considering the CVN impact energy at the aging temperature of 427 °C (800 °F) as the basis, the CVN impact energy at temperatures lower than 475 °C (885 °F) may be extrapolated on the basis of the aging parameter P in Equation 4. Defining $P = 1$ at 427 °C (800 °F) Equation 4 may be rewritten as follows :

$$P(t,T) = \log_{10}(t) + 0.4343\ U/R\ [\ 1/700 - 1/T\ ] \qquad (4a)$$

Assuming the activation energy [40] $U = 24000$ cal/mole and the gas constant $R =$ 1.98 cal/mole - °K Table 6 may be generated for equivalent aging time at 316 °C (600 °F).

Table 6 illustrates the extremely long times required to produce the same embrittlement at 316 °C (600 °F) as compared to the embrittlement at 427 °C (800 °F) i.e. 7841 hours of aging time would be required after aging at 316 °C (600 °F) to obtain the same CVN impact energy which is obtained after aging

at 427 °C (800 °F) for 3000 hours. Equation 4 cannot be used to extrapolate the CVN impact energy at temperatures higher than 475 °C (885 °F) since the activation energy for the precipitates forming at higher temperatures (σ, χ, carbides etc.) is different.

The hardness of cast alloys (SAWQ) was almost independent of the ferrite content, except in the casting which contained 7% ferrite (CF 3M hardness 76 HRB). The lower hardness of this casting was due to greater amount of softer austenite phase in the matrix. Hardness (HRB) of the castings did not change significantly even after the aging treatment as seen from Figures 20 - 24. The trend observed however, was that the hardness after aging at 427 °C (800 °F) was higher than the hardness after aging at 316 °C (600 °F) which was higher than the hardness obtained after aging at 594 °C (1100 °F). The greatest increase in the hardness at 427 °C (800 °F) was probably due to increased precipitation of the embrittling phases in the ferrite as compared to that at 316 °C (600 °F). The CVN impact energy was also affected to a lesser extent after aging at 316 °C (600 °F) as compared to that at 427 °C (800 °F), due to the same reason. Other reason why the hardness was so insensitive to the embrittling phases may be due to the fact that the embrittling phases precipitate in the ferrite phase which has a small volume fraction in the duplex structure.

The small increase in hardness after aging at 594 °C (1100 °F) may be due to two opposing factors; the precipitation of hard σ phase leading to increase in hardness, and the depletion of alloying elements from the ferrite grains (due to formation of σ and carbides), and reduction in the ferrite content as a result of precipitation of the embrittling phases, which leads to decrease in hardness.

These two opposing factors lead to a smaller increase in hardness as a result of aging at 594 ^{0}C (1100 ^{0}F).

The knoop hardness of ferrite phase, Figures 25 - 29, of the unaged castings and those aged at 427 and 316 ^{0}C (800 and 600 ^{0}F) also indicate that the embrittling phases precipitate in ferrite . The greater increase in knoop hardness of the ferrite of castings aged at 427 ^{0}C (800 ^{0}F) as compared to those aged at 316 ^{0}C (600 ^{0}F) corroborates the hardness results. There was no significant change in the Knoop hardness of austenite due to aging at 427 and 316 ^{0}C (800 and 600 ^{0}F) which indicates that there was probably no precipitation in the austenite.

FERRITE CONTENT OF CASTINGS :

The ferrite content of the castings decreased considerably after aging at 594 and 427 ^{0}C (1100 and 800 ^{0}F) as seen from Figures 30 - 34. The non-magnetic σ and α' phases were probably responsible for the decrease. At 594 ^{0}C (1100 ^{0}F), along with precipitation of σ phase there may be formation of γ_2 which is non-magnetic and could lead to a decrease in ferrite content. A slight increase in the ferrite content was observed in castings aged at 316 ^{0}C (600 ^{0}F), the reason for which is unknown. The decrease in ferrite content of the castings aged at 594 ^{0}C (1100 ^{0}F) may partly be due to precipitation of carbides in ferrite or along the ferrite/austenite boundary.

The scatter in measured ferrite content, Figures 30 - 34, may be due to several reasons. Inhomogenity in the distribution, chemical composition and orientation of the ferrite phase, variation in the chemical composition of the

keel blocks from which the CVN impact specimens were obtained and the amount of inclusions in the castings, could all lead to the scatter observed in the ferrite content. The fact that different heats were made using different steel melting practices also can lead to the scatter in the measured ferrite content.

WELDABILITY STUDIES :

There was no appreciable difference in the cracking response of the SAWQ alloys and the aged alloys (Figure 35). The embrittling phases such as σ and the α' dissolved in the molten weld puddle during weld deposition, leaving behind a weld which did not contain any optically observable embrittling phases (Figures 44 and 45). The σ phase did not reform in the weld, and probably the α' phase also did not reform in the weld metal, due to fast cooling rates experienced by the weld. Thus the weld metal deposited on both aged and SAWQ castings may not contain any embrittling phases and hence the cracking tendency was similar in both cases.

The cracking tendency of the weld metal was low so long as the FN of the weld metal was lower than about 22 FN. However, when the ferrite content was about 24 FN, the total crack length in the weld increased as seen from Figure 35. Higher amounts of ferrite in weld metal promoted cracking of the weld metal, the reasons for which are not clear. Another reason why the weld metal with a higher FN showed a greater hot cracking tendency, was that it also contained higher amount of sulphur than all the other alloys (Figure 37) and higher amounts of sulphur are known to promote hot cracking of the weld metal. The

varying amounts of sulphur content in the steel may be due to the different melting practices used for making different heats.

The weld metal ferrite content was higher than that of the base metal on which the weld was deposited, in all the alloys, as shown in Figure 36. This can be explained on the basis of Figure 2. All the welds solidified as primary ferrite first, as is evident from the micrographs in Figure 38. If the cooling rates are fast as in case of welds, the primary ferrite formed in the initial stages of solidification, has insufficient time to transform to austenite as predicted by the vertical section of the Fe-Cr-Ni system. Hence higher amounts of ferrite are retained in the weld metal as compared to the casting of same chemical composition. The Cr_{eq}/Ni_{eq} ratio of all the welds is sufficiently high and hence, the primary ferrite was the first phase to solidify in all the welds.

The increase in hardness of the weld metal as compared to the base metal on which welds were deposited (Table G in the appendix), indicates that the ferrite (higher hardness) content of weld metal was higher. A slight decrease in hardness of the HAZ of aged castings implies that the embrittling phases in the HAZ may have been reconverted to ferrite due to the heating cycles experienced by the HAZ during welding, however there was no evidence of formation of any of the embrittling phases in the HAZ.

OPTICAL MICROSCOPY :

Optical micrographs of castings aged at 594 ^{0}C (1100 ^{0}F), Figures 39, 40 and 41, clearly indicate the precipitation of σ phase in ferrite. Alloy CF 3M

with 20% ferrite in SAWQ condition contained χ phase (Figure 41) in addition to the σ phase in ferrite after aging for more than 3000 hours at 594 ^{0}C (1100 ^{0}F). However, the χ phase did not precipitate in other casting after aging. This indicates that higher amounts of ferrite promote precipitation of χ phase. Carbides formed preferentially in alloys containing Mo (Figure 42). Cb is a strong carbide forming element and thus it may tie up the carbon in the form of Cb carbides. However, the carbides revealed by the Murakami's reagent are of the type $Cr_{23}C_6$, which may have a lesser volume fraction in alloys containing Cb (CF 3) due to lesser amount of carbon being available for the formation of $Cr_{23}C_6$ type carbides. Thus, very few carbides were found in CF 3C type of castings after aging.

FRACTOGRAPHY :

The fractographs of the broken CVN impact specimens (Figures 46 - 48) illustrate that aging at 594 and 427 ^{0}C (1100 and 800 ^{0}F) resulted in a brittle fracture, and that the mode of fracture was ductile after aging at 316 ^{0}C (600 ^{0}F), as is evident from the dimpled fracture surface of specimens shown in Figure 46. The fractographs in Figures 47 and 48 suggest that σ phase and probably the α' phase may be responsible for the brittle fracture in castings aged at 594 and 427 ^{0}C (1100 and 800 ^{0}F). The fracture surface of the specimens aged at 316 ^{0}C (600 ^{0}F), Figure 46, show a large volume fraction of inclusions (mainly sulphides and silicates), which may be one of the reasons why a scatter was observed in the CVN impact energy and the ferrite measurements on the castings.

CONCLUSIONS

The microstructure, mechanical properties and the ferrite content of the unaged and the aged type CF 3M, CG 8M and CF 3C castings were investigated. The weldability test (varestraint test) was performed on each casting before and after aging. The following were the conclusions :

1. Significant decrease in the CVN impact energy resulted after aging the castings at 594 and 427 ^{0}C (1100 and 800 ^{0}F). A small decrease in the CVN impact energy resulted after aging at 316 ^{0}C (600 ^{0}F). The decrease in CVN impact energy after aging at 594 and 427 ^{0}C (1100, 800 and 600 ^{0}F) was due to precipitation of σ and probably the α' phases, respectively. The decrease in CVN impact energy after aging at 316 ^{0}C (600 ^{0}F) is believed to be due to precipitation of phases such as X, M, ML etc. in the ferrite phase of the castings.

2. Increasing CVN impact energy was found to be a function of decreasing Cr_{eq}/Ni_{eq} ratio.

3. Significant decrease in the ferrite content of the castings occurred after aging at 594 and 427 ^{0}C (1100 and 800 ^{0}F). A small increase in ferrite content resulted after aging at 316 ^{0}C (600 ^{0}F).

4. A small increase in the hardness was observed in all the alloys at all the three aging temperatures. A substantial increase in the microhardness of the ferrite phase resulted due to aging at 427 and 316 ^{0}C (800 and 600 ^{0}F).

5. Primary ferrite was the first phase to solidify in all the castings and

welds.

6. The hot crack susceptibility of the weld metal (by varestraint testing) was found to be very low for all the castings in both the aged and unaged condition. Weld metal ferrite levels exceeding about 22 FN, and higher sulphur contents, promoted hot cracking of the weld. No cracking was observed in the HAZ of any of the alloys.

7. There was no significant change in the hot crack susceptibility of the weld metal of the castings which were aged as compared to those which were in the solution annealed and water quenched condition.

8. The ferrite content of the weld metal was always higher than that of the cast metal.

9. There was no evidence of reformation of the σ phase either in the weld metal or the HAZ after welding.

REFERENCES

(1) Chopra O. K. and Ayrault G., Proc. 11th Water Reactor Safety Research Information Meeting, Oct. 24-28, 1983, National Bureau of Standards, Gaithersburg, MD.

(2) DeLong T. J et al., Weld. Jnl., Vol. 52, pp. 281s - 297s, 1973.

(3) ASTM A 800.

(4) Steel Casting Handbook, SFSA 1980.

(5) Bain E. C. and Griffiths W. E., Trans. AIME, Vol. 75, pp. 166-213, 1927.

(6) Pugh J. W. and Nisbet J. O., Trans. AIME, Vol. 188, pp. 268-276, 1950.

(7) Rivlin V. G and Raynor G.V., International Metals Rev., No. 1, 1980.

(8) Lippold J. C. and Savage W. F., Weld. Jnl., Vol. 58, No. 12, pp. 362s-374s, Dec. 1979.

(9) Lippold and Savage, Weld. Jnl., Vol. 59, No. 2, pp. 48s - 58s, 1980.

(10) David S. A. Weld. Jnl., Vol. 60, No. 4, pp. 63s - 71s, April 1981.

(11) Borland J. C and Younger R. N., Report B5/1/59, Brit. Weld. Res. Assoc., Aug. 1959.

(12) Parks J. M., Weld. Jnl., Vol. 34, pp. 568 - 570, 1955.

(13) Thomas R. D., Metal Prog., Vol. 50, pp. 474 - 479, 1946.

(14) Apblett W. R and Pellini W. S., Weld. Jnl., Vol. 33, pp. 83s-90s, 1954.

(15) Hull F. C., Weld. Jnl., Vol. 46, No. 9, pp. 399s-409s, Sep. 1967.

(16) Borland J. C. and Younger R. N., Brit. Weld. Jnl., pp. 22-59, Jan 1960.

(17) Beck F. H et al, ASTM STP No. 369, 1965.

(18) Fontana M. G and Beck F. H., Alloy Casting Institute Project No. 40, Dec.

1962.

(19) Ohmori Y. and Maehara Y., Trans. ISIJ, Vol. 24, pp. 60-68, 1984.

(20) Blenkinsop P. A and Nutting J., JISI, pp. 953-958, Sep. 1967.

(21) Klemetti K et al, Weld. Jnl., Vol. 63, No. 1, pp. 17s-25s, Jan. 1984.

(22) Landerman E. I and Bamford W. H., Winter Annual Meeting of The ASME, San Francisco, CA, Dec. 10-15, 1978.

(23) Vitek J. M and David S. A., Weld. Jnl., Vol. 63, No. 8, pp. 246s-253s, Aug. 1984.

(24) Lai J. K and Galbraith I. F., Jnl. Mater. Sci., Vol. 15, pp. 1297-1305, 1980.

(25) Flowers J. W. et al., Corrosion, pp. 186t-198t, Vol. 19, May 1983.

(26) Brown J. F. et al., Metallurgia, Vol. 56, pp. 215-223, 1957.

(27) Lai J. K. and Haigh J. R., Weld. Jnl., Vol. 58, No. 1, pp. 1s-6s, Jan 1979.

(28) Arata Y. et al., Trans. JWRI, Vol. 5, No. 2, pp. 135-151, 1976.

(29) Solomon H. D. and Levinson L. M., Acta Met., Vol. 26, pp. 429-442, 1978.

(30) Tavassoli A. A. et al., Metal Sci., Vol. 18, pp. 345-350, July 1984.

(31) Gauzzi F. and Verdini B., Met. Sci. Technol., Vol. 2, No. 2, pp. 48-53, 1984.

(32) Hull F. C., Weld. Jnl., Vol. 52, No. 3, pp. 104s-113s, March 1973.

(33) Hendry A. et al., Metal Sci., pp. 482-486, August 1979.

(34) Grobner P. J., Met. Trans., Vol. 14, pp. 251-260, Jan. 1973.

(35) Lagneborg R., Trans. ASM, Vol. 60, pp. 67-78, 1967.

(36) Cook A. J. and Jones F. W., JISI, Vol. 148, pp. 217p-226p, 1943.

(37) Barcik J., Met. Trans., Vol. 14A, p. 635-641, April 1983.

(38) Nichol T. J. et al., Met. Trans. A, Vol. 11A, pp. 573-585, April 1980.

(39) Shehata M. T et al., Microstructural Sci., Vol. 11, pp. 89-99, 1983.

(40) Spruiell J. E. et al., Met. Trans., Vol. 4, pp. 1533-1544, June 1973.

(41) Weiss B. and Stickler R., Met. Trans., Vol. 3, pp. 851-866, April 1972.

(42) Trautwein A. and Gysel W., GF Spectrum, Vol 5, pp. 38-58, May 1981.

(43) Solomon H. D. and Devine T. M., Duplex Stainless Steels - Tale of two phases, General Electric Company, Technical information series No. 82CRD276, Nov. 1982.

(44) Thomas R. G. and Yapp D., Weld. Jnl, 361s-366s, Dec. 1978.

(45) Beck F. H., ACI, SFSA Project A-56, May 1975, Ohio State University.

(46) Robert R and Nicodemi W., Avesta Stainless Bull., Vol. 2, pp. 14-17,

(47) C. P. Sullivan and M. J. Donachie, Jr., Metals Engg. Qurtly, Vol. 11, pp. 1 - 20, 1971.

(48) Ludwigson D. C. and Link N. S., ASTM, STP No. 369, p. 299, 1965.

(49) Shortsleeve F. J and Nicholson M. E., Trans. ASM, Vol. 43, p.142, 1951.

(50) Foley F. B., Trans. ASM., Vol. 43, p. 156, 1951.

(51) Wegrzyn J. and Klimpel A., Weld. Jnl., Vol. 60, No. 8, Aug. 1981.

(52) Chopra O. K. and Chung H. M., Annual Report Oct 1983 - Sep. 1984, Argonne National Laboratory, Illinois.

(53) Lena A. J and Hawkes M. F., Trans. AIME, Vol. 6, pp. 607 - 615, 1954.

(54) Fisher R. M. et al., Trans. AIME, Vol. 197, pp. 690 - 695, 1953.

(55) Courtnall M. and Pickering F. B., Metal Sci., Vol. 10, p. 273, 1976.

(56) Lundin C. D. and Spond D. F., Weld. Jnl., Nov. 1976.

(57) Savage W. F. and Lundin C. D., Weld. Jnl., Vol. 44, no. 10, 433s-442s, 1965.

(58) C. D. Lundin et al., WRC Bull., No. 280, August 1982.

(59) Finch L., ESCO Corporation, Portland, Oregon. Unpublished Research.

Table 1 : Precipitation of various phases (Ref. 52) in cast stainless steels aged between 300 - 475 °C (572 - 885 °F).

Alloy	Aging conditions		Precipitate phases				
	Temp., °C (°F)	Time, hr	α′	Type P	Type M	Type X	Type ML
26Cr-1Mo	475 (885)	1000	yes				
	400 (752)	1000	no	no			
29Cr-4Mo-2Ni	475 (885)	1000	yes	yes			
	400 (752)	1000	no	yes			
CF 8	475 (885)	1000	yes		yes		
heat B	400 (752)	1000	no	no	no	no	no
CF 8	400 (752)	66,650	no		yes	yes	
heat 280	400 (752)	10,000	no		yes	yes	
	300 (572)	70,000	no		yes	yes	
CF 8	400 (752)	70,000	no		yes		
heat 278	350 (662)	70,000	no		yes	yes	
	300 (572)	70,000	no		yes	yes	
CF 8M	400 (752)	10,000	no		yes		yes
heat 286							

Table 2 : Chemical analysis of the castings.

Alloy	C	Mn	Si	Cr	Ni	Mo	S	P	N	%Ferrite	Cr_{eq}/Ni_{eq}
CF 3M	0.03	0.51	0.61	19.76	10.37	2.18	0.007	0.028	0.114	7	1.12
CF 3M	0.01	0.34	1.34	19.54	9.42	2.2	0.02	0.019	0.031	20	1.5
CG 8M	0.04	0.38	1.25	18.65	10.12	3.09	0.014	0.014	0.04	10	1.34
CF 3C	0.016	0.24	1.24	20.65	9.40	Cb 0.23	0.017	0.015	0.016	14	1.4
CF 3C	0.03	0.49	1.13	20.9	8.86	0.38	0.012	0.032	0.066	15	1.28

%Ferrite - measured by Ferrite Scope
Solution annealing conditions :
CF 3C (14% ferrite) - 1700 ^{0}F, 1 hr, water quenched.
Rest of the castings - 2050 ^{0}F, 1 hr, water quenched.
Cr_{eq}/Ni_{eq} ratio calculated on the basis of ASTM A800.

Table 3 : CVN impact and varestraint test specimen aging schedule.

CVN * impact Specimen Aging Schedule

Aging Temperature	Aging Time (hours)
316 °C and 427 °C	200,300,450,700,1000,1400,2000, 3000,4500,7000,10,000,14,000
594 °C	10,200,300,450,700,1000,1400, 2000,3000,4500,7000,10,000

Varestraint ** test specimen aging schedule

Aging Temperature	Aging Time (hours)
427 °C	10,000
594 °C	8000, 10,000

* - 2 specimens per alloy per aging time and Temperature
Alloys aged at 594 °C for 7000 and 10,000 hours were solution annealed at 1900 °F and water quenched.

** - 3 specimens per alloy aged at 427 °C
1 specimen, alloy CF 3M (20% ferrite) aged at 594 °C for 8000 hours.
1 specimen per alloy aged at 594 °C for 10,000 hours.

Table 4 : Welding parameters used in the varestraint test.

Electrode	W + 2% ThO_2
Electrode - workpeice gap	1.56 mm (1/16 ")
Electrode extension	5 mm (1/5 ")
Electrode dia	3.125 mm (1/8 ")
Travel speed	125 mm/min (4.9 ")
Gas flow rate	1 m^3/hr (35 cfh)
Current	310 - 315 A
Voltage	15 - 16 V

Table 5 : CVN impact, ferrite content and Cr_{eq}/Ni_{eq} ratio of castings.

Alloy	CVN impact energy (ft-lbs)	Ferrite content(%)			Cr_{eq}/Ni_{eq} ratio
		calc.	MG	FS	
CF 3M	145	28.5	20	20	1.5
CF 3C	135	20.7	12.5	14	1.4
CG 8M	159	18	9	10	1.34
CF 3C	>264	15	13	15	1.29
CF 3M	>264	7.7	6	7	1.12

calc. - calculated
MG - Magna Guage
FS - Ferrite Scope
Cr_{eq}/Ni_{eq} - ASTM A800.

Table 6 : Equivalent aging time at 316 °C considering 427 °C as the base. Activation energy 24000 cal/mole.

Aging Parameter P	Aging Time in hours at	
	427 °C (800 °F)	316 °C (600 °F)
1.000	10	26
2.301	200	5251
2.477	300	7841
2.653	450	11,761
2.845	700	18,295
3.000	1000	26,136
3.146	1400	36,591
3.301	2000	52,273
3.477	3000	78,409
3.653	4500	117,614
3.845	7000	182,955
4.000	10,000	261,364
4.146	14,000	365,910

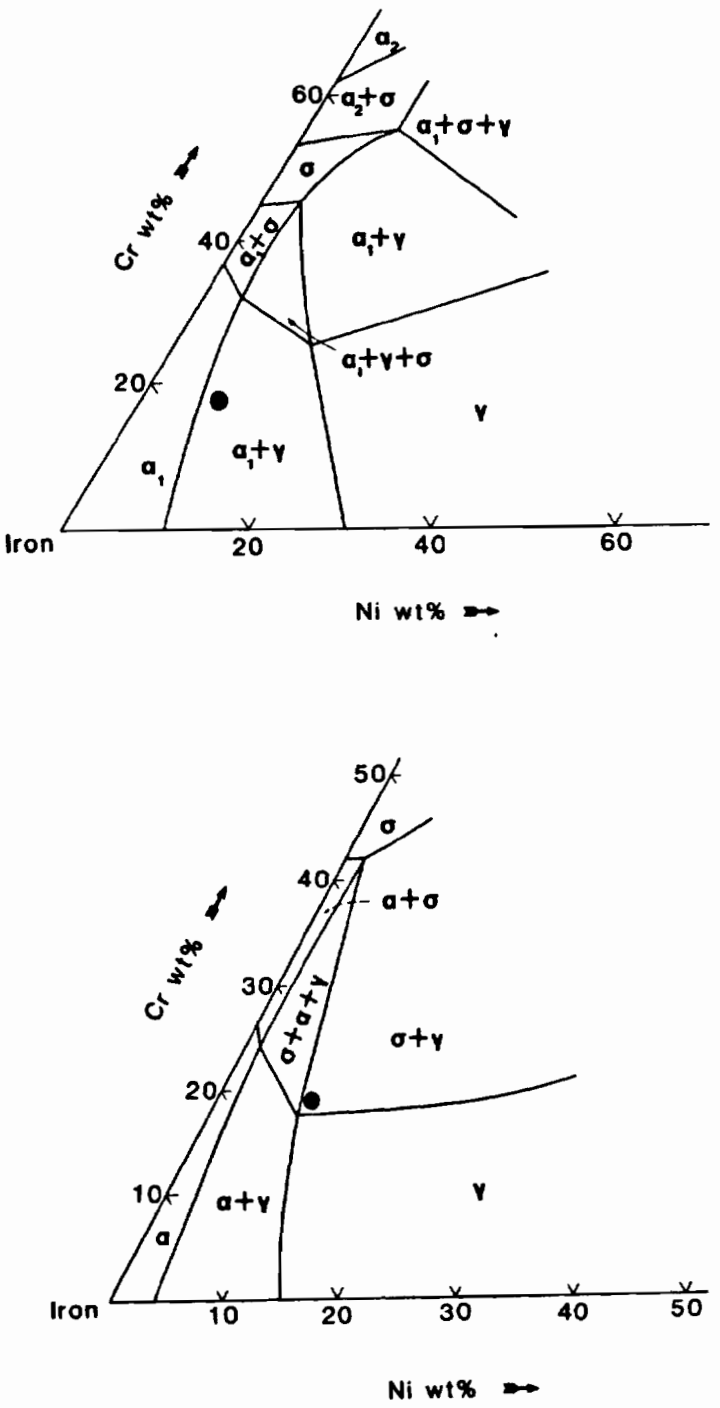

Figure 1 : Isothermal sections of the Fe-Cr-Ni system (a) at 400 °C (752 °F), (b) at 650 °C (1202 °F) (Ref. 7).

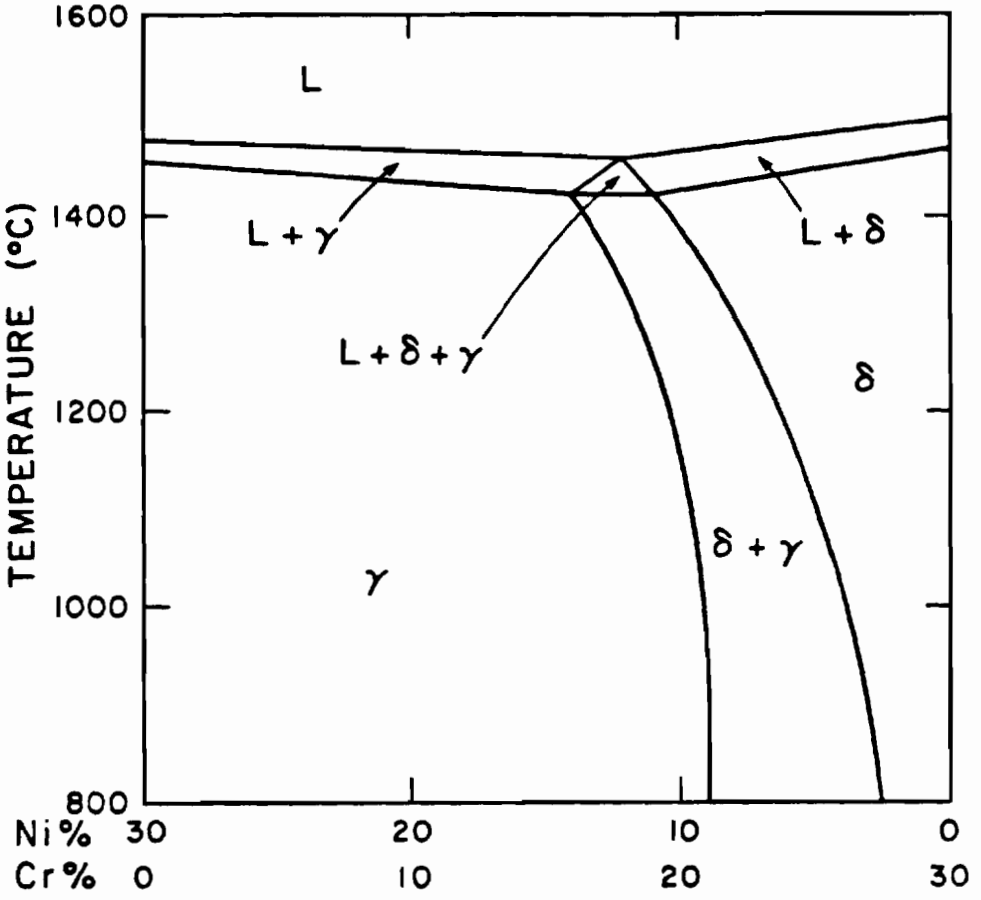

Figure 2 : Vertical section of the Fe-Cr-Ni system for 70% Fe (Ref. 8).

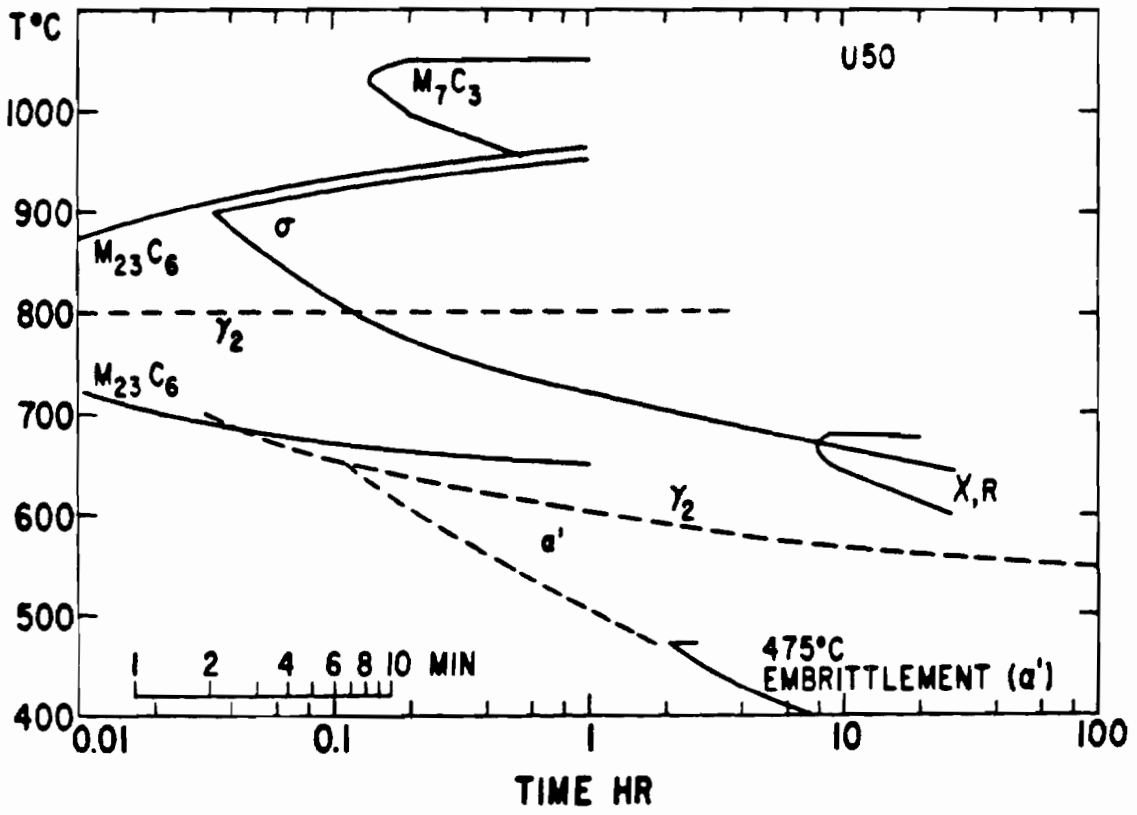

Figure 3 : Time temperature diagram for the precipitation in a duplex stainless steel alloy U50 (Ref. 43).

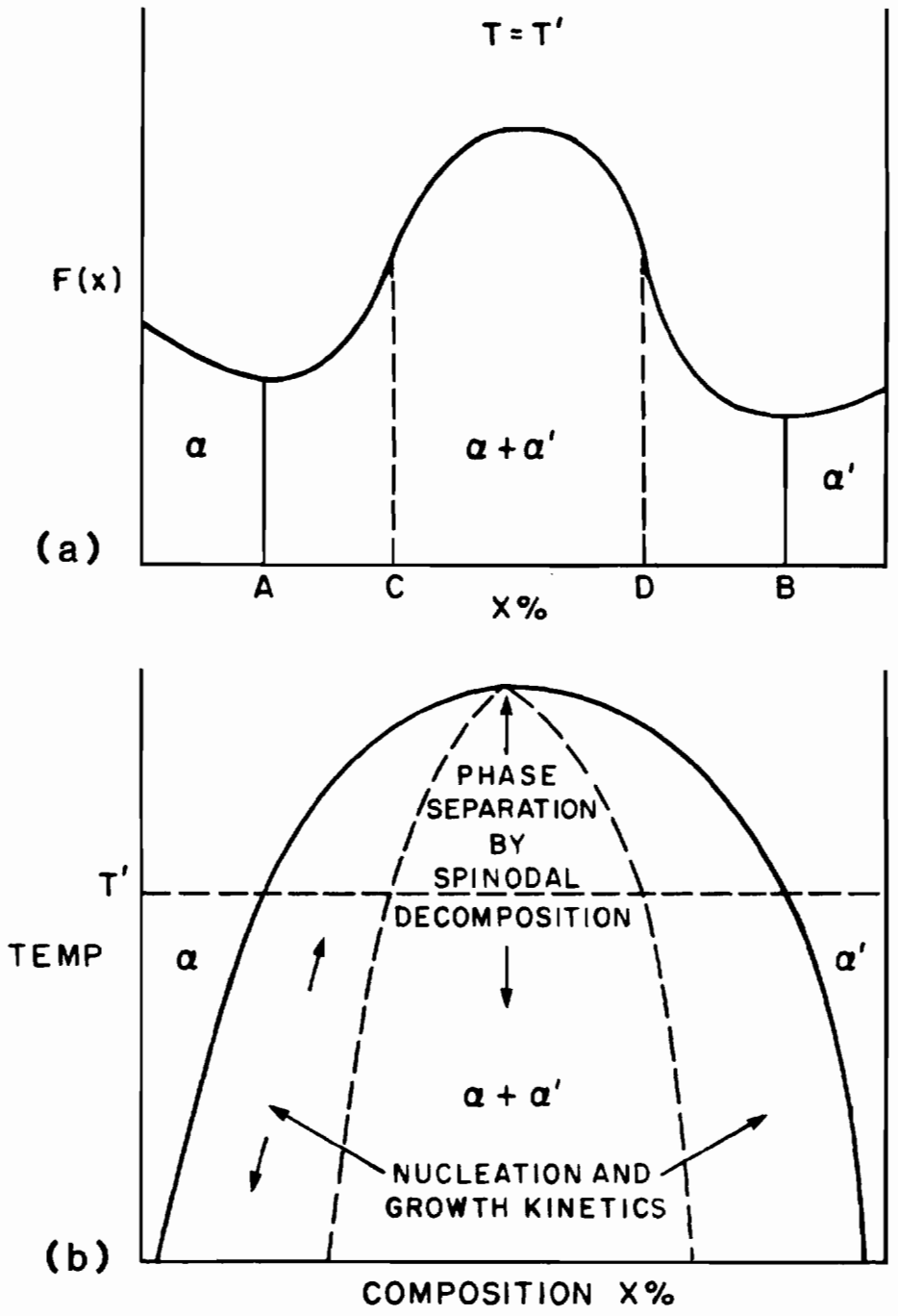

Figure 4 : Schematic spinodal decomposition mechanism for the formation of α' phase for Fe-Cr system. (a) free energy diagram, (b) binary diagram.

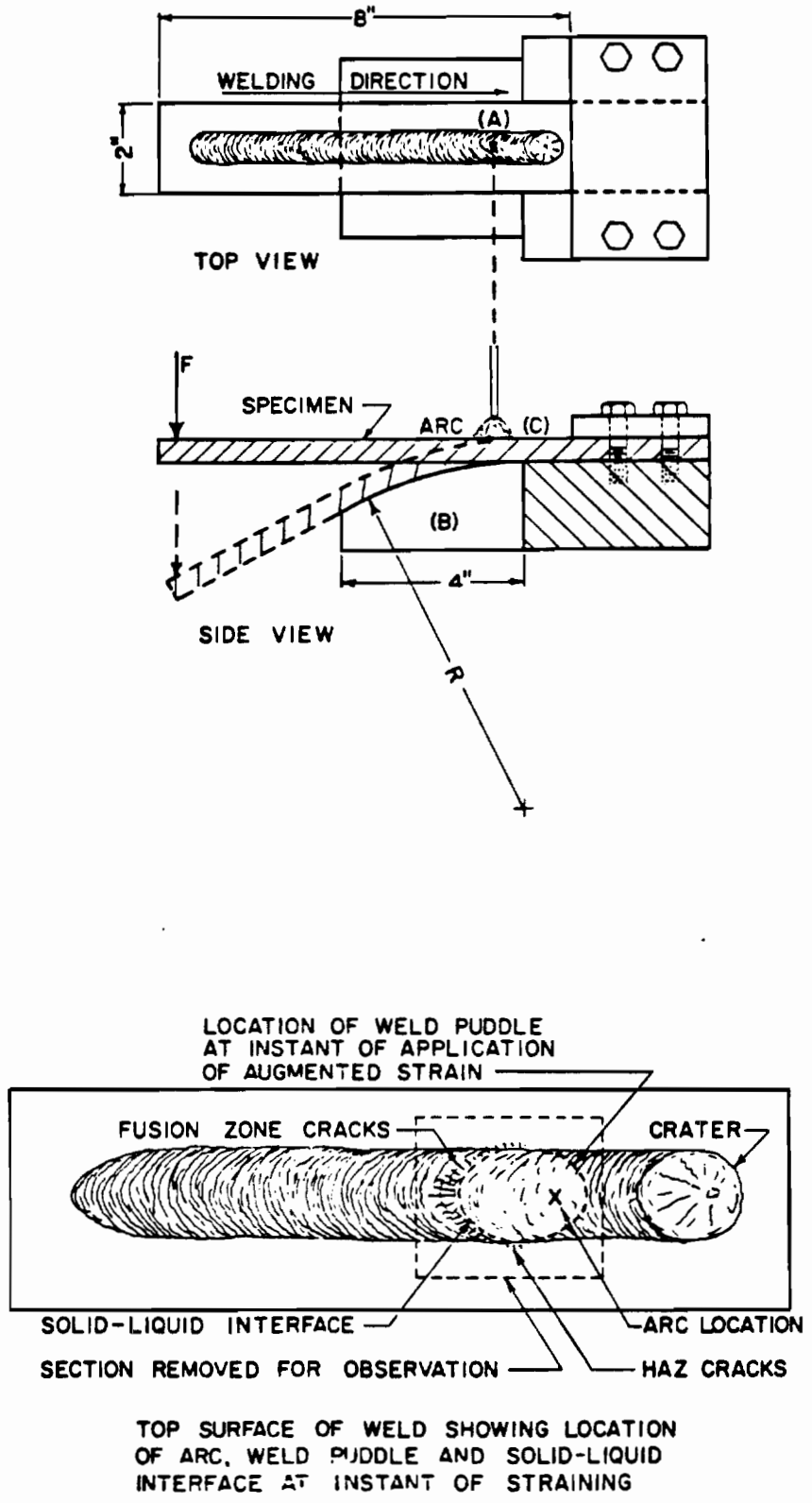

Figure 5 : Schematic illustration of the varestraint test jig and specimen set up (AWS B4.0).

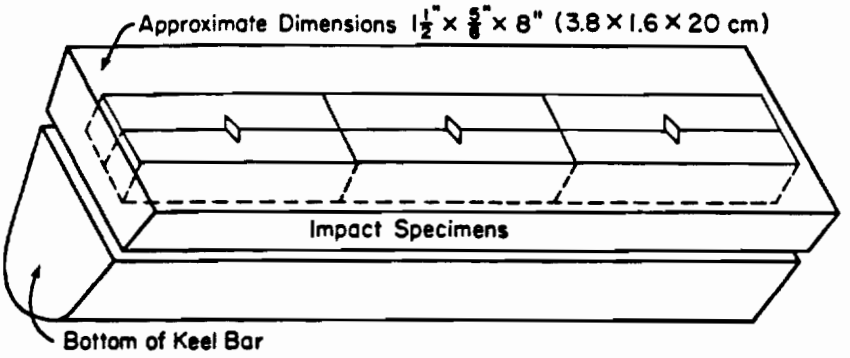

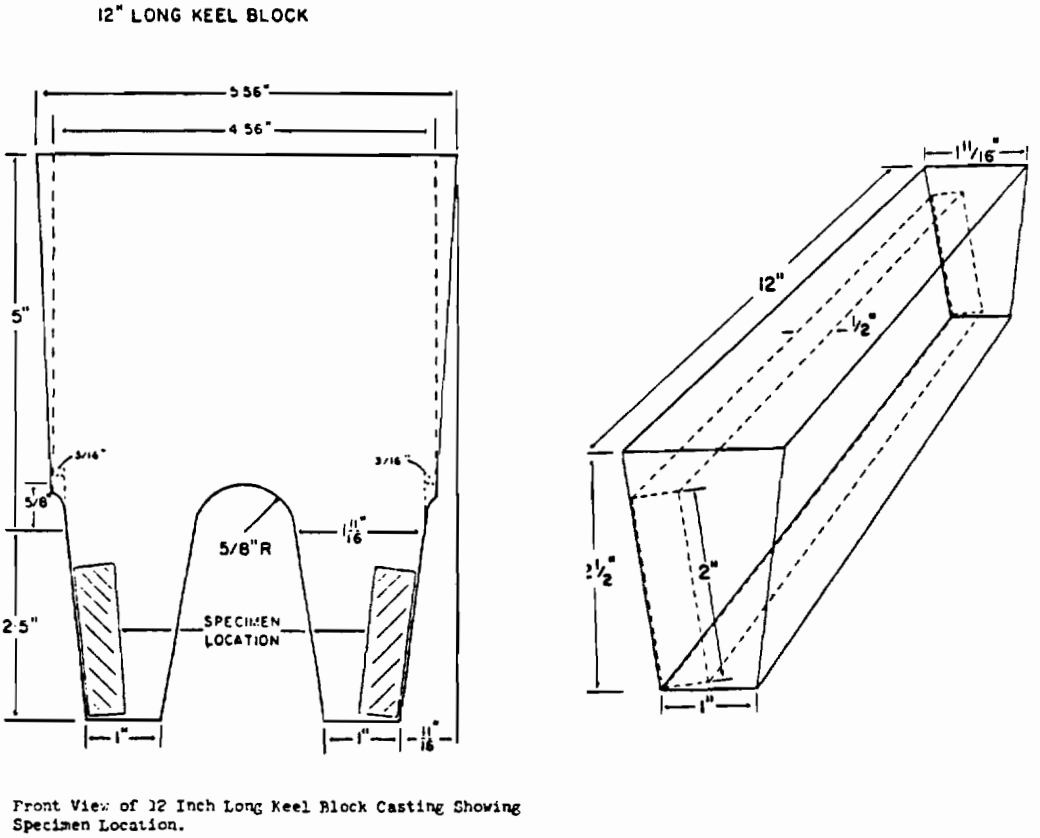

Front View of 12 Inch Long Keel Block Casting Showing Specimen Location.

Figure 6 : Location of the CVN impact and varestraint test specimens in the keel block casting.

(a)

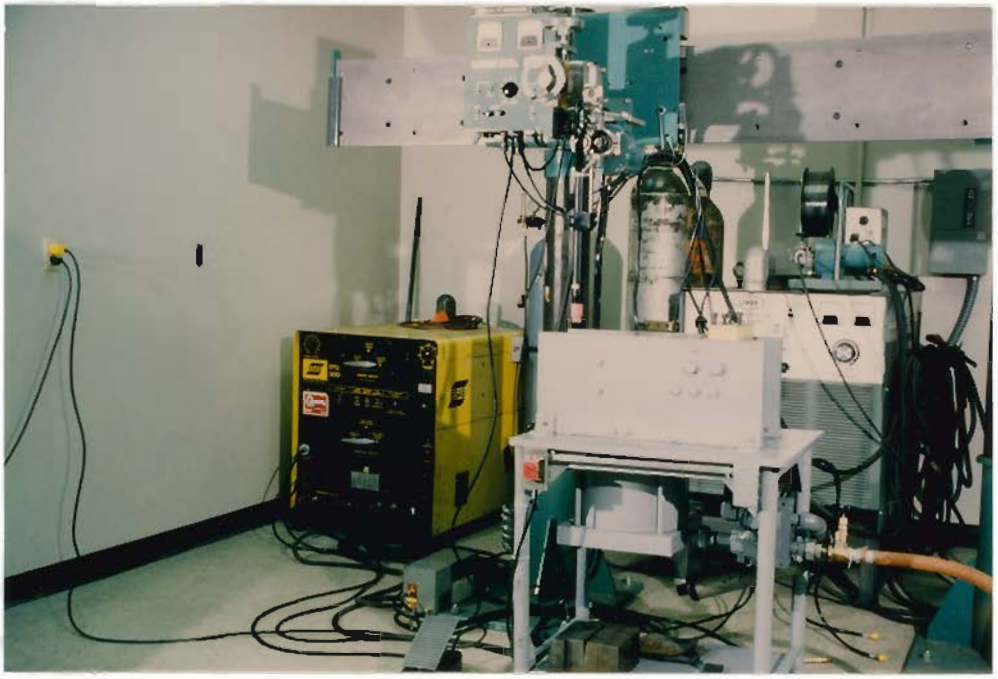

(b)

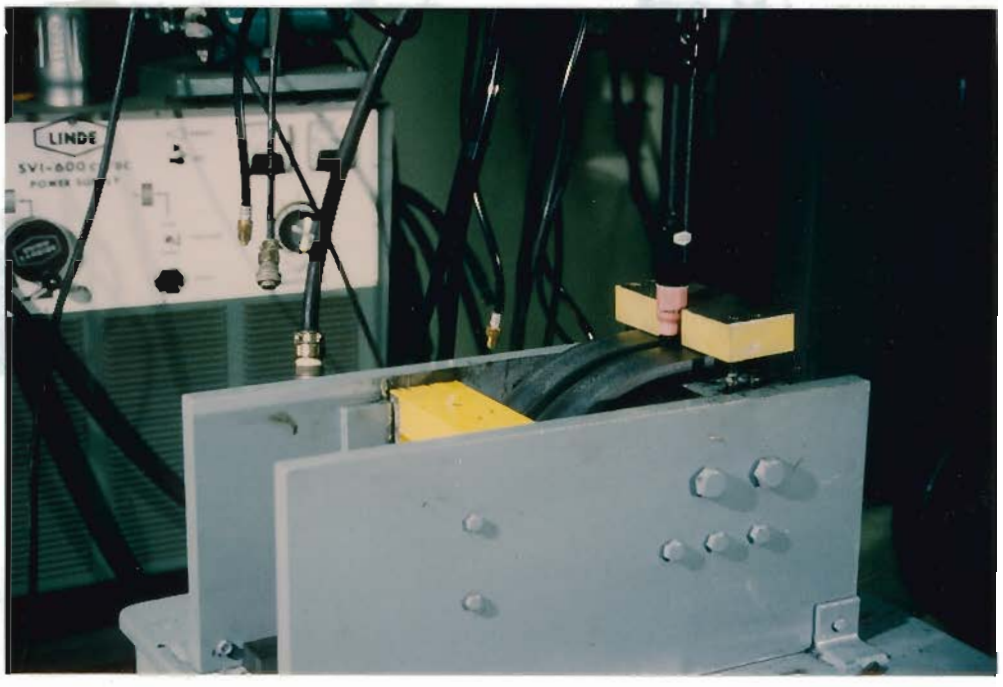

Figure 7 : Experimental set up of the varestraint test jig and specimen. a) actual set up b) close up of the set up after the test has been performed.

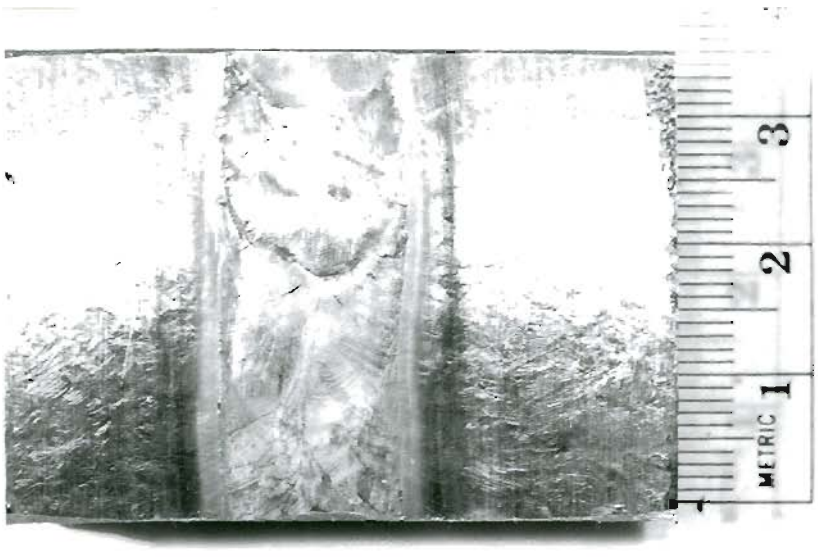

Figure 8 : A specimen removed from the varestraint test bar for the examination of cracks in the weld metal and the HAZ.

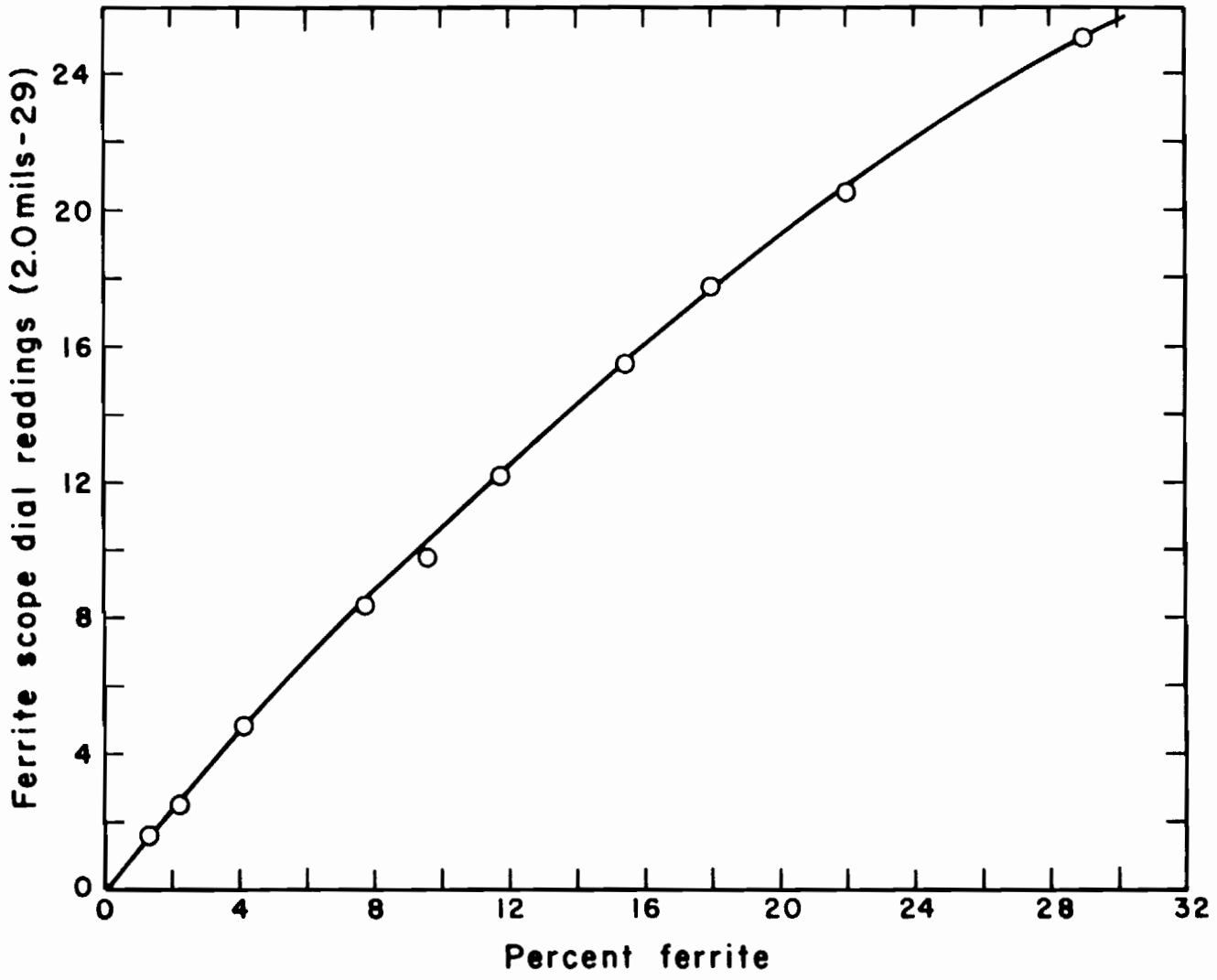

Figure 9 : Conversion of ferrite number (FN) to ferrite content (vol. %) for castings (Ref. 59).

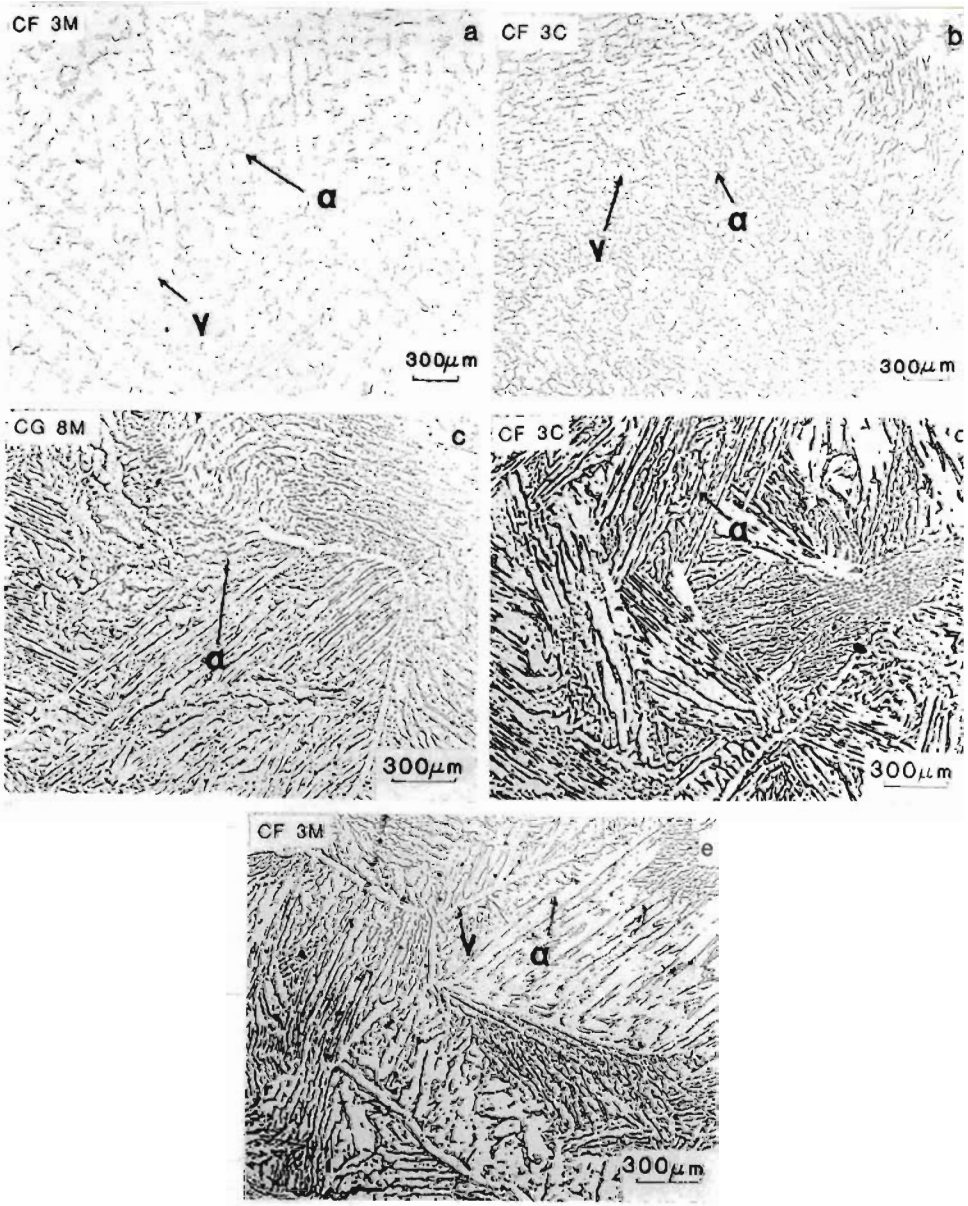

Figure 10 : Solidification structure of castings.
Cr_{eq}/Ni_{eq} a) 1.12, b) 1.28, c) 1.34, d) 1.4, e) 1.5
Dark phase - ferrite, light phase - austenite.
Electrolytic etch - 10% oxalic acid.

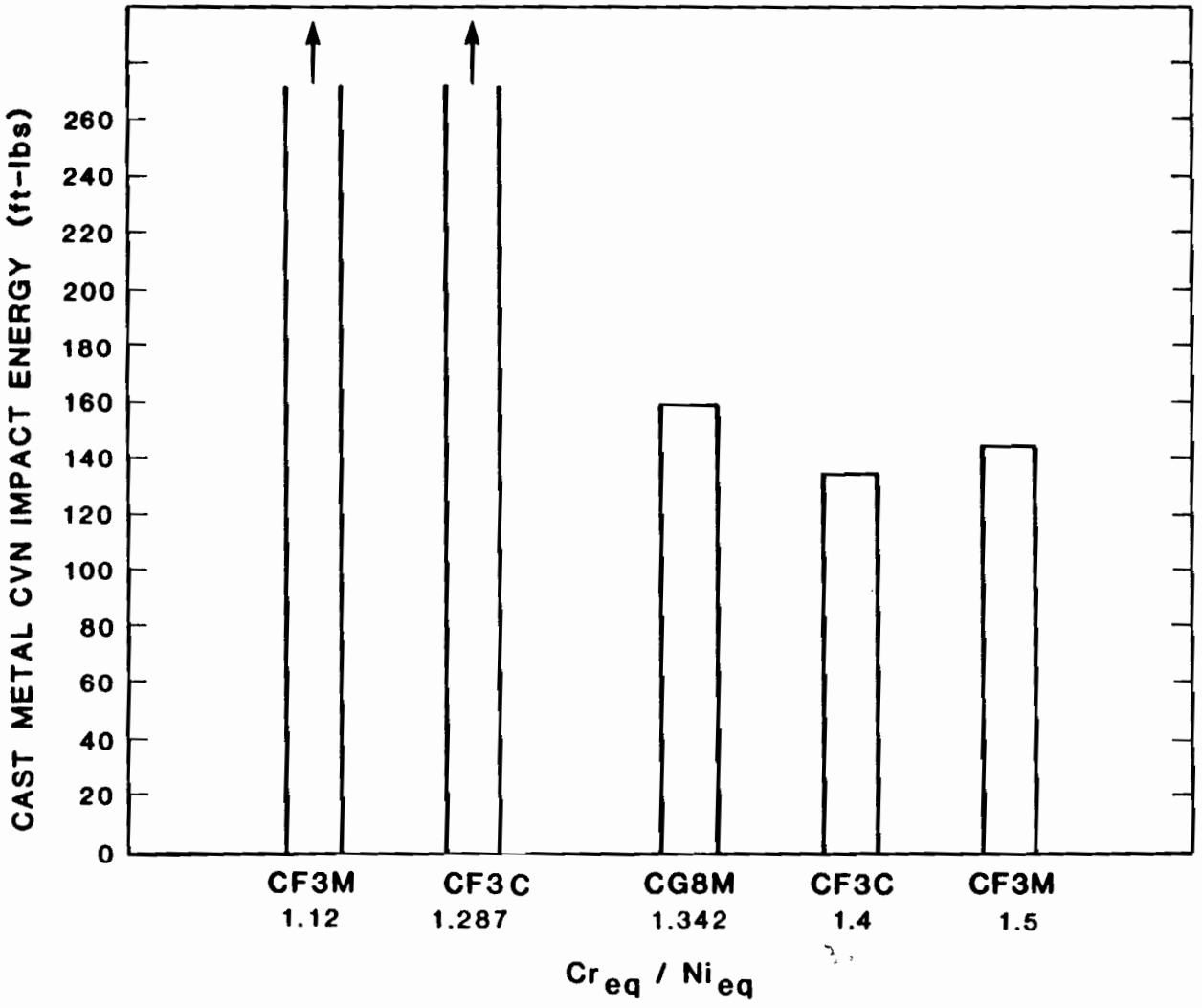

Figure 11 : Effect of Cr_{eq}/Ni_{eq} ratio on the impact energy of castings in SAWQ condition.

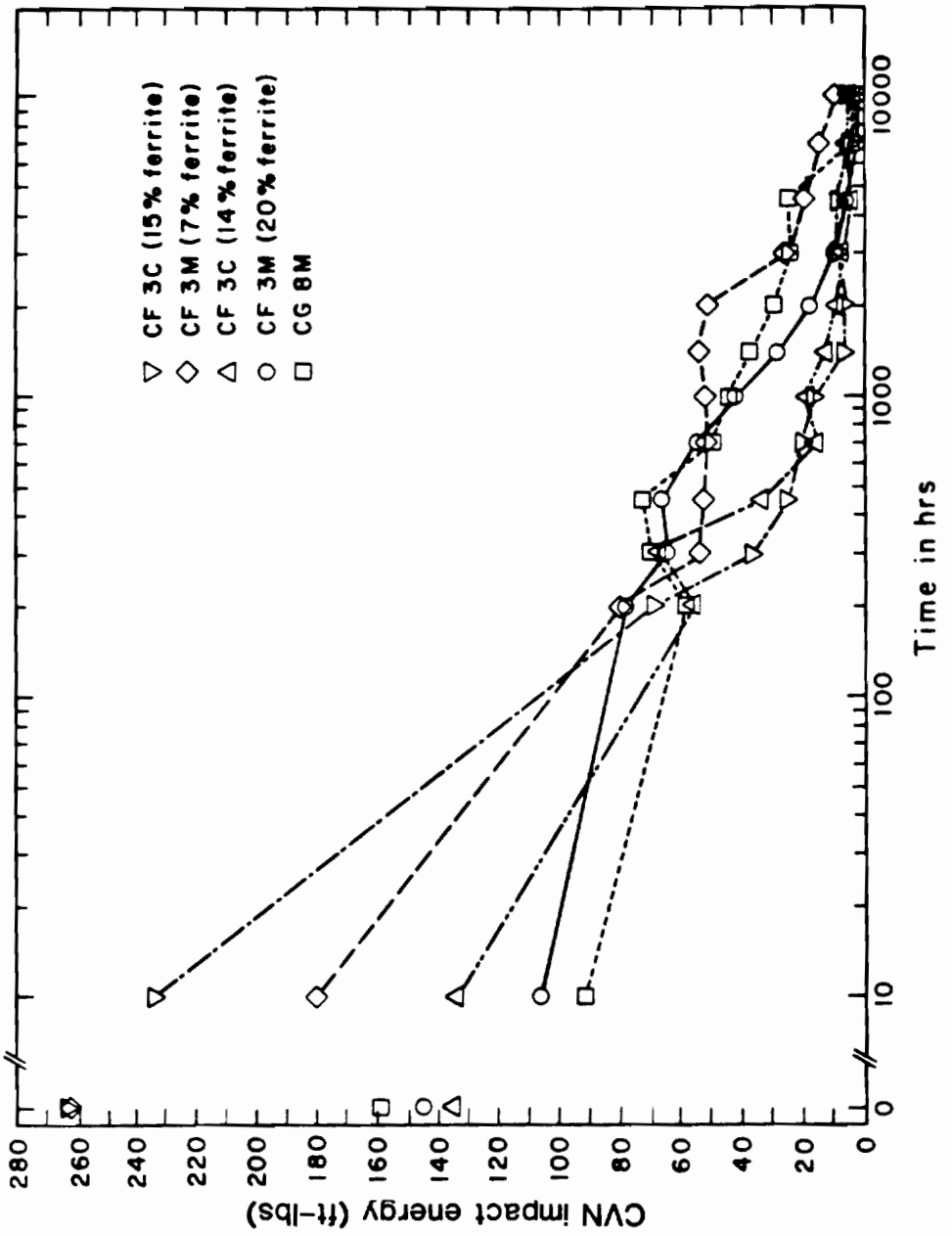

Figure 12 : CVN impact energy of castings (at room temperature) after aging at 594 °C (1100 °F).

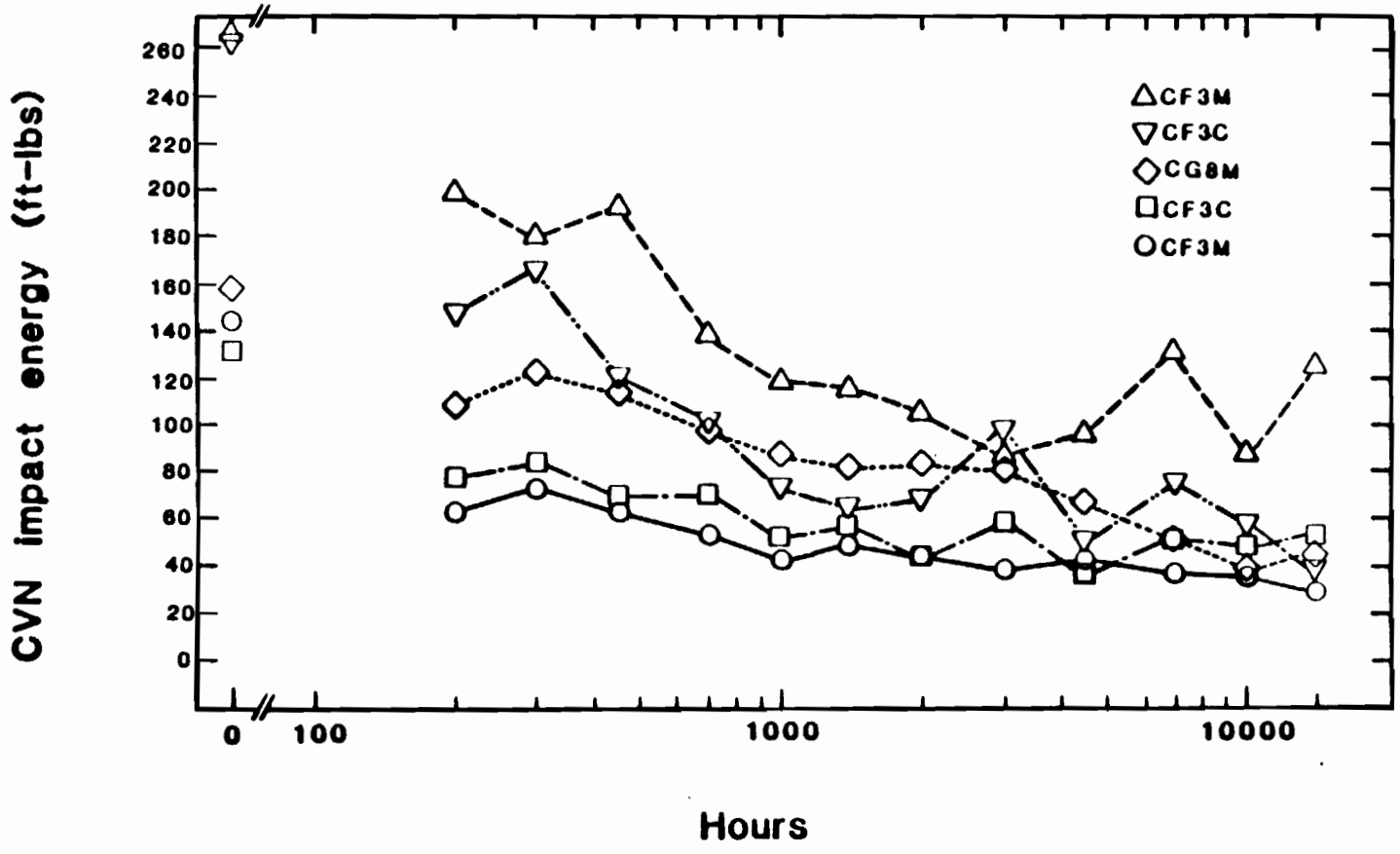

Figure 13 : CVN impact energy of castings (at room temperature) after aging at 427 ^{0}C (800 ^{0}F).

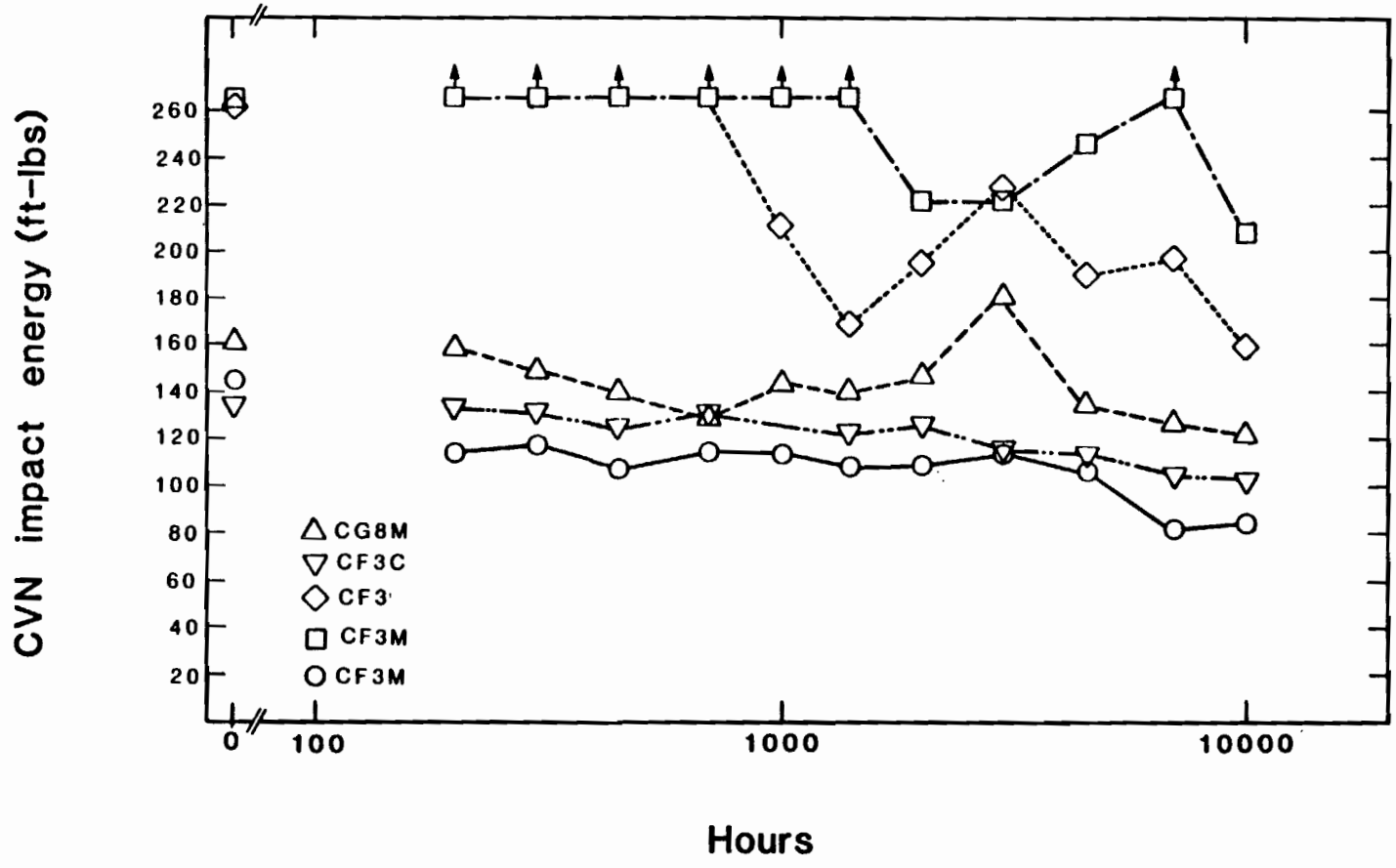

Figure 14 : CVN impact energy of castings (at room temperature) after aging at 316 ^{0}C (600 ^{0}F).

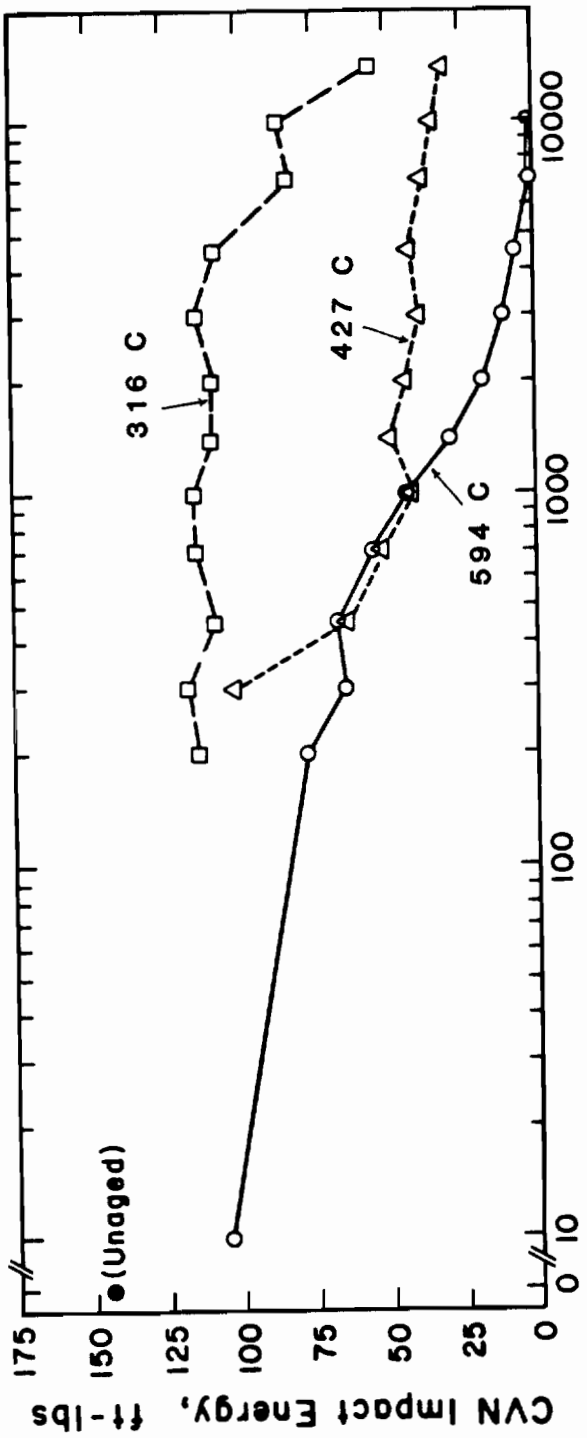

Figure 15 : CVN impact energy for alloy CF 3M (containing 20% ferrite in SAWQ condition) after aging.

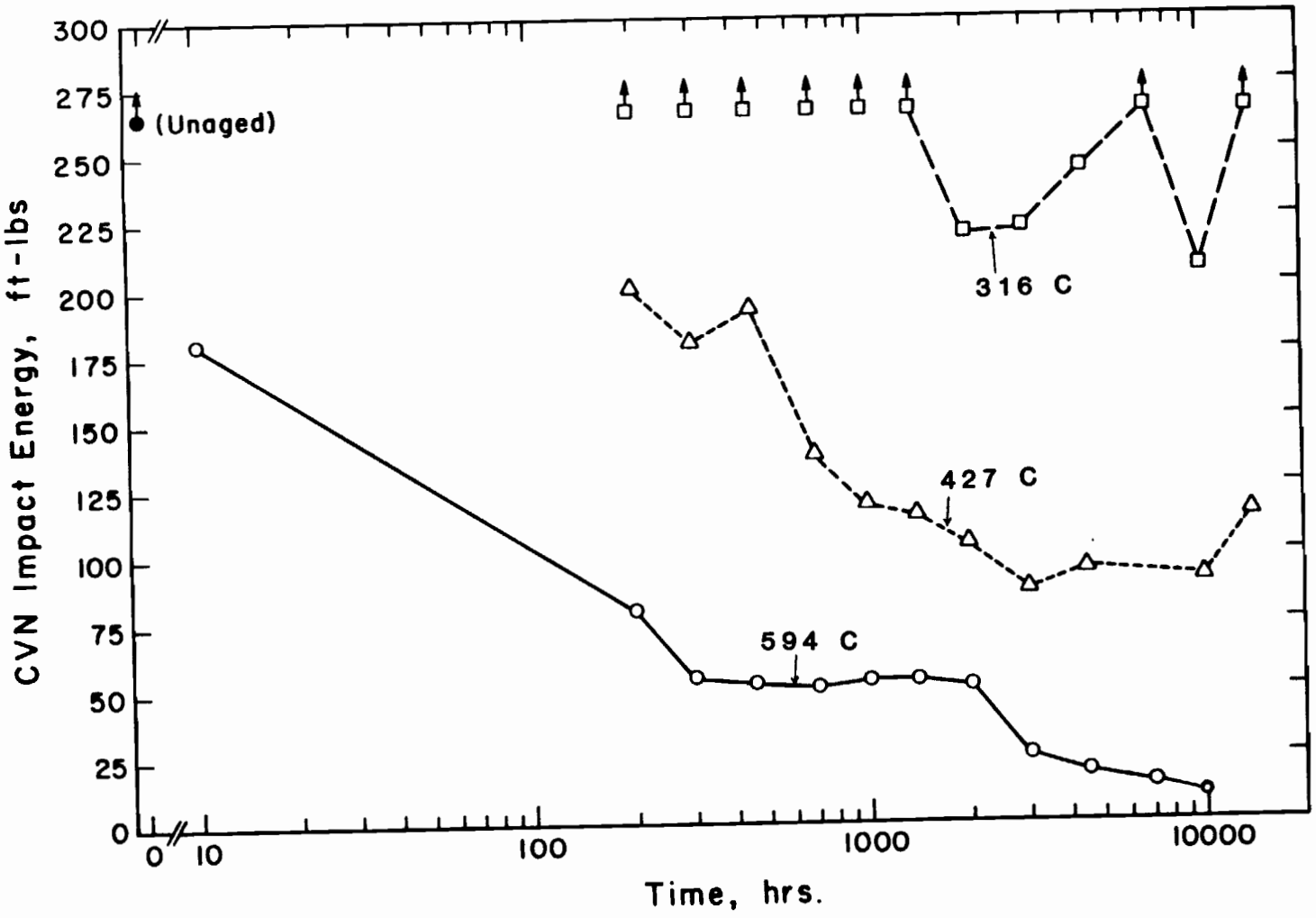

Figure 16 : CVN impact energy for alloy CF 3M (containing 7% ferrite in SAWQ condition) after aging.

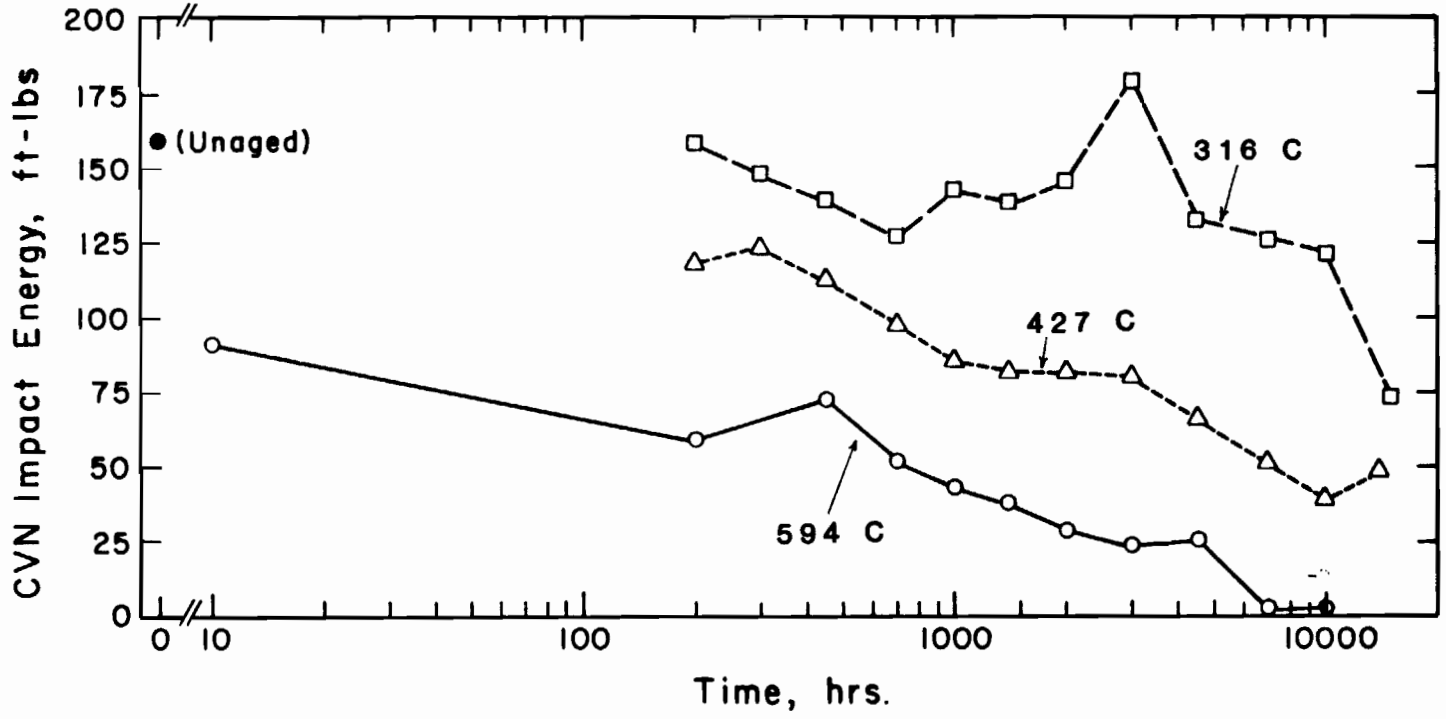

Figure 17 : CVN impact energy for alloy CG 8M (containing 10% ferrite in SAWQ condition) after aging.

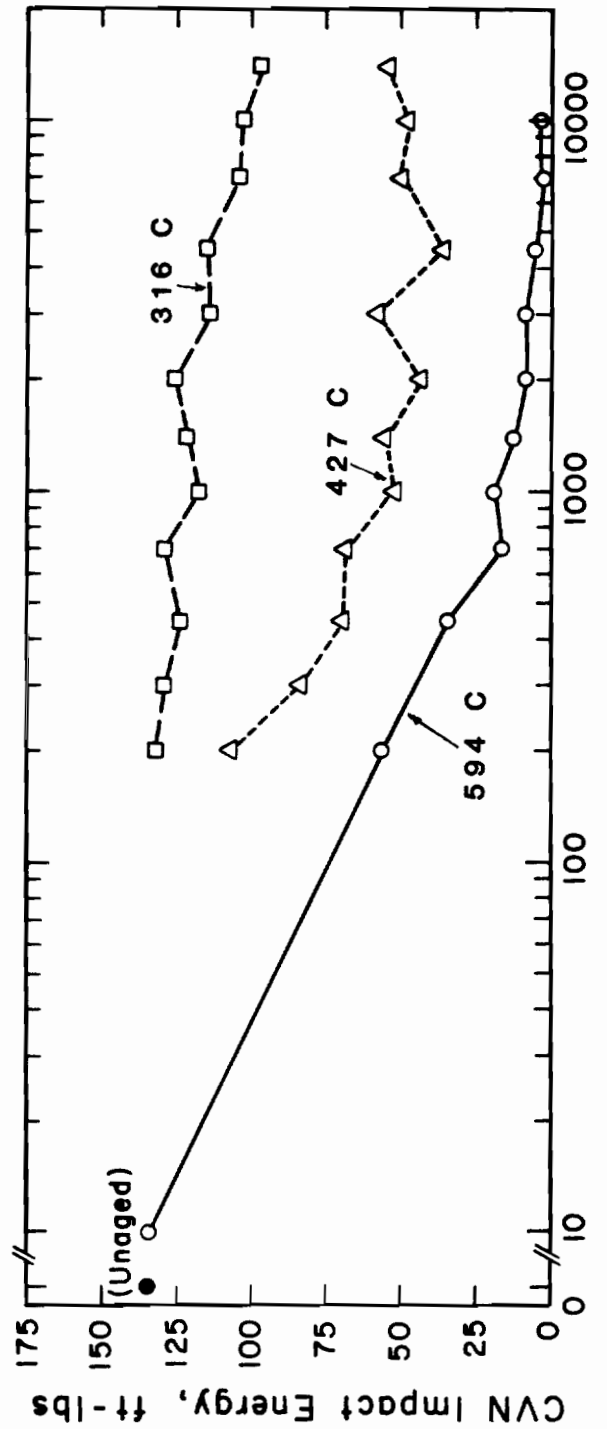

Figure 18 : CVN impact energy for alloy CF 3C (containing 14 % ferrite in SAWQ condition) after aging.

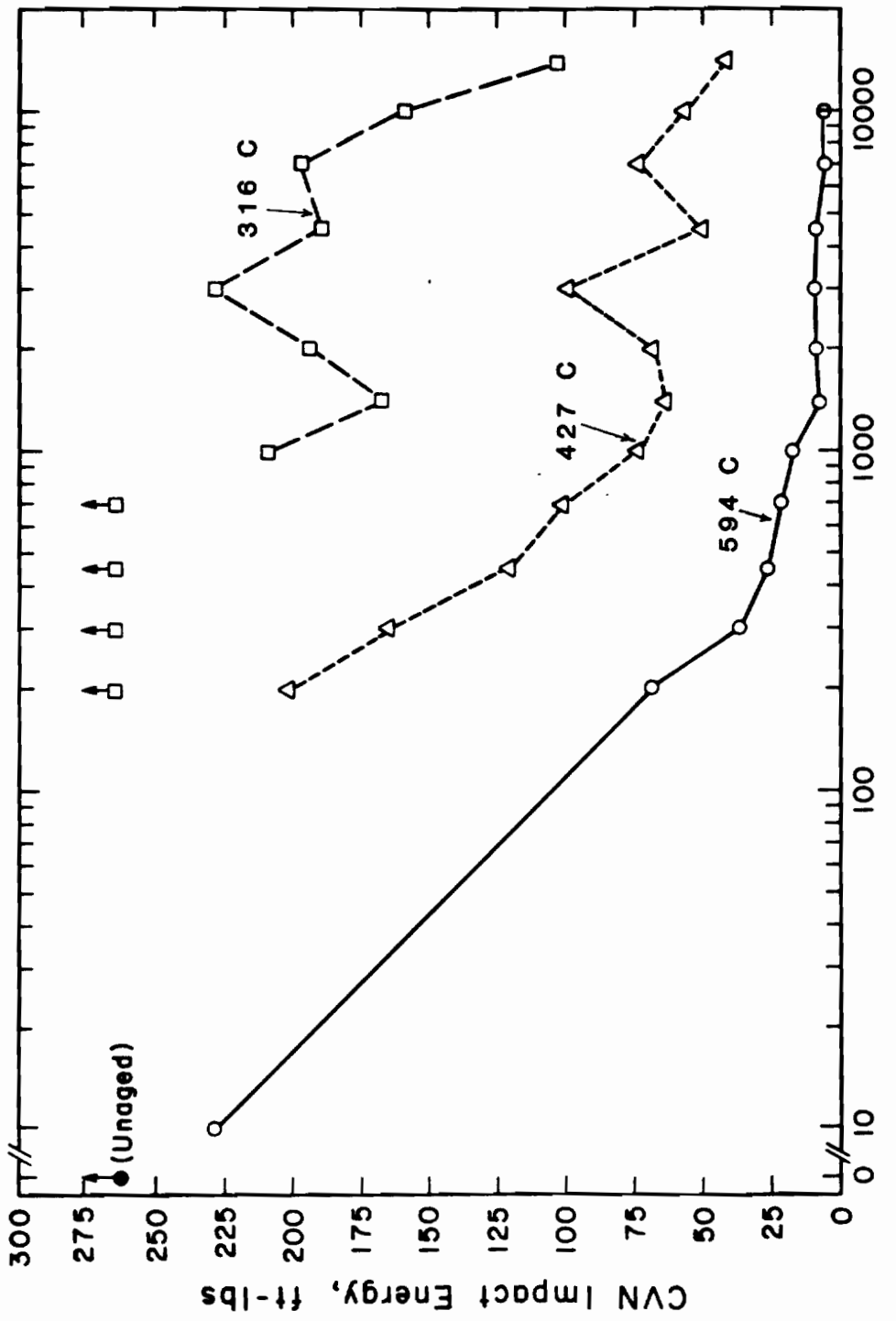

Figure 19 : CVN impact energy for alloy CF 3C (containing 15% ferrite in SAWQ condition) after aging.

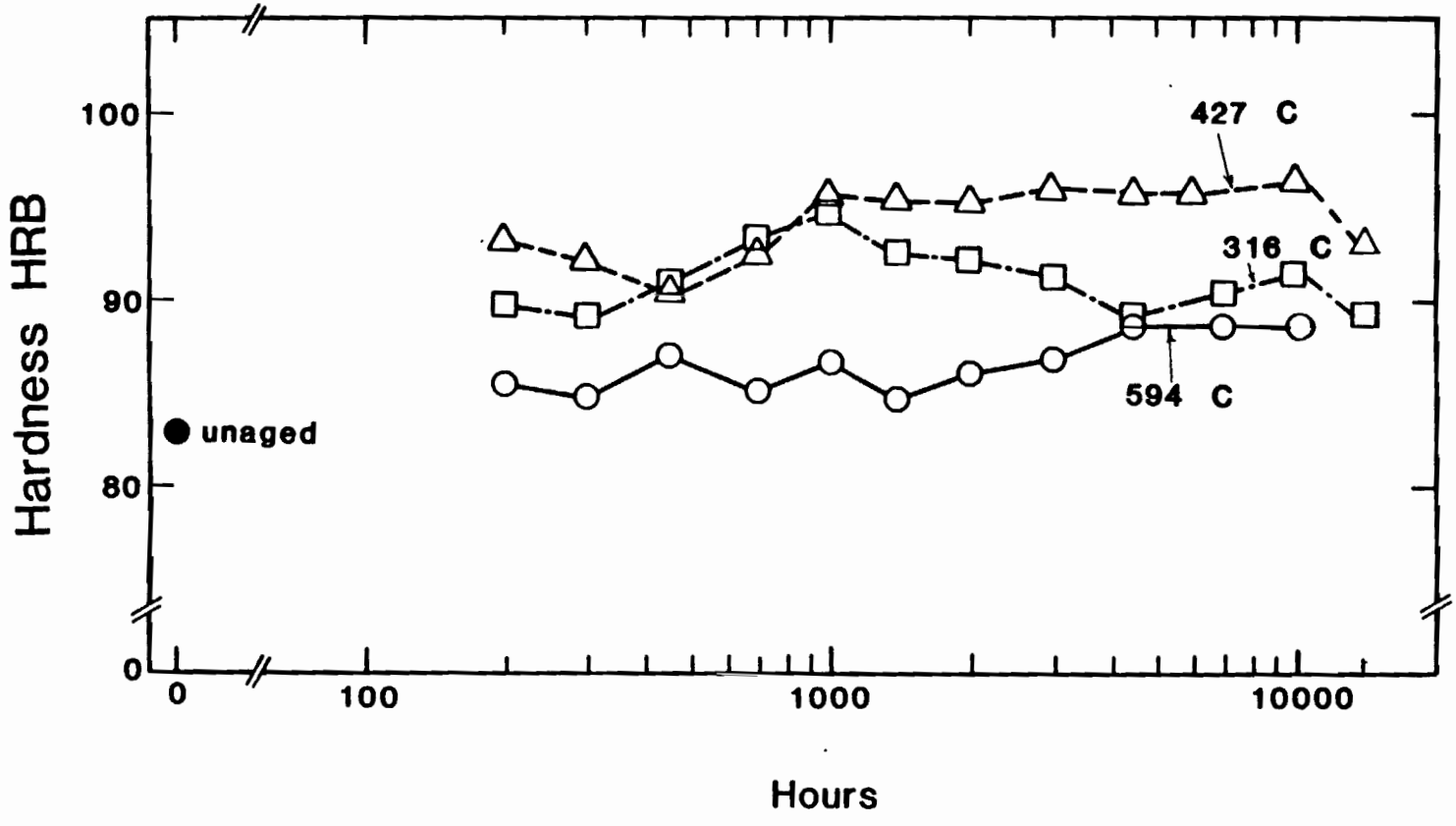

Figure 20 : Hardness for alloy CF 3M (containing 20% ferrite in SAWQ condition) after aging.

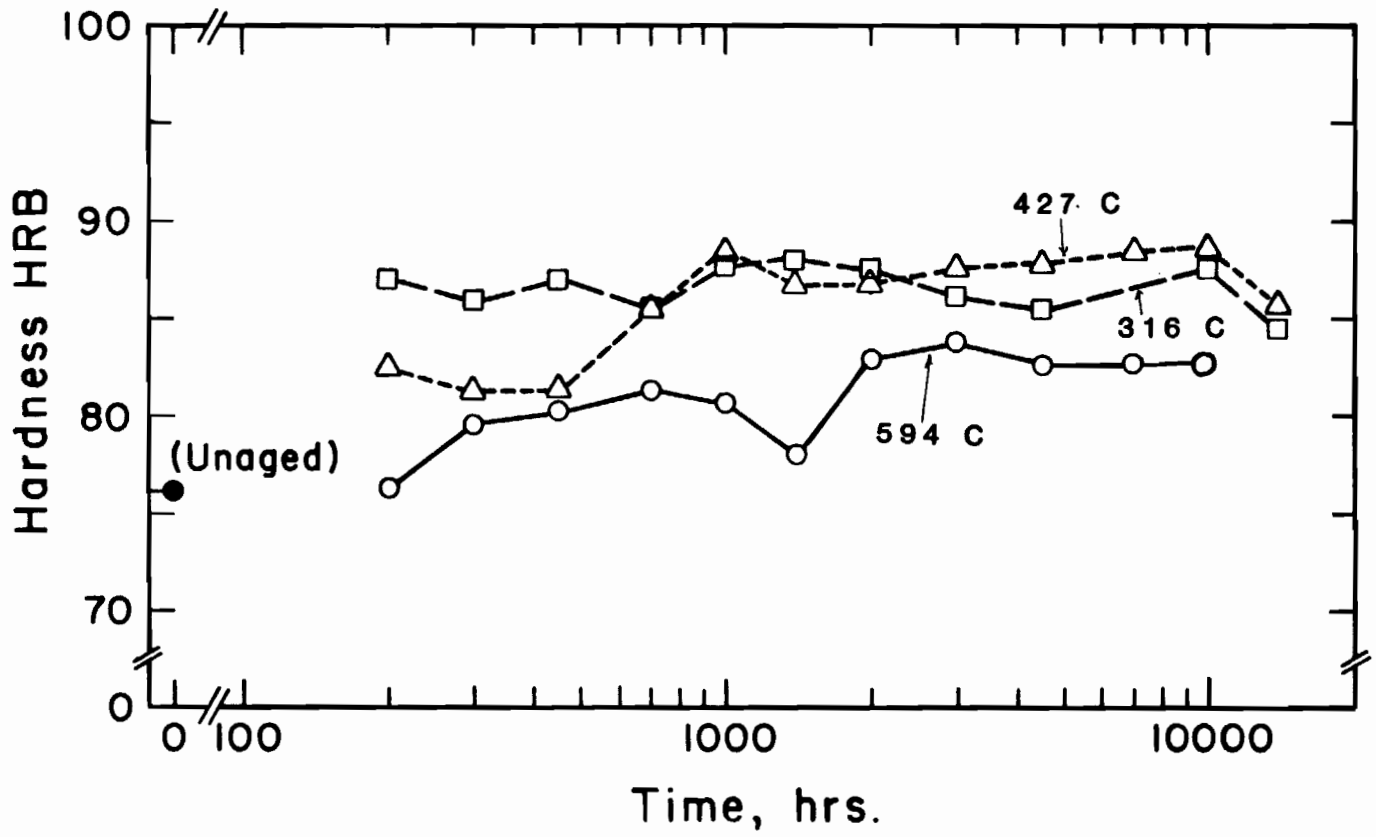

Figure 21 : Hardness for alloy CF 3M (containing 7% ferrite in SAWQ condition) after aging.

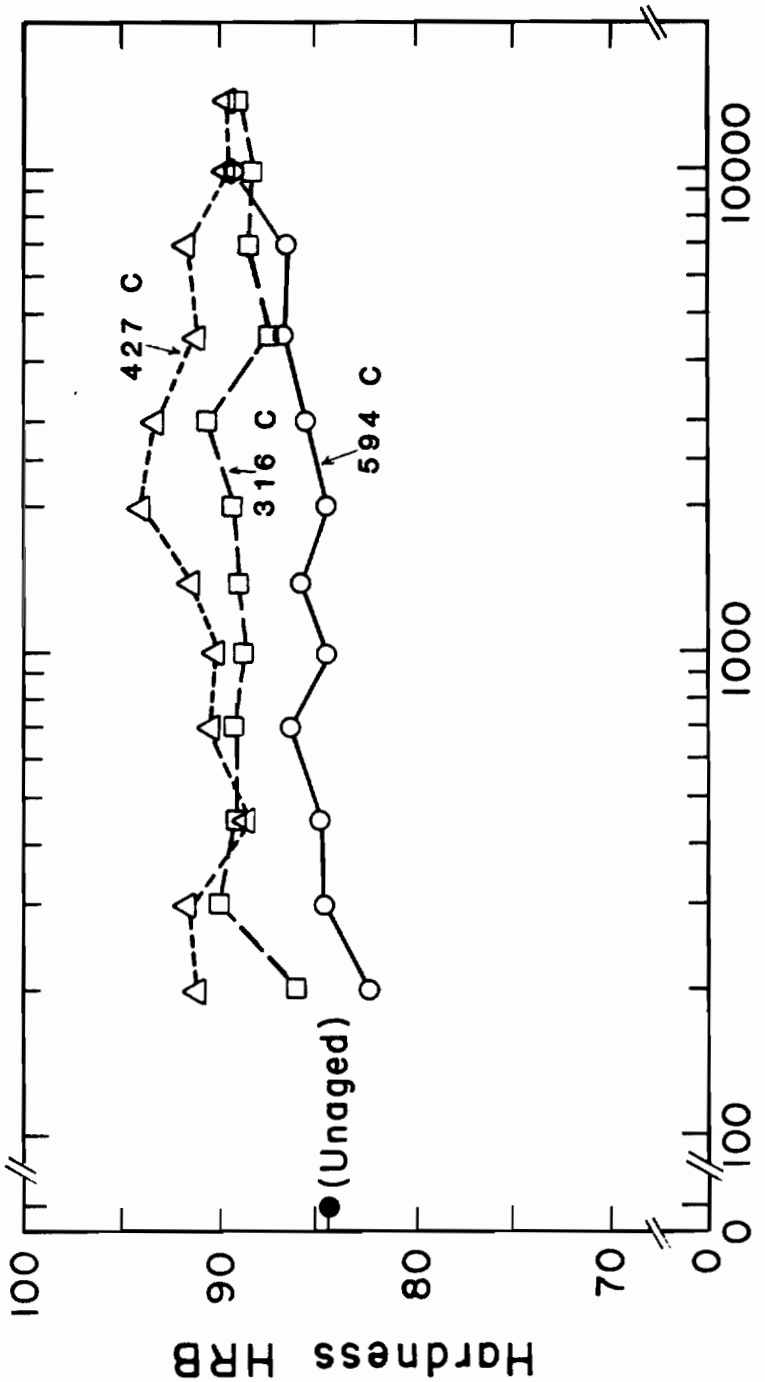

Figure 22 : Hardness for alloy CG 8M (containing 10% ferrite in SAWQ condition) after aging.

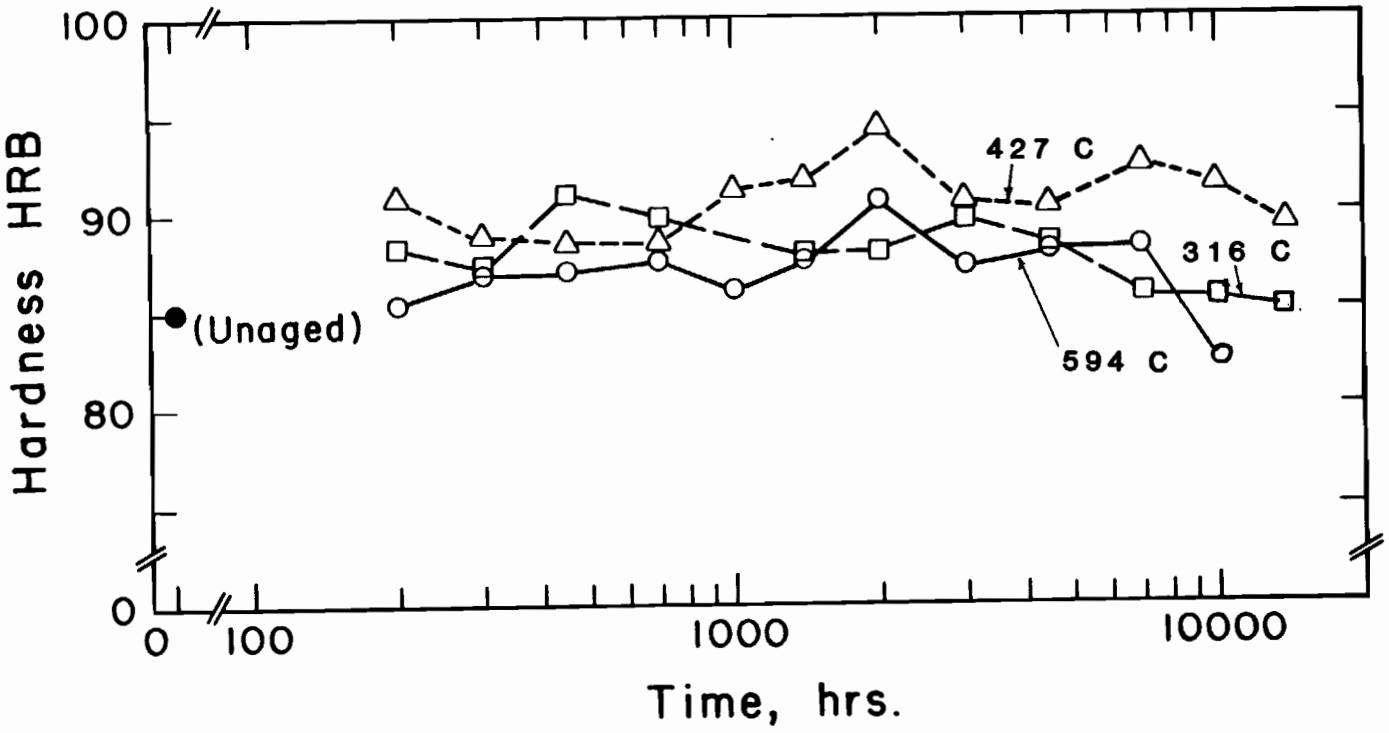

Figure 23 : Hardness for alloy CF 3C (containig 14% ferrite in SAWQ condition) after aging.

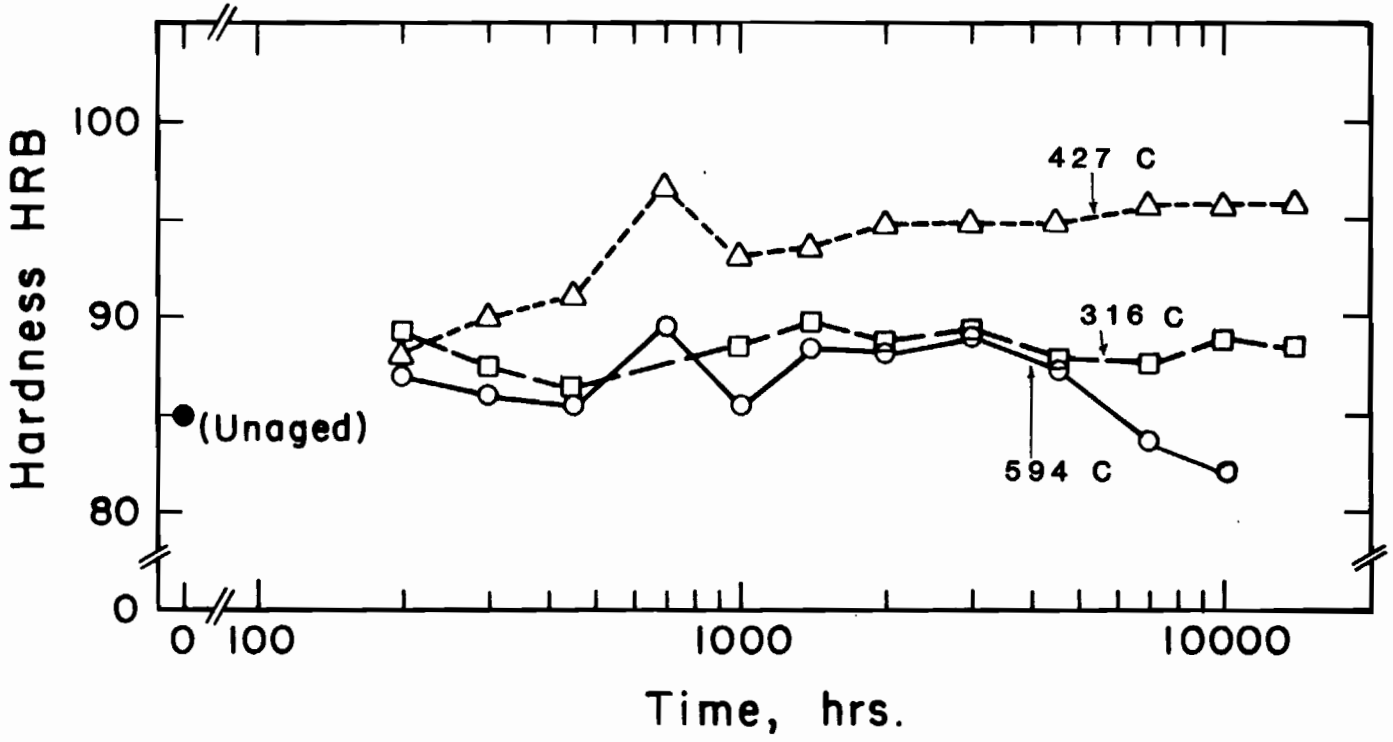

Figure 24 : Hardness for alloy CF 3C (containig 15% ferrite in SAWQ condition) after aging.

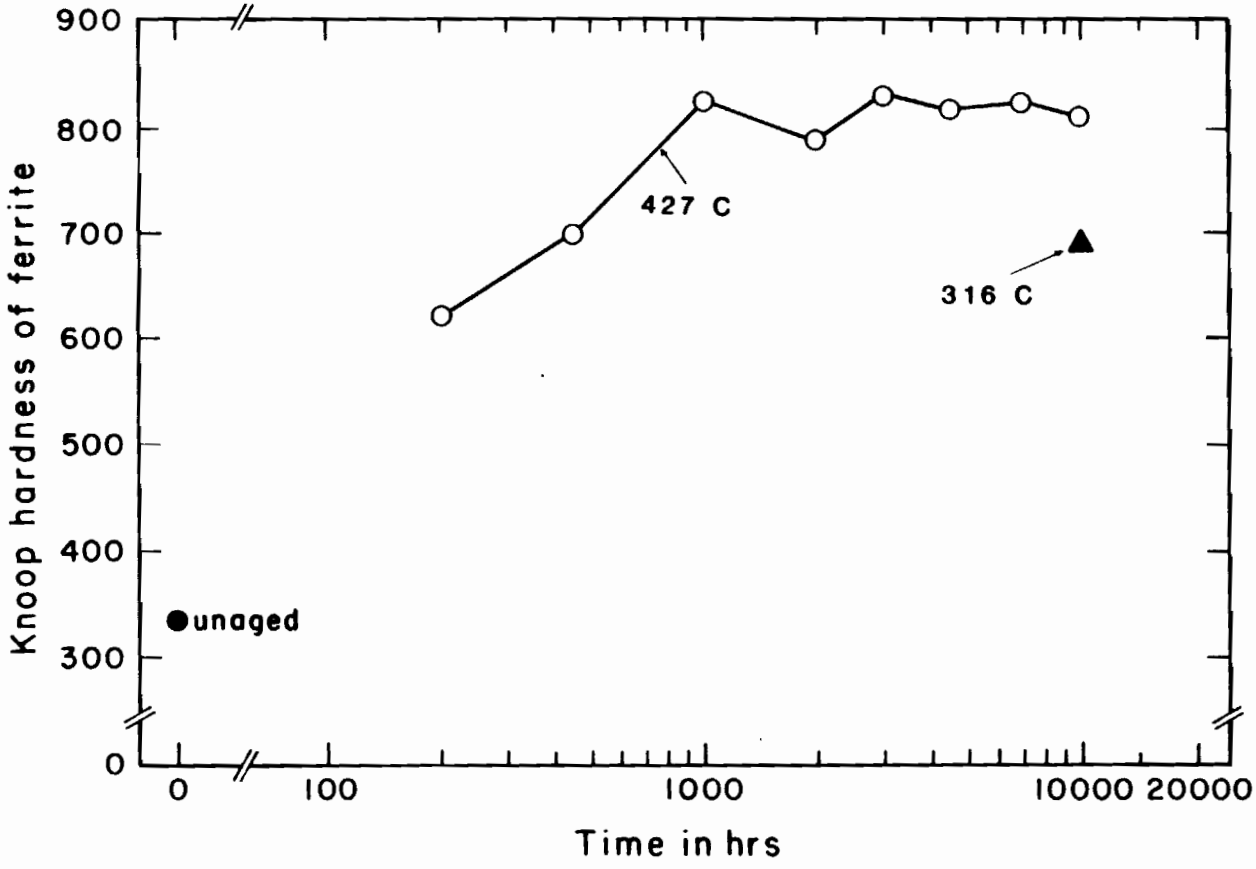

Figure 25 : Knoop hardness (50 gm load) of ferrite for alloy CF 3M (containing 20% ferrite in SAWQ condition) after aging.

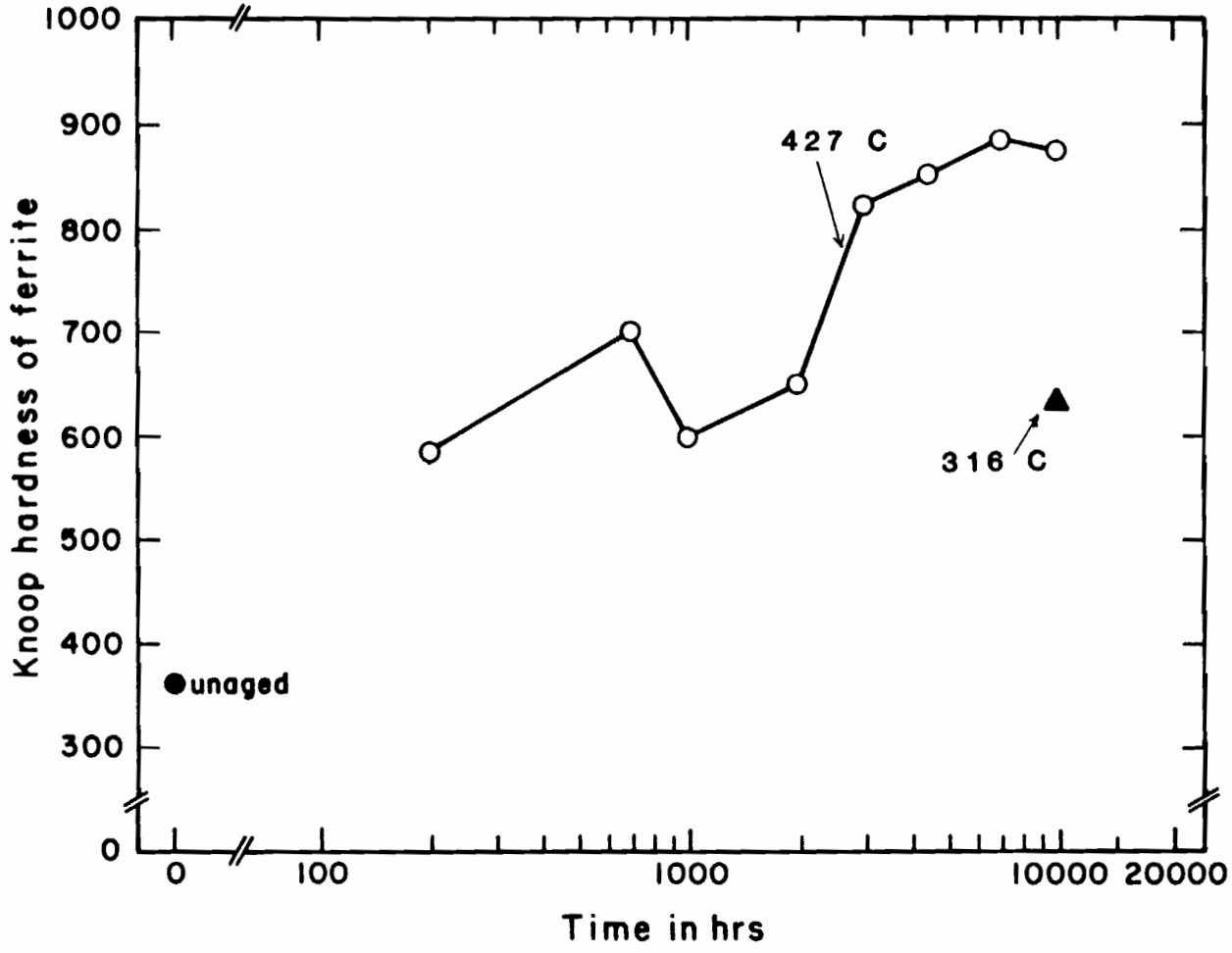

Figure 26 : Knoop hardness (50 gm load) of ferrite for alloy CF 3M (containing 7% ferrite in SAWQ condition) after aging.

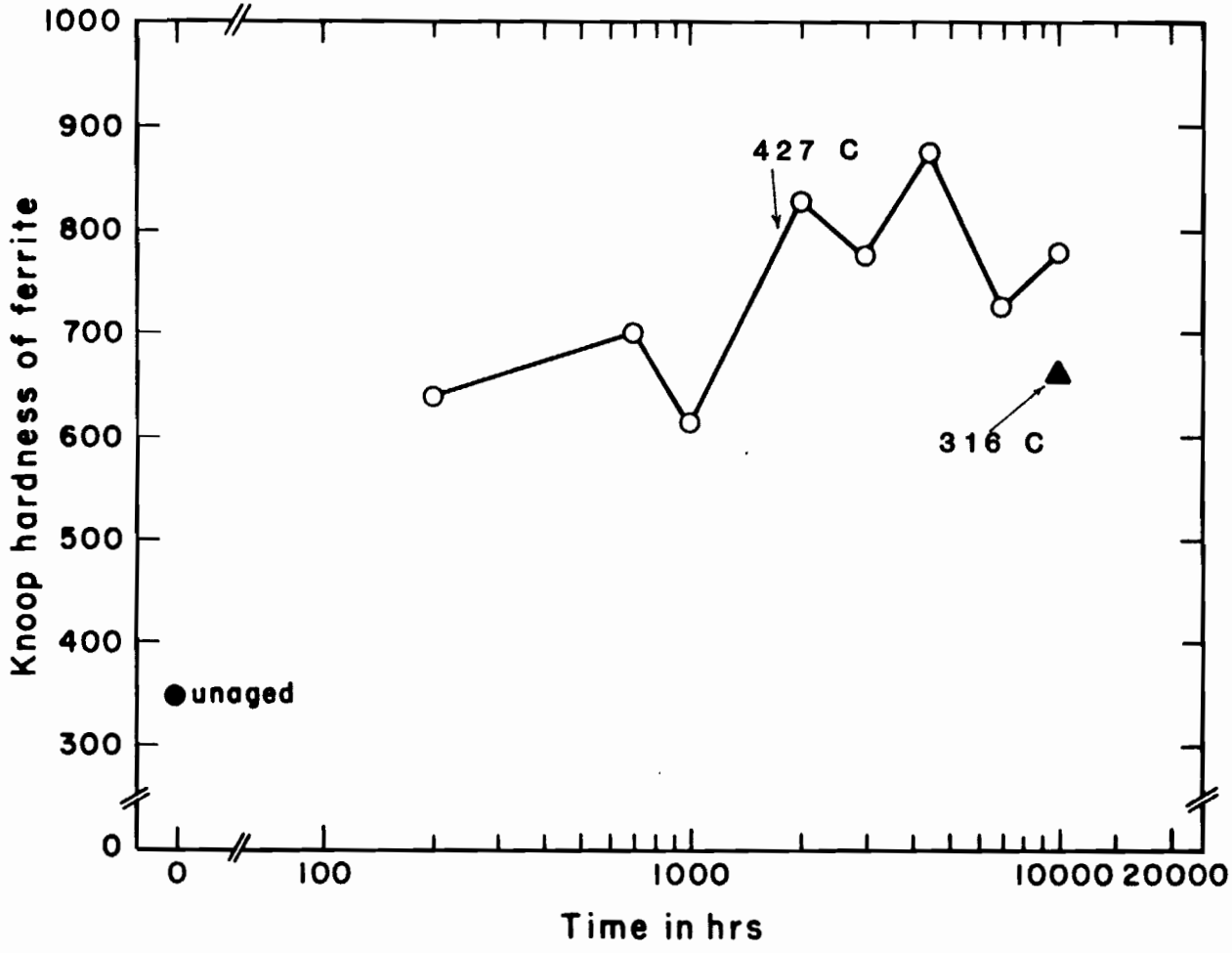

Figure 27 : Knoop hardness (50 gm load) of ferrite for alloy CG 8M (containing 10% ferrite in SAWQ condition) after aging.

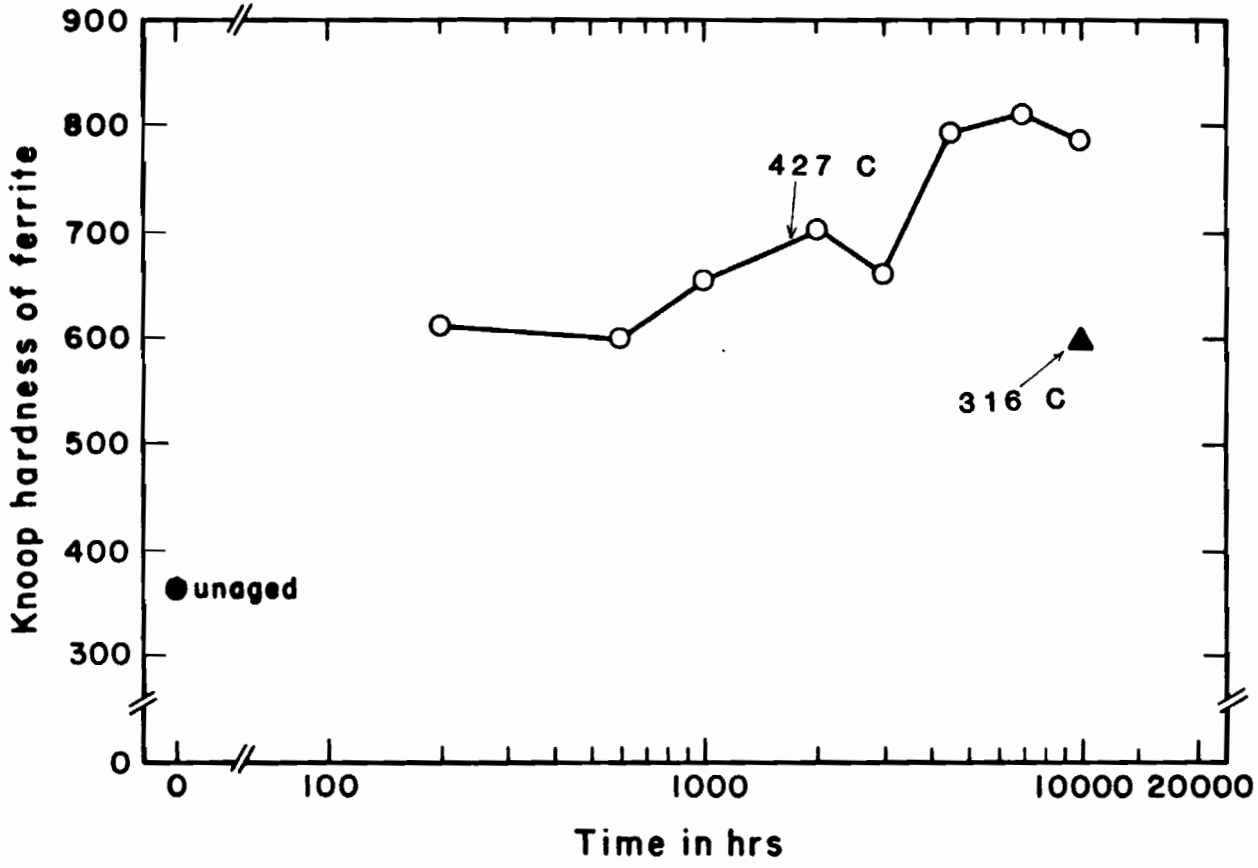

Figure 28 : Knoop hardness (50 gm load) of ferrite for alloy CF 3C (containig 14 % ferrite in SAWQ condition) after aging.

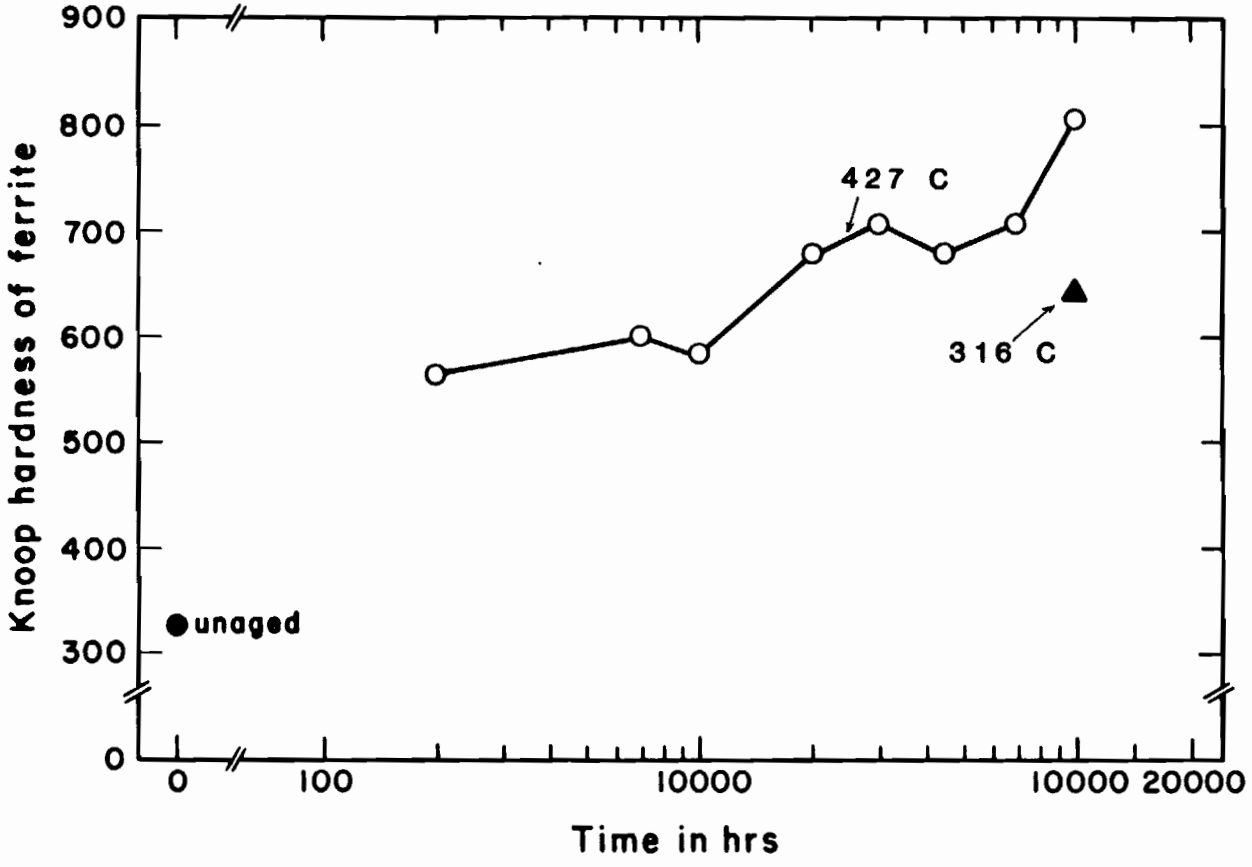

Figure 29 : Knoop hardness (50 gm load) of ferrite for alloy CF 3C (containig 15% ferrite in SAWQ condition) after aging.

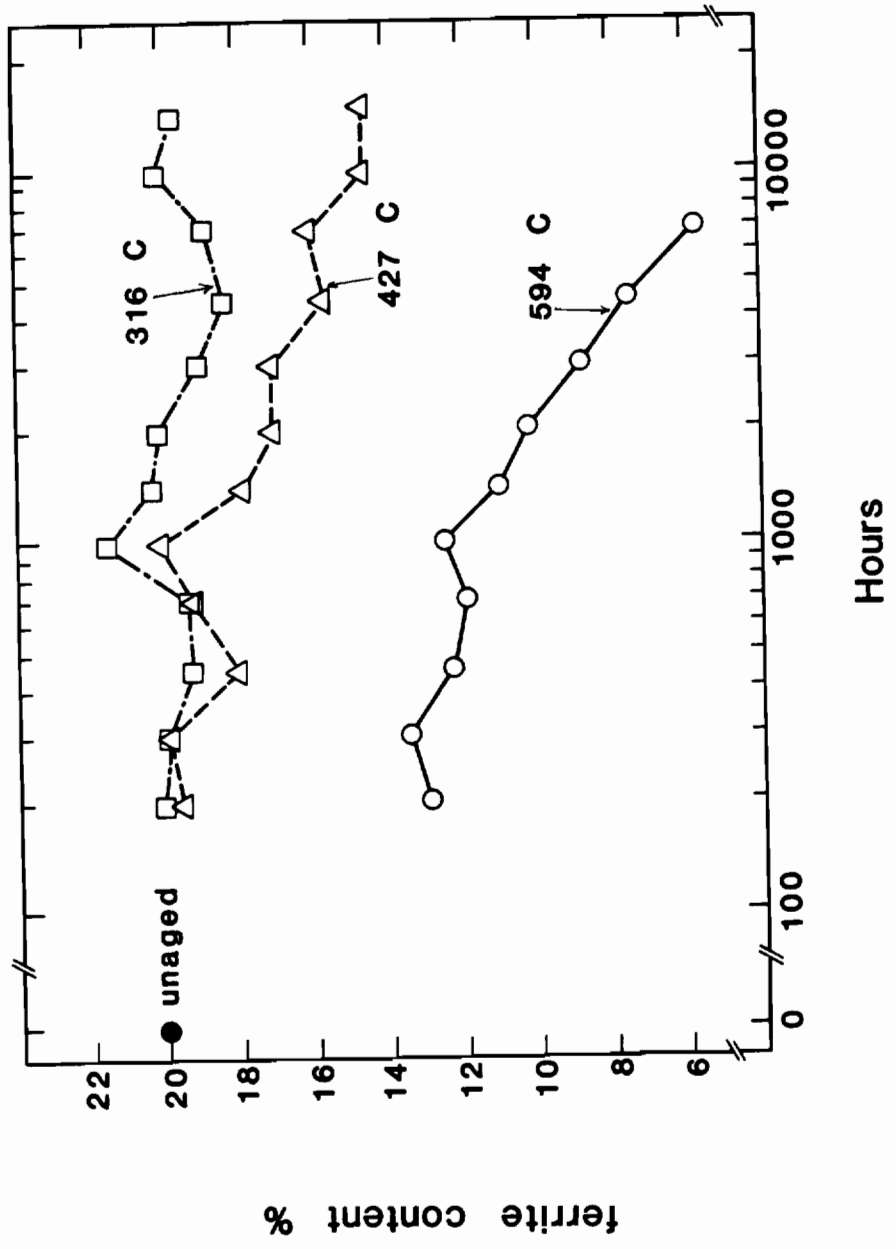

Figure 30 : Ferrite content for alloy CF 3M (20% ferrite in SAWQ condition) after aging.

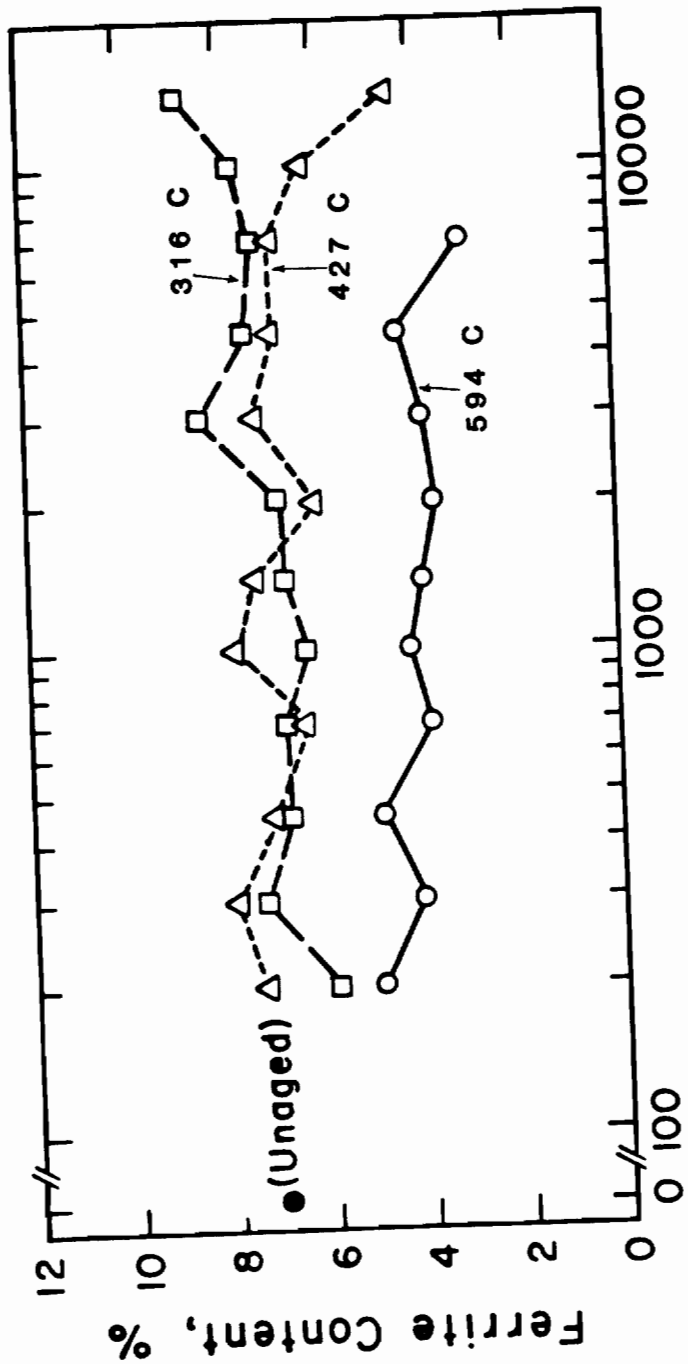

Figure 31 : Ferrite content for alloy CF 3M (7% ferrite in SAWQ condition) after aging.

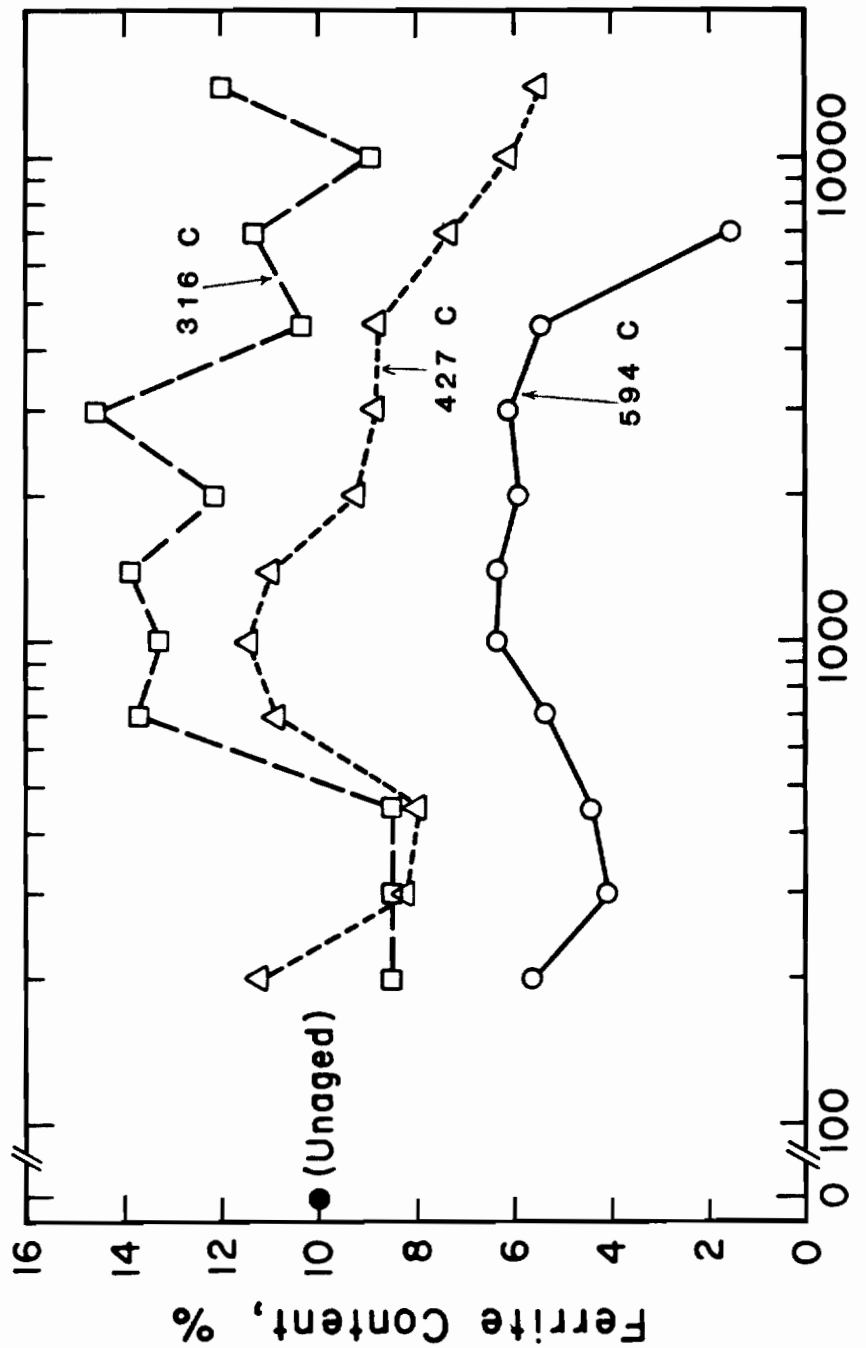

Figure 32 : Ferrite content for alloy CG 8M after aging.

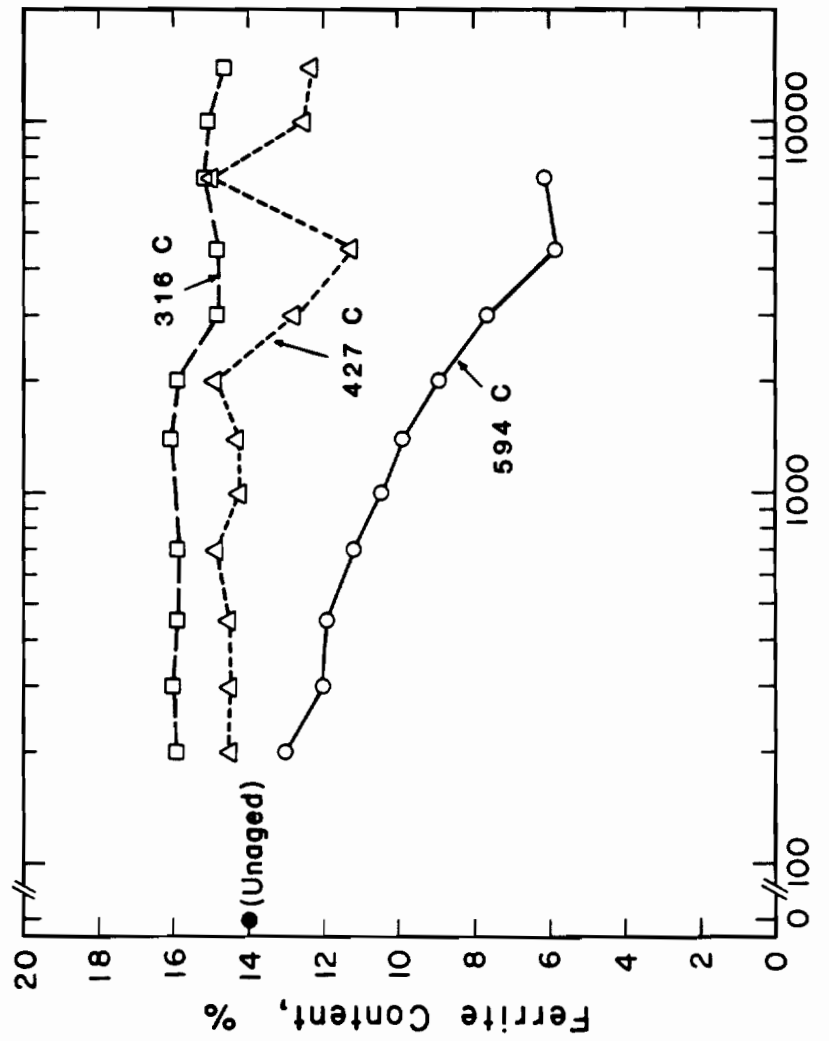

Figure 33 : Ferrite content for alloy CF 3C (14% ferrite in SAWQ condition) after aging.

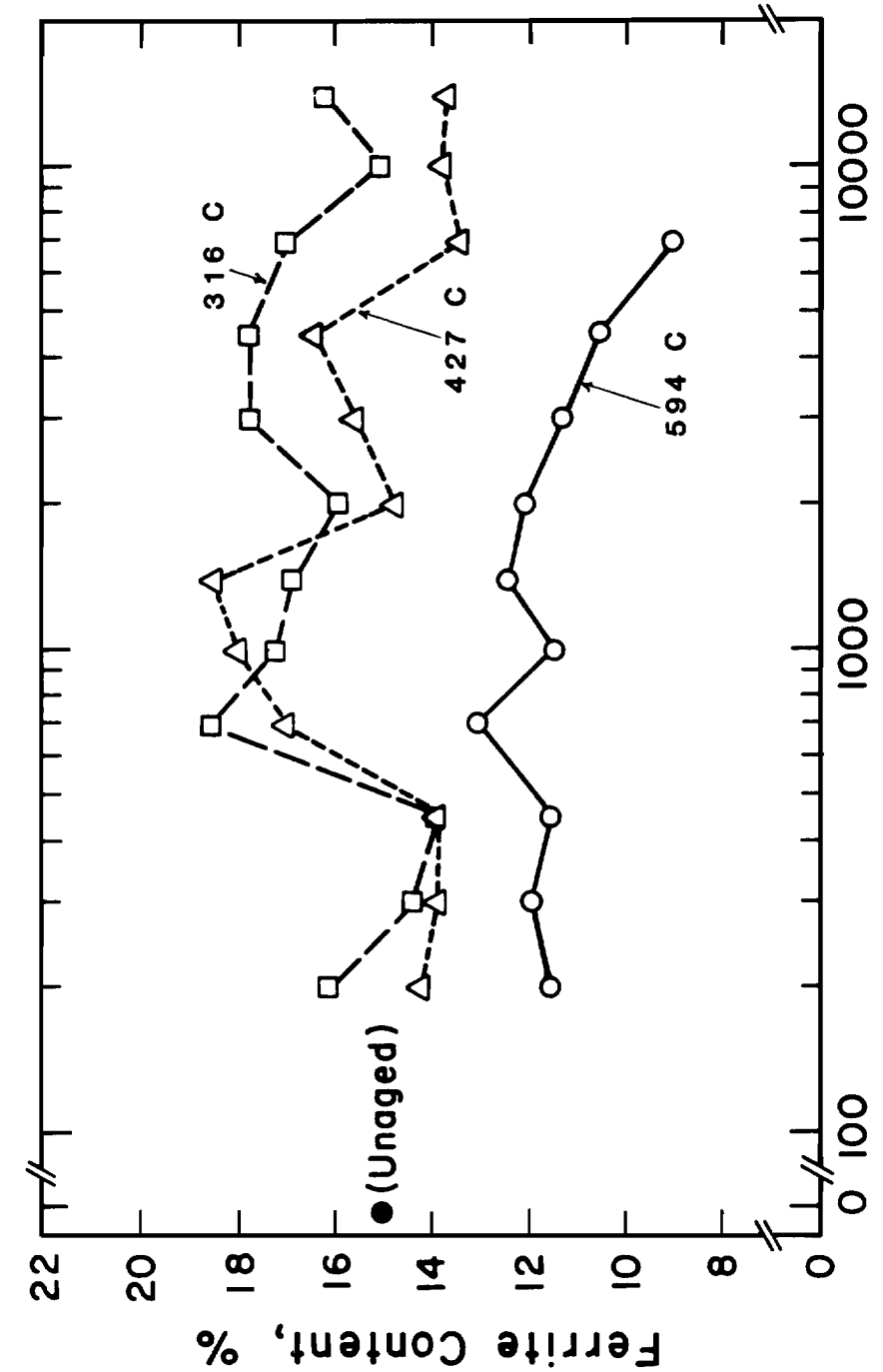

Figure 34 : Ferrite content for alloy CF 3C (15% ferrite in SAWQ condition) after aging.

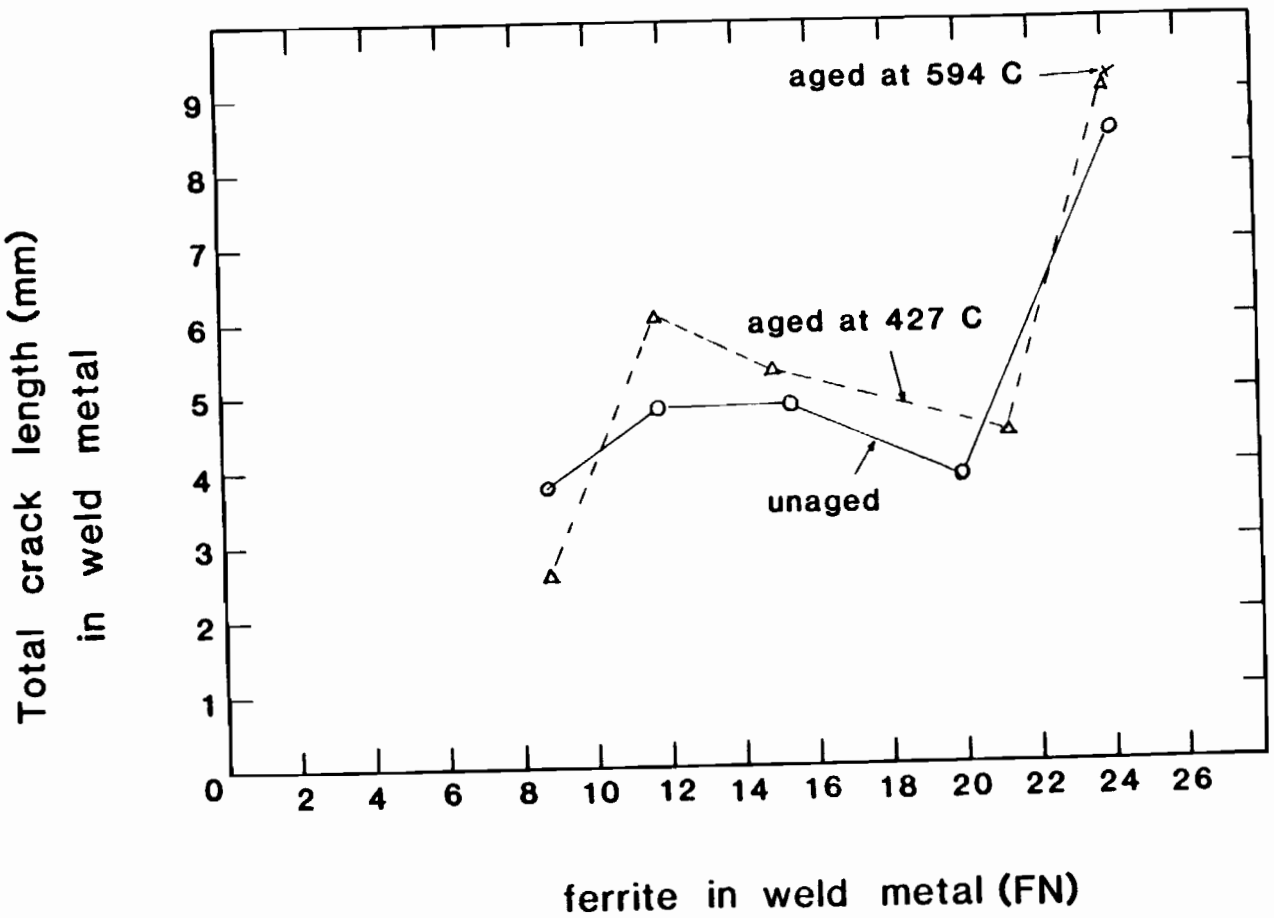

Figure 35 : Total crack length as a function of FN of weld metal for duplex stainless steel castings CF 3M, CG 8M and CF 3C.

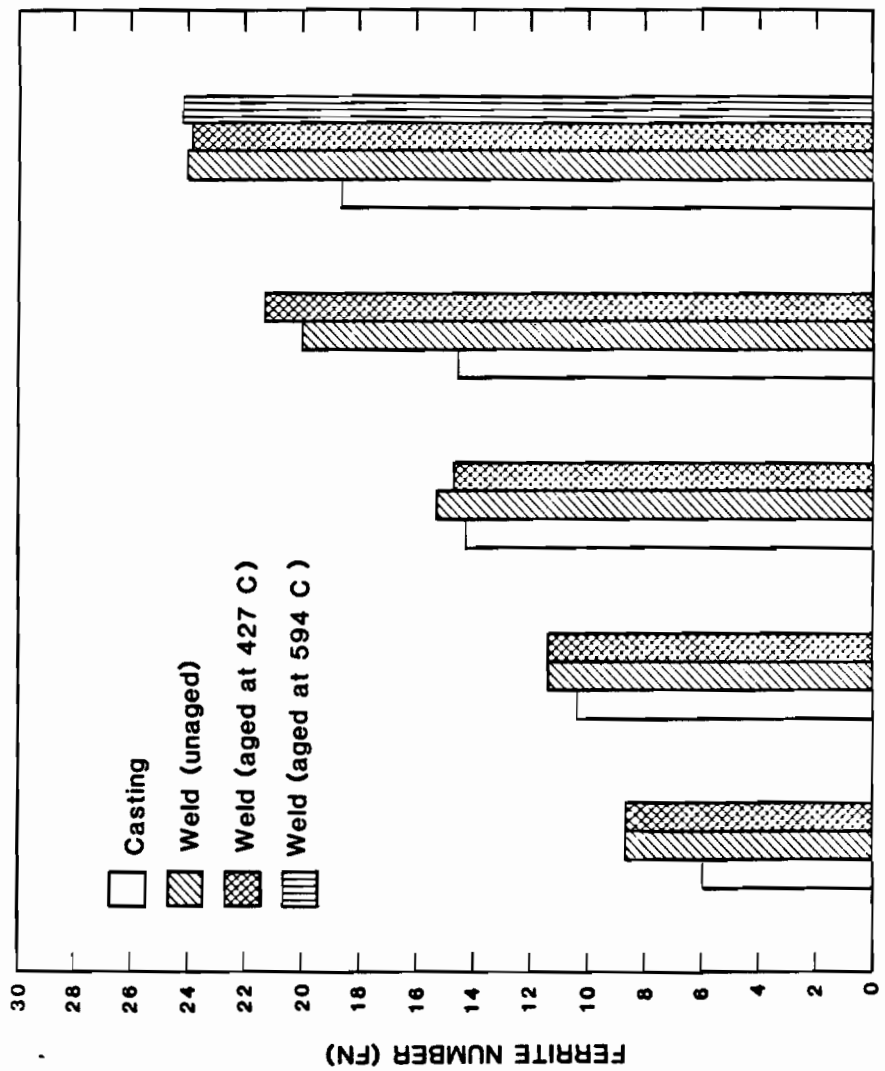

Figure 36 : FN of weld metal as compared to the FN of casting, on which the weld was deposited.

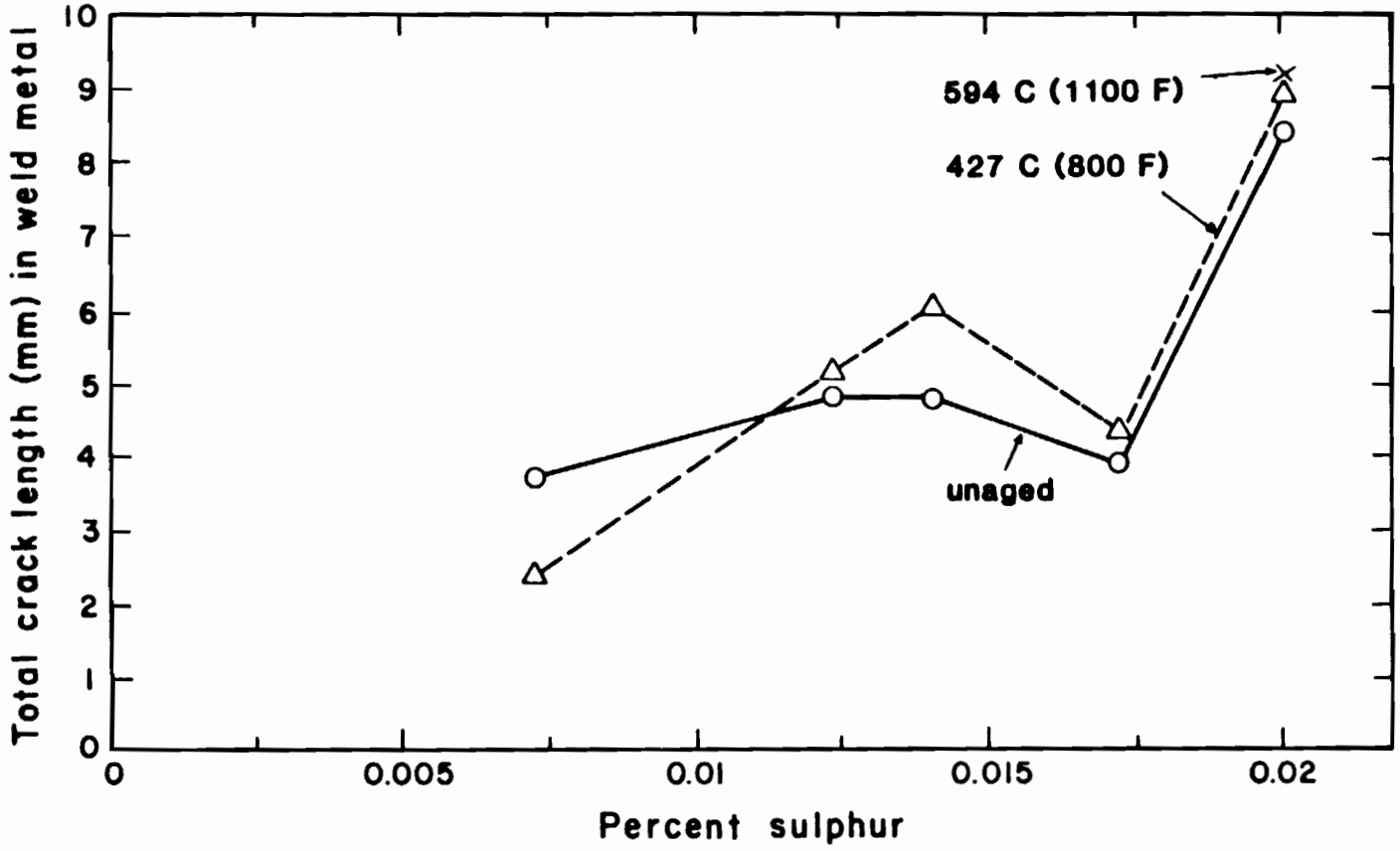

Figure 37 : Effect of S on the hot cracking susceptibility of the weld metal deposited on duplex stainless steel castings CF 3M, CG 8M and CF 3C.

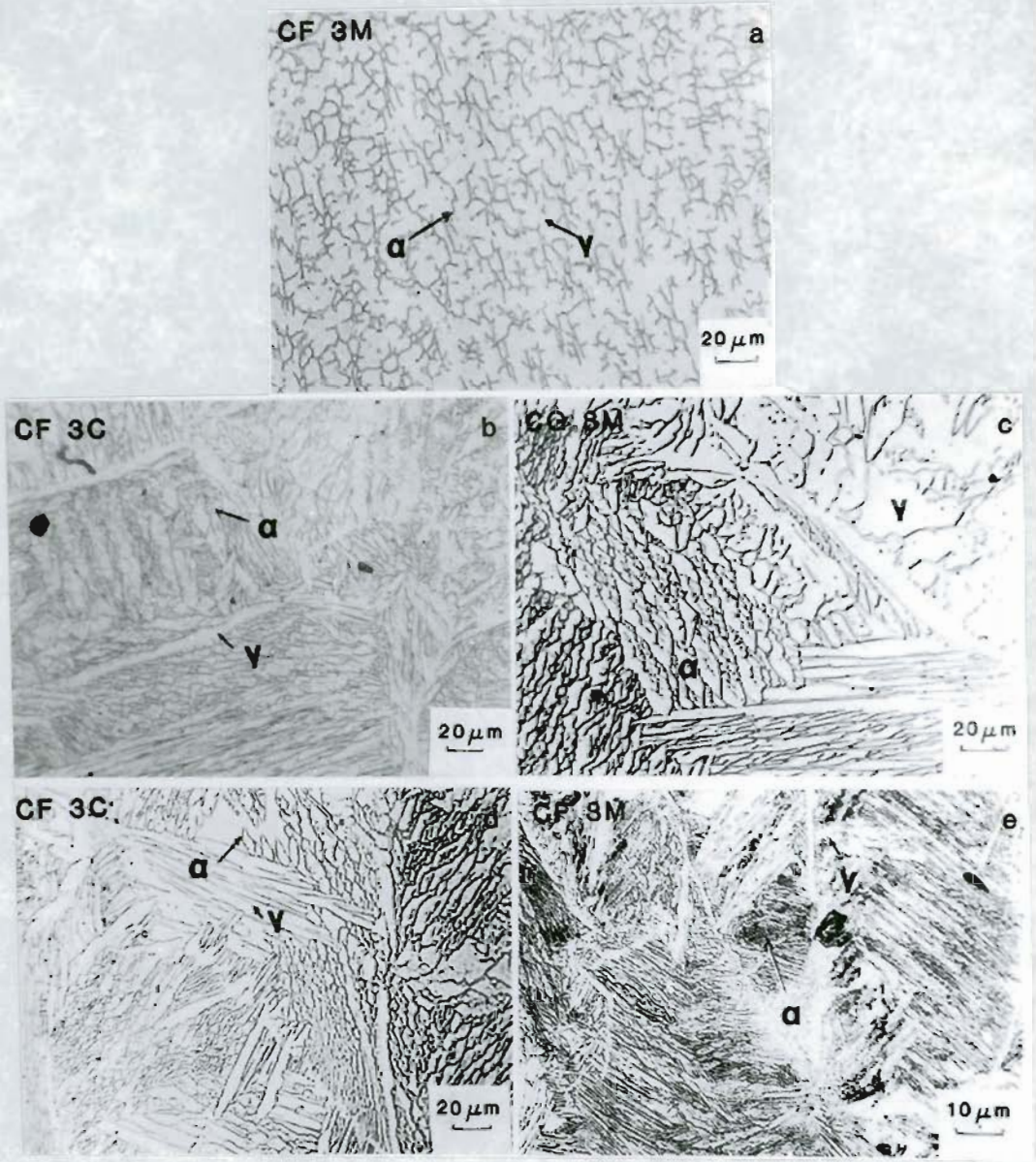

Figure 38 : Solidification structure of welds deposited on duplex stainless steel castings. a) CF 3M (7% ferrite) b) CF 3C (15% ferrite), c) CG 8M, d) CF 3C (14% ferrite) e) CF 3M (20% ferrite). Electrolytic etch with 10 % oxalic acid.

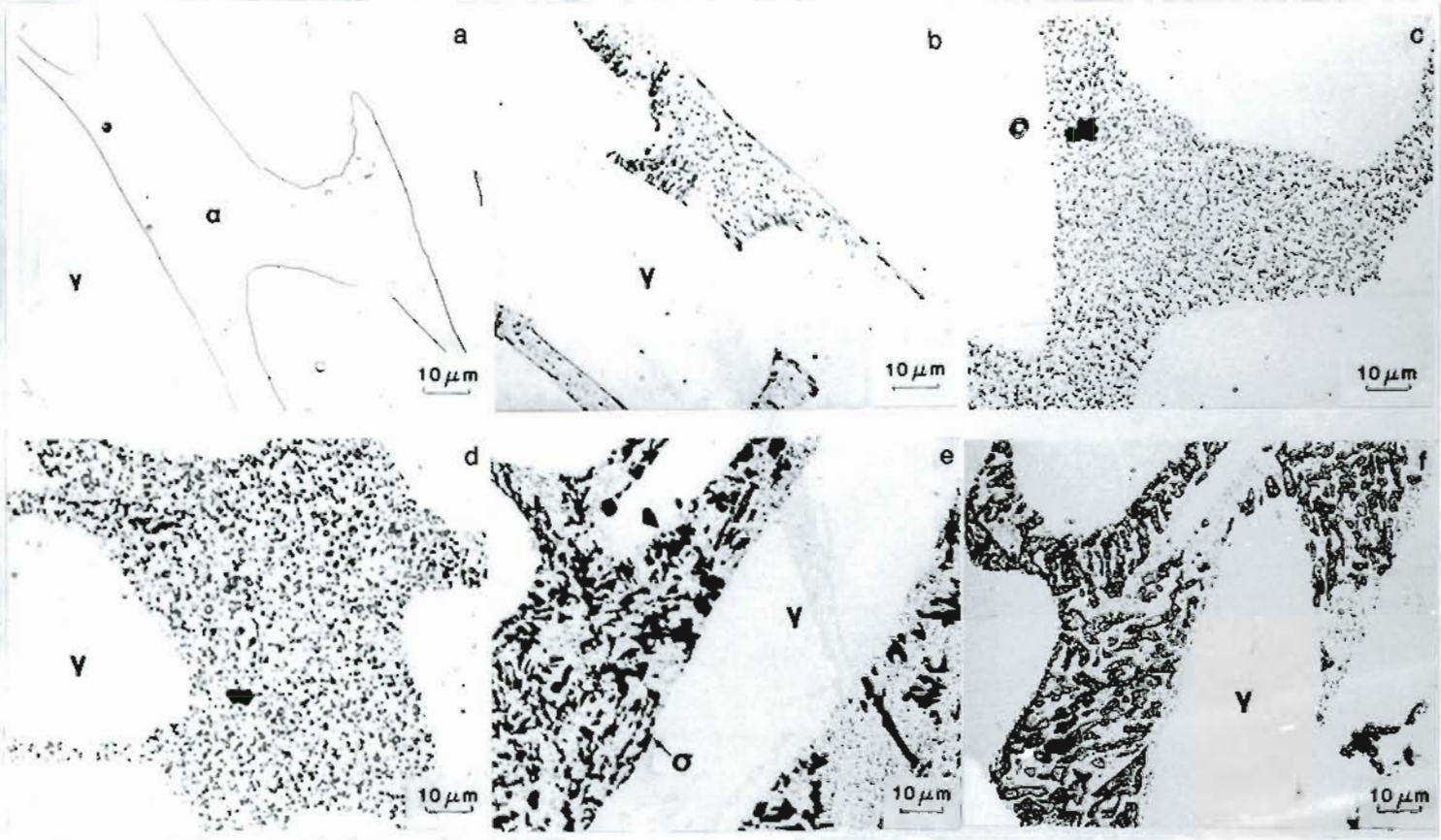

Figure 39 : Microstructures of casting CF 3M (20% ferrite in SAWQ condition) aged at 594 °C (1100 °F) for a) 0 hr, b) 10 hr, c) 200 hr, d) 1000 hr, e) 3000 hr, f) 7000 hr. Large dark patches in ferrite are sigma phase precipitates and the small particles are the precipitates of carbides and the sigma phase. Electrolytic etch - 5N KOH.

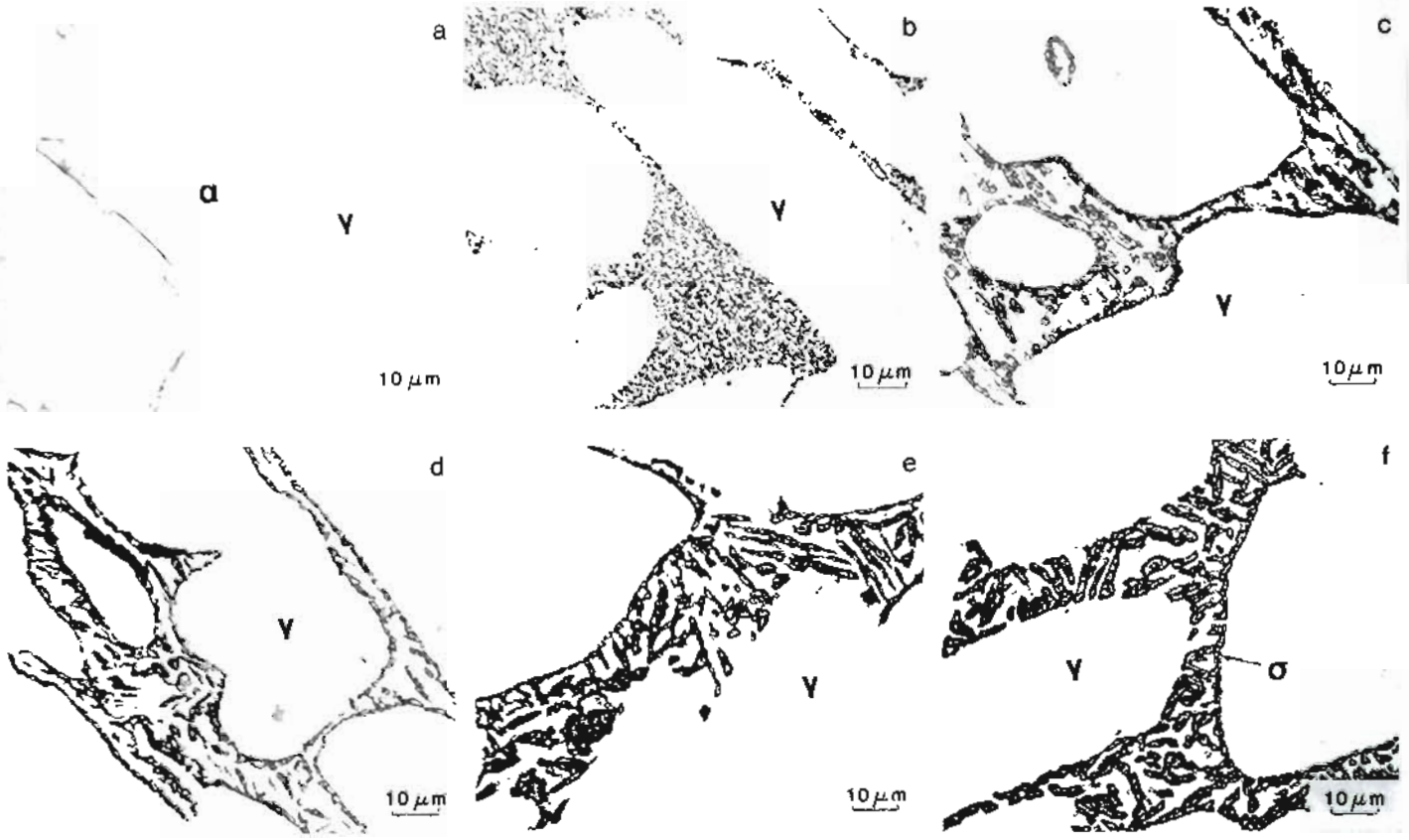

Figure 40 : Microstructures of casting CF 3C (14% ferrite in SAWQ condition) aged at 594 °C (1100 °F) for a) 200 hr, b) 300 hr, c) 700 hr, d) 1000 hr, e) 3000 hr, f) 7000 hr. Large dark patches are sigma phase precipitates and the small particles are precipitates of carbides and the sigma phase. Electrolytic etch - 5N KOH.

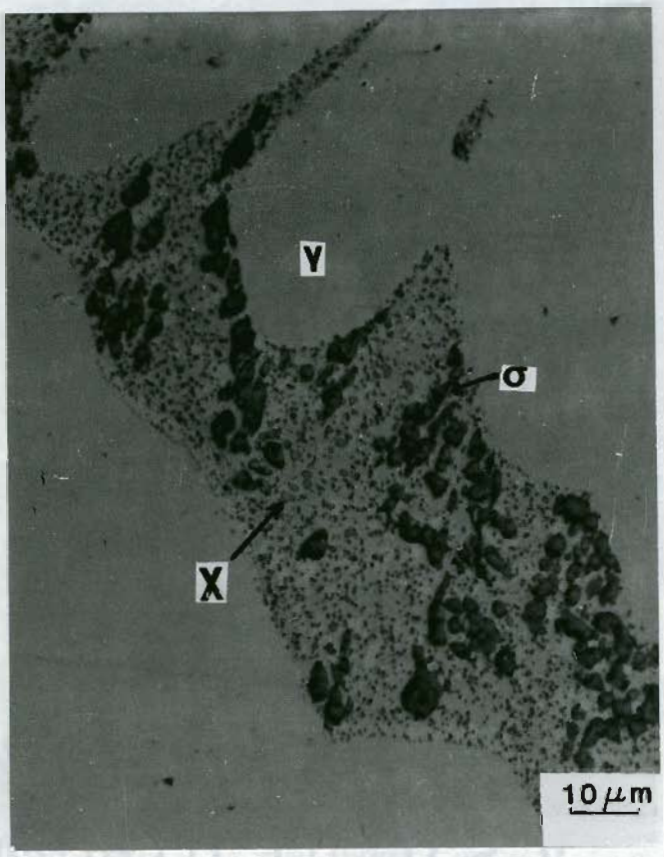

Figure 41 : Microstructure of casting CF 3M (20% ferrite in SAWQ condition) aged at 594 °C (1100 °F) for 3000 hr showing precipitation of sigma, chi and carbide phases. Electrolytic etch - saturated NaOH solution.

Figure 42 : Microstructure of alloy CF 3M (20% ferrite in SAWQ condition) aged at 594 °C (1100 °F) for 10 hr showing precipitation of carbides in ferrite. Etchant - Murakami's reagent.

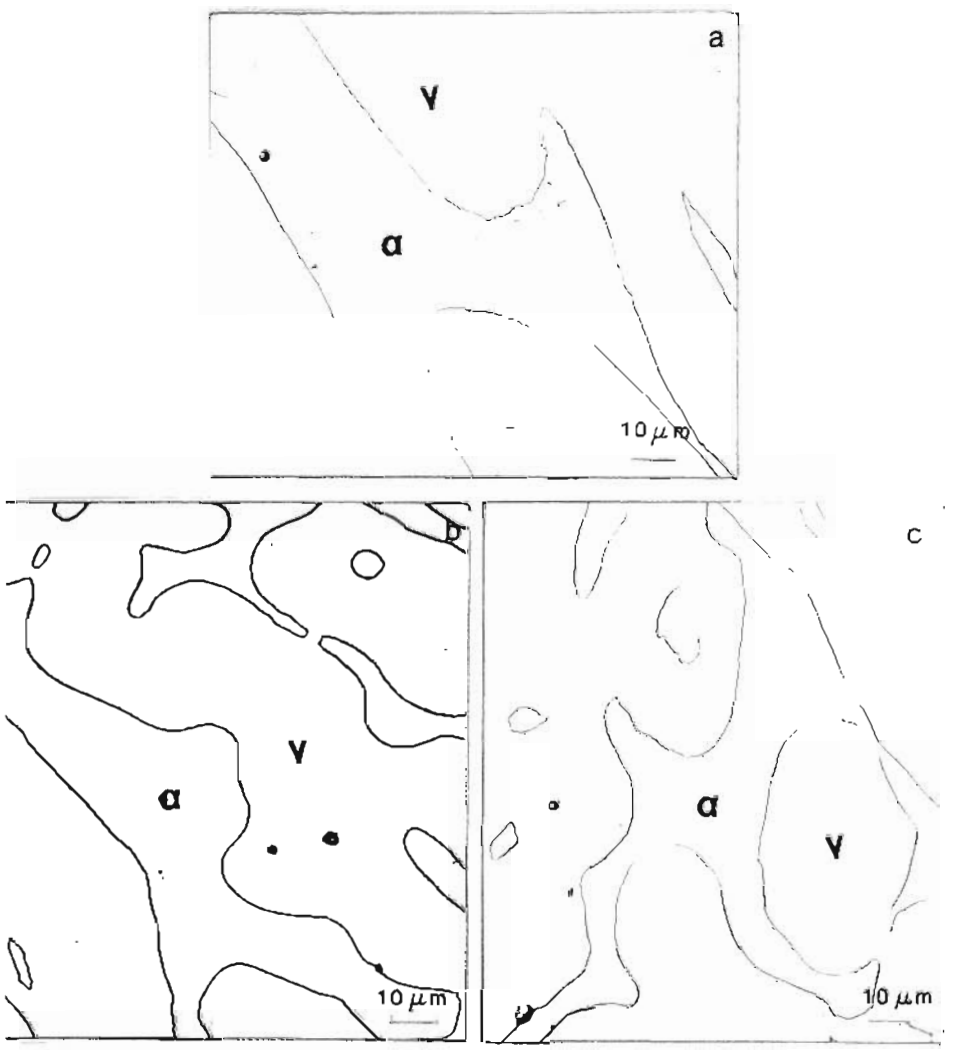

Figure 43 : Microstructures of alloy CF 3M (20% ferrite in SAWQ condition) after aging. a) SAWQ, b) 316 °C (600 °F) for 14,000 hr, c) 427 °C (800 °F) for 14,000 hr. Electrolytic etch - 10% oxalic acid.

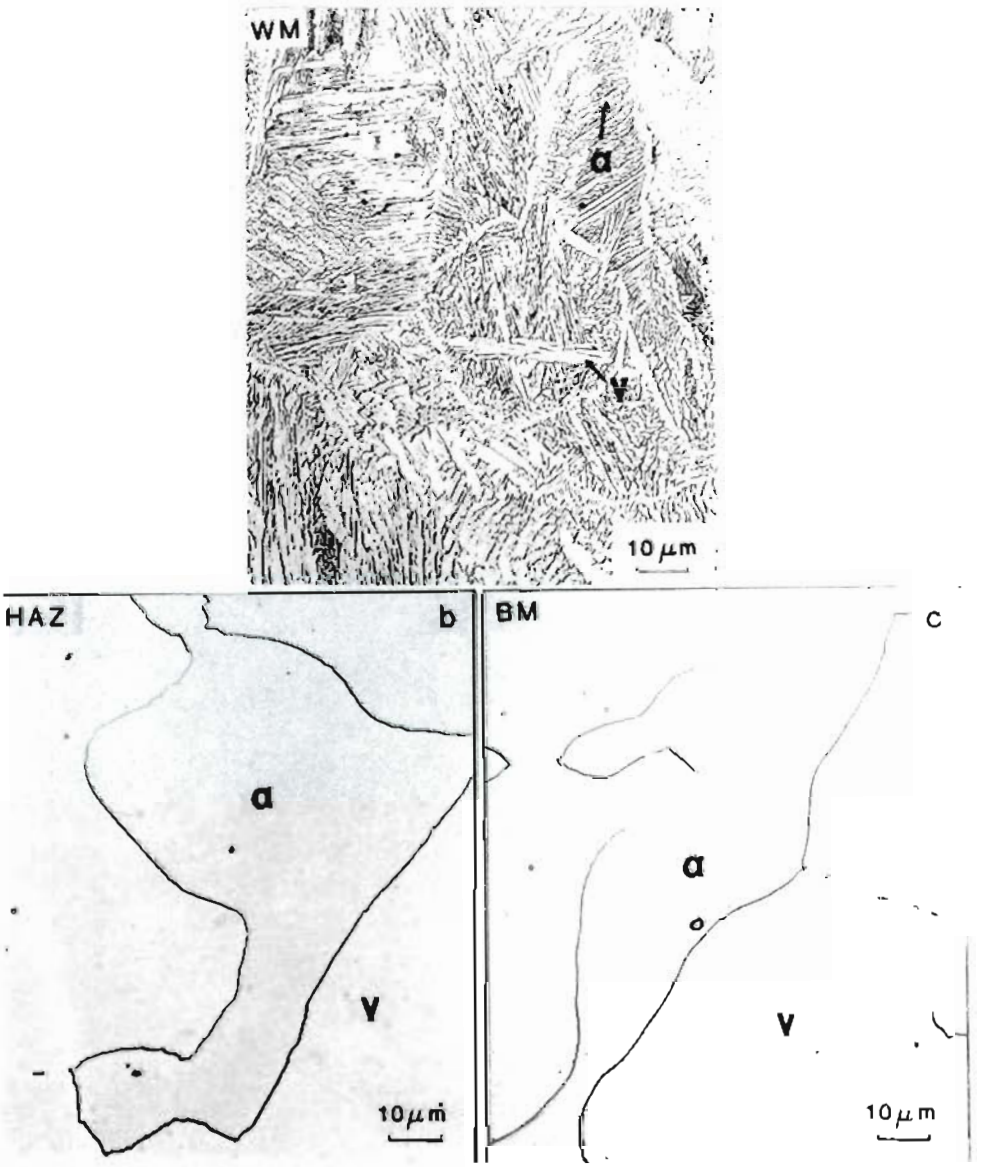

Figure 44 : Microstructures of weld metal, HAZ and base metal for alloy CF 3M (20% ferrite in SAWQ condition). Weld deposited on casting aged at 427 °C (800 °F) for 14,000 hr. Electrolytic etch - 10% oxalic acid.

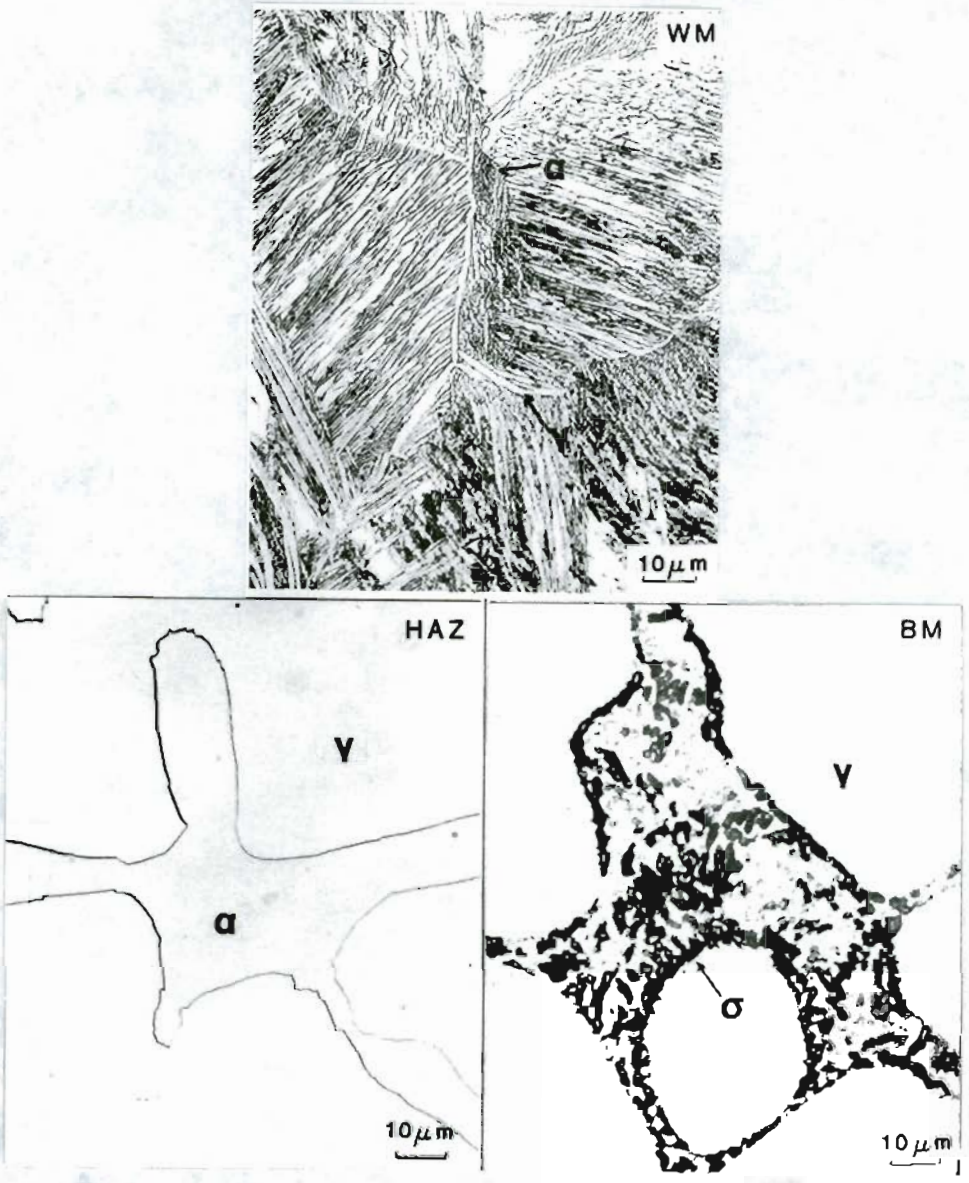

Figure 45 : Microstructures of weld metal, HAZ and base metal for alloy CF 3M (7% ferrite in SAWQ condition). Weld deposited on casting aged at 594 °C (1100 °F) for 10,000 hr. Electrolytic etch - 5N KOH.

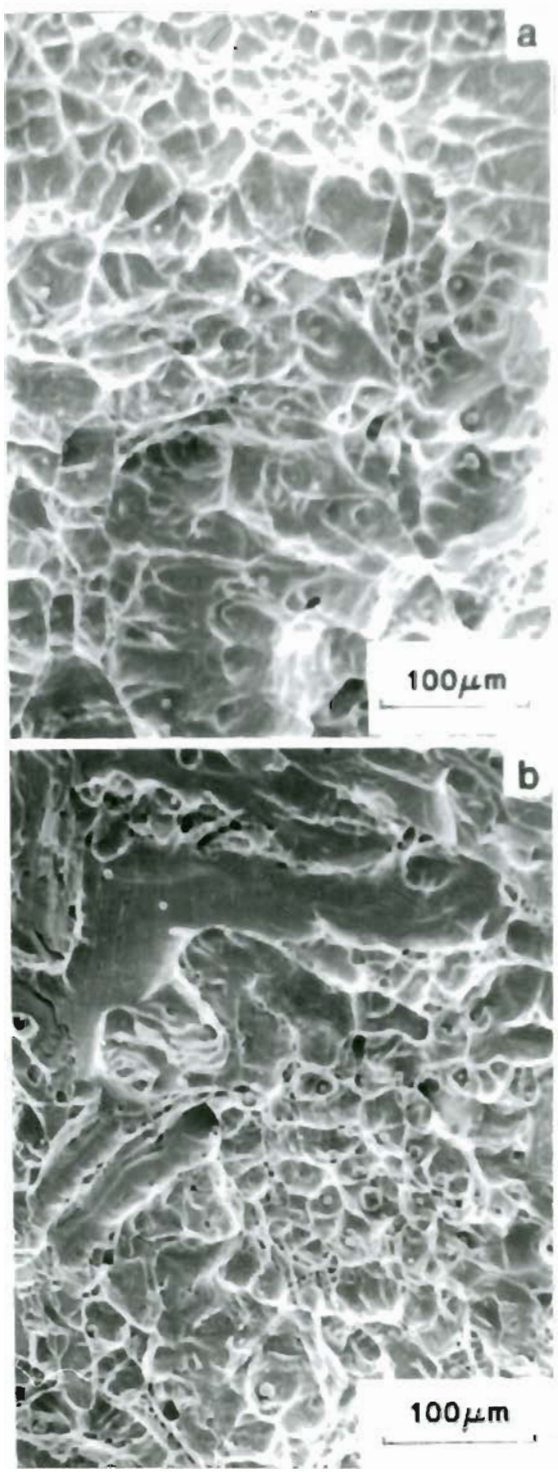

Figure 46 : Fractographs of casting CF 3M (20% ferrite in SAWQ condition). a) SAWQ, b) aged at 316 °C (600 °F) for 14,000 hr.

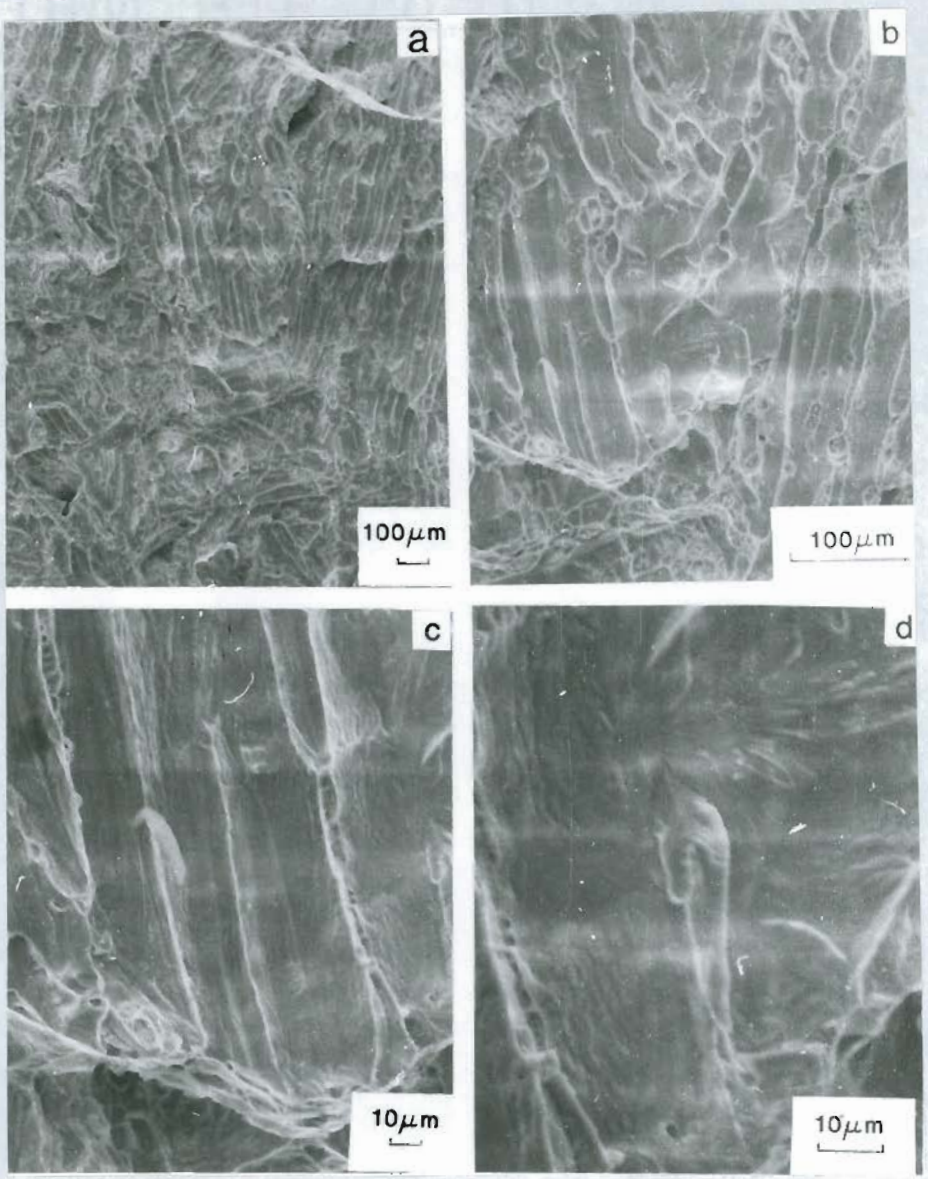

Figure 47 : Fractographs of casting CF 3M (20% ferrite in SAWQ condition) aged at 427 °C (800 °F) for 14,000 hr.

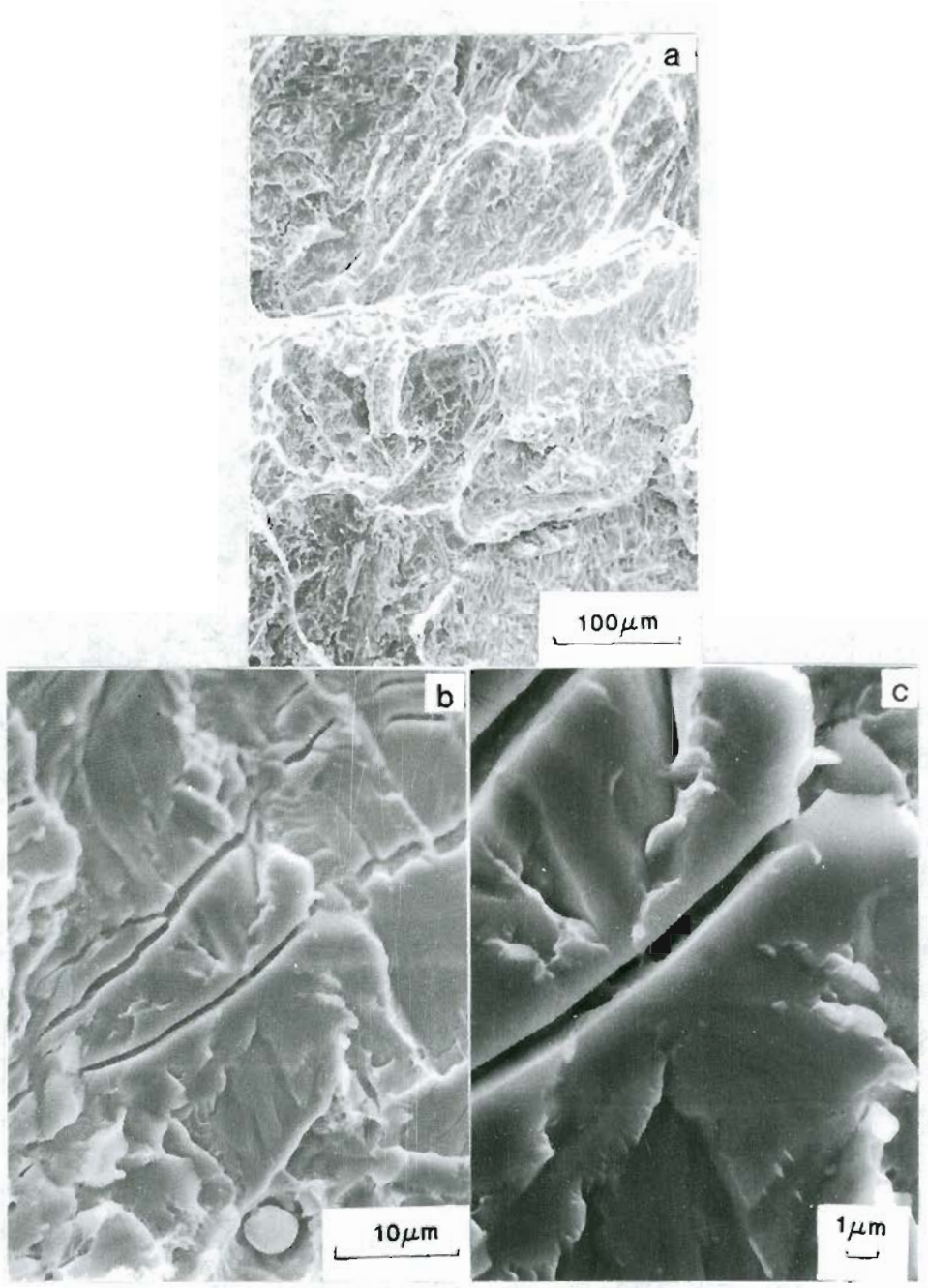

Figure 48 : Fractographs of casting CF 3M (20 % ferrite in SAWQ condition) aged at 594 °C (1100 °F) for 10,000 hr.

APPENDIX

Table A : Average CVN impact energy data for cast stainless steels.

Material	Treatment Duration (hours)	Average CVN Impact Energy (ft-lbs) Treatment Temperature, °C		
		316	427	594
CF 3M	0	145.5	145.5	145.5
20%	10			105
ferrite	200	114	64	78
	300	117	74	65
	450	107	63	67
	700	114	53	55
	1000	114	42	43
	1400	108	49	29
	2000	108	43	18
	3000	114	38	10
	4500	106	41.75	6.5
	7000	81	37.5	2.5
	10,000	84.25	34.75	3.5
	14,000	54.4	30	-
CF 3M	0	>264	>264	>264
7%	10			180
ferrite	200	>264	199	80
	300	>264	179	55
	450	>264	192	53
	700	>264	137	52
	1000	>264	118	53
	1400	>264	115	55
	2000	219	104	52
	3000	220	86	26
	4500	243.5	94.5	19.25
	7000	>264	129.25	15.25
	10,000	205	86	10
	14,000	245	115	-

Table A (cont.) : Average CVN impact energy data for cast stainless steels.

Material	Treatment Duration (hours)	Average CVN Impact Energy (ft-lbs) Treatment Temperature, °C		
		316	427	594
CF 3C	0	135	135	135
14%	10	-	-	135
ferrite	200	131	78	56
	300	129	84	68
	450	124	69	34
	700	130	69	16
	1000	-	52	19
	1400	121	56	13
	2000	125	43	9
	3000	114	58	9
	4500	115	36	5.25
	7000	104.25	50	-
	10,000	102.5	48	7
	14,000	96.75	55.25	-
CF 3C	0	>264	>264	>264
15%	10	-	-	227
ferrite	200	201	147	69
	300	>264	165	37
	450	>264	165	37
	700	>264	101	21
	1000	210	73	17
	1400	167	64	7
	2000	193	68	8
	3000	227	99	9
	4500	188.25	50	9.5
	7000	195.75	73.75	5.25
	10,000	158.25	56.25	7
	14,000	103.5	41.5	-

Table A (cont.) : Average CVN impact energy data for cast stainless steels.

Material	Treatment Duration (hours)	Average CVN Impact Energy (ft-lbs) Treatment Temperature, ^{0}C		
		316	427	594
CG 8M	0	159.5	159.5	159.5
10%	-	-	91	
ferrite	200	159	118	59
	300	148	122	70
	450	139	113	73
	700	128	98	51
	1000	143	85	44
	1400	139	82	38
	2000	145	82	30
	3000	180	80	25
	4500	133.25	65.5	25.5
	7000	125.5	50.5	3.5
	10,000	121	39	4
	14,000	73.25	47.75	-

Table B : Average hardness (HRB) data for cast stainless steels.

Material	Treatment Duration (hours)	Average Hardness HRB Treatment Temperature, ^{0}C		
		316	427	594
CF 3M 20% ferrite	0	82.5	82.5	82.5
	200	89.4	93.6	85.4
	300	89	92.6	84.7
	450	90.7	90.8	87
	700	93.8	92.3	85
	1000	94.6	96	86.8
	1400	92.5	96	84.6
	2000	92.1	95.2	86
	3000	91.1	95.9	86.7
	4500	89.1	95.7	88.3
	7000	90.2	95.6	86.1
	10,000	91.1	96.2	88.4
	14,000	89.4	92.5	-
CF 3M 7% ferrite	0	76	76	76
	200	87	82.5	76.5
	300	86.5	81.1	79.8
	450	86.7	81.5	80.2
	700	85.7	85.5	81.2
	1000	87.5	88.4	80.6
	1400	88.7	86.8	78
	2000	87.6	86.9	82.8
	3000	86.6	87.6	83.8
	4500	85.3	87.8	83.8
	7000	-	88.3	81.8
	10,000	87.5	88.6	83.5
	14,000	85.6	84.5	-

Table B (cont.) : Average hardness (HRB) data for cast stainless steels.

Material	Treatment Duration (hours)	Average Hardness HRB Treatment Temperature, °C		
		316	427	594
CF 3C 14% ferrite	0	84.7	84.7	84.7
	200	88.5	90.9	85.4
	300	87.3	88.9	87
	450	91	88.5	87
	700	90	88.5	87.9
	1000	86	91.1	86.1
	1400	87.4	91.8	87.3
	2000	87.4	94	90.7
	3000	89.3	90.3	87.2
	4500	88.5	90	88.1
	7000	86	92.2	86.1
	10,000	85.5	91.2	82.6
	14,000	84.9	89.6	-
CF 3C 15% ferrite	0	84.8	84.8	84.8
	200	89	88.2	87.4
	300	87.6	89.8	86.3
	450	86.3	91.5	85.2
	700		96.6	89.8
	1000	88.7	93.1	85.1
	1400	89.4	93.4	88.5
	2000	88.2	94.6	88.5
	3000	86	94.4	88.2
	4500	87.3	93.3	87.7
	7000	87.5	95.4	84.1
	10,000	88.8	95.4	82.4
	14,000	88.5	90.6	-

Table B : Average hardness (HRB) data for cast stainless steels.

Material	Treatment Duration (hours)	Average Hardness HRB Treatment Temperature, °C		
		316	427	594
CG 8M	0	84.4	84.4	84.4
10%	200	86.9	91.1	82.3
ferrite	300	90.1	91.7	84.7
	450	88.6	88.4	84.9
	700	89.6	90.4	86.3
	1000	87.9	90	84.5
	1400	88.2	91.5	85.7
	2000	89.3	94	84.3
	3000	90.9	93.2	-
	4500	87.3	90.6	86.5
	7000	88.3	91.2	87.7
	10,000	88.1	89	89.7
	14,000	89.1	89.3	-

Table C : Knoop hardness (50 gm load) of ferrite after aging.

Treatment Duration (hours) (at 427 ^{0}C)	CF 3M 20% ferrite	CF 3M 7% ferrite	CG 8M 10% ferrite	CF 3C 14% ferrite	CF 3C 15% ferrite
0	333	361	352	357	331
200	630	588	644	612	565
700	704	715	716	600	599
1000	858	594	615	661	584
2000	775	646	838	714	678
3000	864	829	767	647	714
4500	835	853	877	798	676
7000	857	884	755	828	721
10,000	830	876	780	791	823
14,000					
(at 316 C) 10,000	696	634	657	599	641

Table D : Average ferrite content (%) data for cast stainless steels.

Material	Treatment Duration (hours)	Average Ferrite Content (%) Treatment Temperature, °C		
		316	427	594
CF 3M 20% ferrite	0	19.7	19.7	19.7
	200	20	19.5	12.8
	300	19.8	19.8	13.5
	450	19.3	18	12.2
	700	19.2	19.3	11.9
	1000	21.5	20.1	12.5
	1400	20.3	17.9	11
	2000	20.2	17.2	10.2
	3000	19	17.3	8.8
	4500	18.4	15.7	7.5
	7000	18.6	16	5.7
	10,000	84.25	34.75	-
	14,000	19.6	14.4	-
CF 3M 7% ferrite	0	8.3	8.3	8.3
	200	5.8	7.5	3.6
	300	7.3	7.8	4.2
	450	6.6	7.1	4.8
	700	6.7	6.5	3.9
	1000	6.4	7.7	4.2
	1400	6.7	7.4	4.0
	2000	6.9	6.2	3.7
	3000	8.5	7.5	4.0
	4500	7.5	7.1	4.9
	7000	-	8.4	3.0
	10,000	7.7	6.3	-
	14,000	8.8	4.5	-

Table D (cont.) : Average ferrite content (%) data for cast stainless steels.

Material	Treatment Duration (hours)	Average Ferrite Content (%) Treatment Temperature, °C		
		316	427	594
CF 3C 14% ferrite	0	14.2	14.2	14.2
	200	15.8	14.7	13
	300	16	14.6	12
	450	15.7	14.6	11.8
	700	15.3	14.8	11.1
	1000	-	15.3	10.4
	1400	16	14.7	9.9
	2000	15.8	14.8	8.7
	3000	14.7	12.8	7.7
	4500	13.2	-	6.7
	7000	14.7	12	6.1
	10,000	14.7	12.5	-
	14,000	14.6	12.4	-
CF 3C 15% ferrite	0	15.2	15.2	15.2
	200	16.2	14.2	11.5
	300	14.4	13.8	11.9
	450	13.7	13.8	11.3
	700	18.5	17	13
	1000	17.2	18	11.5
	1400	16.9	18.6	12.2
	2000	15.5	14.3	12.1
	3000	17.6	15.5	11.4
	4500	17.7	16.4	10.5
	7000	16.7	13.3	8.9
	10,000	15.1	13.7	-
	14,000	16.2	13.7	-

Table D (cont.) : Average ferrite content (%) data for cast stainless steels.

Material	Treatment Duration	Average Ferrite Content (%) Treatment Temperature, °C		
CG 8M	0	10	10	10
10%	200	8.5	11.3	5.7
ferrite	300	8.6	8.3	4.2
	450	8.3	8.0	4.5
	700	13.8	10.9	5.4
	1000	13.2	11.5	6.3
	1400	13.8	10.6	6.2
	2000	12.3	9.2	5.9
	3000	14.6	8.5	6.3
	4500	10.9	8.9	5.5
	7000	11.3	7.4	1.6
	10,000	8.9	6.2	-
	14,000	12	5.5	-

Table E : Varestraint test data for castings.

Alloy	Total Crack Length(TCL) (mm)		Average TCL (mm)		
	unaged	aged at 427 °C	unaged	aged at 427 °C	aged at 594 °C
CF 3M	7.17	8.85			
20%	8.24	10.88			
ferrite	10.08	7.32	8.49	9.01	9.07
CF 3M	4.29	3.2			
7%	3.51	2.05			
ferrite	3.44	2.16	3.76	2.47	2.7
CG 8M	4.09	6.39			
10%	5.94	8.81			
ferrite	4.44	8.92	4.82	8.04	7.1
CF 3C	4.64	5.79			
14%	2.88	3.45			
ferrite	4.31	4.08	3.94	4.44	4.15
CF 3C	3.72	7.27			
15%	5.23	3.9			
ferrite	5.69	4.80	4.88	5.32	5.1

Table F : Ferrite content (FN) of the weld metal of the varestraint specimens.

Alloy	Average Ferrite Number (FN) Aging temperature, °C (°F)		
	unaged	427 °C (800 °F)	594 °C (1100 °F)
CF 3M 20% ferrite	24.1	24	24.1
CF 3M 7% ferrite	8.6	8.6	
CG 8M	11.8	11.8	
CF 3C 14% ferrite	20	21.2	
CF 3C 15% ferrite	15.4	14.8	

Table G : Hardness of the weld metal, HAZ and the base metal.

Alloy	Aging condition	Hardness (HRB) of		
		weld metal	HAZ	base metal
CF 3M (20% ferrite)	As cast	95.3	88.8	84.8
	427 °C	94.9	89.4	98.9
	594 °C			
CF 3M (7% ferrite)	As cast	89.7	87.9	87.7
	427 °C	90.1	86.5	85.6
CG 8M	As cast	90	88	84.5
	427 °C	90.3	87.4	89.4
CF 3C (14% ferrite)	As cast	92.6	85	85.4
	427 °C	95.3	85.9	88
CF 3C (15% ferrite)	As cast	89.5	86.6	85.6
	427 °C	92.4	87.8	91.1

BIOGRAPHICAL NOTE

The author was born on March 28, 1960, in Murud Janjira, India. He attended the Elizabeth High School between 1965 and 1972, and S. E. S. High School between 1972 and 1976 and graduated with a H. S. S. Certificate (XI) in April 1976. He then joined the Ruia College at Bombay, India, and obtained a H. S. S. Certificate (XII) in Science in May 1977. He then joined the Sardar Vallabbhai Patel College of Engineering, Bombay. Later the author enrolled at the Indian Institute of Technology, Bombay, and graduated with a B. Tech. degree in Metallurgical Engineering in May 1983. He subsequently joined the Materials Science Department at the Oregon Graduate Center, Beaverton, Oregon, U. S. A., in fall 1983, where he completed the requirements for the degree Master of Science in August 1985.